The Geometry of Gravitational Lensing: Magnification Relations, Observables, and Kerr Black Holes

by

Amir Babak Aazami

Department of Mathematics
Duke University

Date: _____

Approved:

_____
Arlie O. Petters, Advisor

_____
Hubert L. Bray

_____
Charles R. Keeton

_____
Marcus C. Werner

Dissertation submitted in partial fulfillment of the requirements for the degree of
Doctor of Philosophy in the Department of Mathematics
in the Graduate School of Duke University
2011

Abstract

(Mathematics)

The Geometry of Gravitational Lensing: Magnification Relations, Observables, and Kerr Black Holes

by

Amir Babak Aazami

Department of Mathematics
Duke University

Date: _____

Approved:

_____
Arlie O. Petters, Advisor

_____
Hubert L. Bray

_____
Charles R. Keeton

_____
Marcus C. Werner

An abstract of a dissertation submitted in partial fulfillment of the requirements for the degree of Doctor of Philosophy in the Department of Mathematics in the Graduate School of Duke University
2011

Abstract

Gravitational lensing is the study of the bending of light by gravity. In such a scenario, light rays from a background star are deflected as they pass by a foreground galaxy (the "lens"). If the lens is massive enough, then multiple copies of the light source, called "lensed images," are produced. These are magnified or demagnified relative to the light source that gave rise to them. Under certain conditions their sum is an invariant: it does not depend on where these lensed images are in the sky or even the details of the lens mass producing them. One of the main results of this thesis is the discovery of a new, infinite family of such invariants, going well beyond the previously known class of two. The application of this result to the search for dark matter in galaxies is also discussed.

The second main result of this thesis is a new general lens equation and magnification formula governing lensing by Kerr black holes, for source and observer lying in the asymptotically flat region of the spacetime. The reason for deriving these quantities is because the standard gravitational lensing framework assumes that the gravitational field of the lens is weak, so that a Newtonian potential can be applied to model it. This assumption obviously breaks down in the vicinity of a black hole, where the gravity is immense. As a result, one has to go directly to the Kerr metric and its associated geometric quantities, and derive an equation for light bending from first principles. This equation is then solved perturbatively to obtain lensing observables (image position, magnification, time delay) beyond leading order.

to my father, mother, and sister, with love

Contents

List of Tables

List of Figures

Acknowledgements

From Yale, I would like to thank Richard Easther for his early support, and especially Priyamvada Natarajan; without her help this thesis would not have been possible. I also thank Hubert Bray, Charles Keeton, and Jeffrey Rabin for being fantastic collaborators, as well as Marcus Werner for stimulating discussions. Most especially, however, I thank my adviser and mentor Arlie Petters, from whom I have learned so much.

1

Introduction

Gravitational lensing is the study of the bending of light by gravity. In such a scenario, light rays from a background star are deflected as they pass by a foreground galaxy (the "lens"). This effect was predicted by Einstein in 1911 as a consequence of his general theory of relativity, and first observed by Eddington in 1919. The field is now a vibrant area of research in astronomy, physics, and mathematical physics (see, e.g., Schneider et al. (1992); Petters et al. (2001); Petters (2010)). The phenomenon of light bending is an extraordinary one: if the lens is massive enough, then multiple copies of the light source, called "lensed images," are produced; see Fig. 1.1 for examples.

1.1 Magnification Relations

Chapters 2 and 3 of this dissertation focus on an important aspect of this phenomenon: lensed images are *magnified* or *demagnified* relative to the light source that gave rise to them. Formally, the magnification is a ratio of solid angles, subtended by the lensed image and source. Surprisingly, under certain conditions the *sum* of the magnifications of lensed images is an *invariant:* it does not depend on

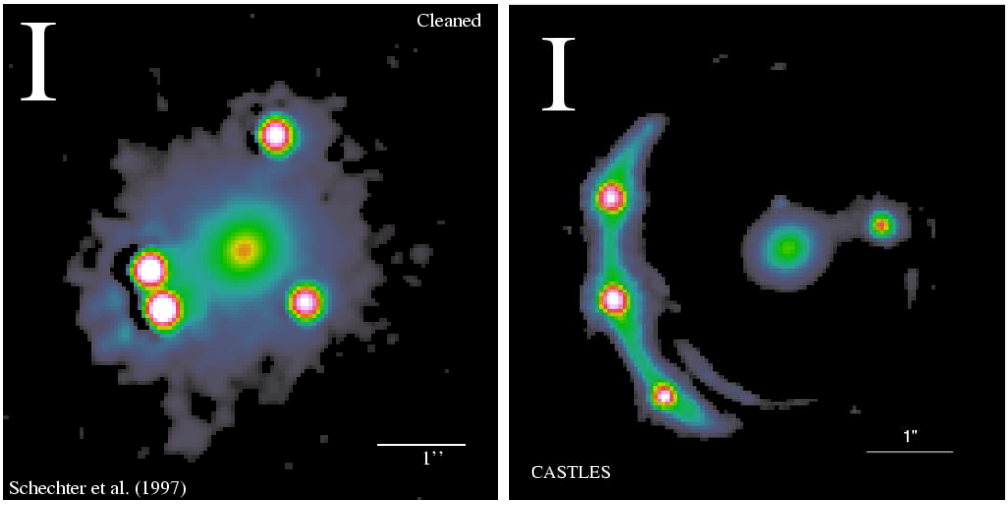

FIGURE 1.1: Two observations of four lensed images of a background source by a foreground galaxy (central bulge in each panel). In each panel the source is a quasar, though it is not visible. The letter "I" indicates that the images are being observed in the near-infrared I-band. Courtesy of the CASTLES lens sample (http://www.cfa.harvard.edu/castles).

where these lensed images are in the sky or even the details of the lens mass producing them. These invariants are known as "magnification relations," and they are used by astronomers to infer the presence of dark matter in galaxies, among other things (see Keeton et al. (2003, 2005) and references therein). But they are also mathematically noteworthy because they are *geometric* invariants.

A Brief Introduction to Gravitational Lensing

Due to the large distances traversed by light rays in a typical lensing scenario (much larger than the spatial extent of the lens mass), we work under the assumption that the lens is essentially two-dimensional and lies on a plane perpendicular to our line of sight, known as the *lens plane* $L \subseteq \mathbb{R}^2$. When we speak of the "location of a lensed image in the sky," we mean its vector position $\mathbf{x} \in L$. The position $\mathbf{x}$ is where a light ray gets deflected (geometrically, light rays are modeled as null geodesics in general relativity). Likewise, we can think of the source as lying at a particular (fixed) vector position $\mathbf{y}$ in the *source plane* $S = \mathbb{R}^2$ (far behind L but parallel to it); see Fig. 1.2.

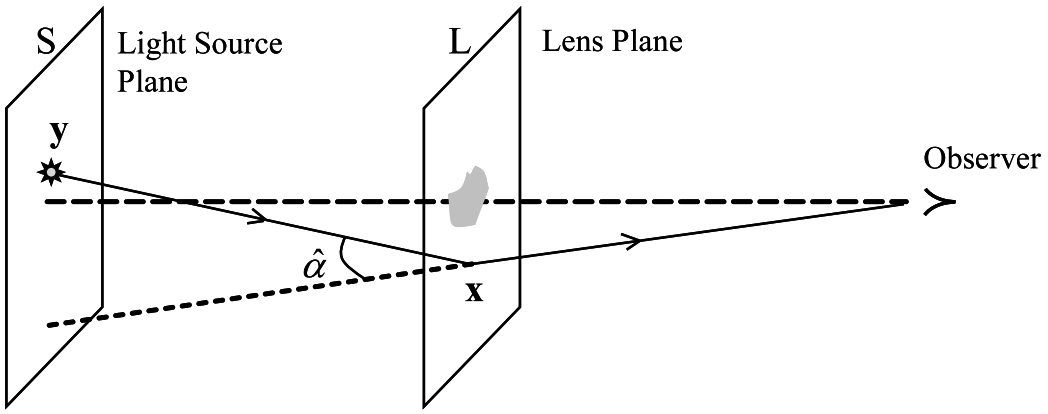

FIGURE 1.2: Schematic of gravitational lensing. A light ray emitted from a source at $\mathbf{y} \in S$ is deflected by an angle $\hat{\alpha}$ at the lens plane at $\mathbf{x} \in L$. An observer thus sees (one copy of) the source at $\mathbf{x} \in L$. Courtesy of Petters (2010).

With these quantities in hand, one can then ask: "If a light ray is deflected by the lens and then reaches us, how much longer is its arrival time compared to a light ray that would have directly reached us in the absence of a lens?" We quantify this "time delay" by the *time delay function*, a smooth real-valued function $T_{\mathbf{y}} \colon L \longrightarrow \mathbb{R}$. This function actually contains within it the core of gravitational lensing theory. We now apply Fermat's principle of "least time," which says that light rays emitted from a source that reach us are realized as critical points of the time delay function (and so the mathematical origins of gravitational lensing theory ultimately lie in symplectic geometry). In other words, a lensed image of a light source at $\mathbf{y}$ is a critical point of $T_{\mathbf{y}}$, i.e., a solution $\mathbf{x} \in L$ of the equation $(\operatorname{grad} T_{\mathbf{y}})(\mathbf{x}) = \mathbf{0}$, where the gradient is taken with respect to $\mathbf{x}$. With this information in hand, we can now geometrically define the notion of magnification: the *signed magnification* of a lensed image $\mathbf{x} \in L$ of a light source at $\mathbf{y} \in S$ is

$$\mu(\mathbf{x}; \mathbf{y}) = \frac{1}{\operatorname{Gauss}(\mathbf{x}, T_{\mathbf{y}}(\mathbf{x}))} \ ,$$

where $\operatorname{Gauss}(\mathbf{x}, T_{\mathbf{y}}(\mathbf{x}))$ is the Gaussian curvature of the graph of $T_{\mathbf{y}}$ at the critical point $(\mathbf{x}, T_{\mathbf{y}}(\mathbf{x}))$. This definition makes clear why magnification relations are

geometric invariants. (Though not obvious, it is equivalent to the definition given in terms of solid angles above.) But it also begs the question: What happens if $\text{Gauss}(\mathbf{x}, T_{\mathbf{y}}(\mathbf{x})) = 0$? Any $\mathbf{y} \in S$ giving rise to such an $\mathbf{x}$ is called a *caustic point*. The set of all caustic points typically forms smooth curves, but could also include isolated points. Since we do not expect to see lensed images with infinite magnification in the sky (mathematically, caustics form a set of measure zero), the important question then becomes whether a source lies *near* a caustic. If it does, then very interesting things happen, as we shall see below. Indeed, in Fig. 1.1 above, the source in each case lies near a caustic, and this accounts for the particular configuration the four lensed images assume (in the left panel, notice that two images lie very close together, while in the right panel there is a triplet of images positioned away from the fourth). To better understand this relation between caustics and the observed positions of lensed images, one must delve into the mathematical subject known as *singularity theory,* which is the systematic analysis of the critical point and caustic structure of families of smooth functions.

A Brief Introduction to Singularity Theory

In one of the major achievements in singularity theory, Vladimir Arnold in 1973 classified the possible types of stable caustics that can occur (Arnold's classification incorporated and went beyond an earlier classification by René Thom in the 1960s). Specifically, Arnold classified all stable simple Lagrangian map-germs of n-dimensional Lagrangian submanifolds by their generating family $F_{\mathbf{c},\mathbf{y}}$ (these are analogous to the time delay function $T_{\mathbf{y}}$); see Arnold (1973). In the process, he found a remarkable connection between his classification and the Coxeter-Dynkin diagrams of the simple Lie algebras of types A_n $(n \geqslant 2)$, D_n $(n \geqslant 4)$, E_6, E_7, E_8. This is now known as Arnold's A, D, E *classification of caustic singularities;* see Table 2.2 of Chapter 2.

The time delay function $T_{\mathbf{y}}(\mathbf{x})$ can be viewed as a two-parameter family of functions with parameter the light source position $\mathbf{y} \in S$. In this two-dimensional setting, it can be shown that a "generic" time delay function will give rise to only two types of "generic" caustic points: *folds* and *cusps* ("generic" is here used in a well-defined sense; ultimately, we are living in the Whitney C^∞-topology in a given space of mappings). Folds are arcs on the source plane that abut isolated cusp points. These are the simplest examples of caustic singularities in Arnold's classification. Now, let $T_{c,\mathbf{y}}(\mathbf{x})$ denote a family of time delay functions parametrized by the source position $\mathbf{y}$ and $c \in \mathbb{R}$. (In the context of gravitational lensing, the parameter c may denote the core radius of the galaxy acting as lens, or the redshift of the source, or some other physical input.) The three-parameter family $T_{c,\mathbf{y}}(\mathbf{x})$ gives rise to a more sophisticated and higher-order caustic structure. Varying c causes the caustic curves in the light source plane S to evolve with c. This traces out a caustic surface in the three-dimensional space $\mathbb{R} \times \mathbb{R}^2 = \{(c, \mathbf{y})\}$. The source plane S would then be a particular "c-slice" of this caustic surface. Beyond folds and cusps, these surfaces are classified into three generic types, namely, *swallowtails, elliptic umbilics*, and *hyperbolic umbilics*. And so on; more and more parameters give rise to higher- and higher-order caustic surfaces, with ever-more beautiful (and strange) shapes. In Arnold's classification, it turns out that the fold, cusp, swallowtail, and umbilics are classified by the Dynkin diagrams A_2, A_3, A_4, and D_4, respectively.

Having said this, there is no reason to restrict the notion of magnification to time-delay functions alone. Indeed, consider a smooth n-parameter generating family $F_{\mathbf{c},\mathbf{y}}(\mathbf{x})$ of functions on an open subset of $\mathbb{R}^2$ that exhibits a caustic singularity classified by Arnold's A, D, E classification. We can then define the *magnification* of $F_{\mathbf{c},\mathbf{y}}(\mathbf{x})$ at a critical point $\mathbf{x}$ in exactly the same way as we did for time-delay

functions, namely, as

$$\mathfrak{M}(\mathbf{x};\mathbf{y}) = \frac{1}{\text{Gauss}(\mathbf{x}, F_{\mathbf{c},\mathbf{y}}(\mathbf{x}))} \ ,$$

where we use the symbol $\mathfrak{M}$ to distinguish magnification in the generic sense from its use in gravitational lensing. Armed with this definition, we can now inquire whether we can uncover "magnification relations" for any of the caustic singularities in Arnold's family. The surprising answer is that *all* of them exhibit a magnification relation of the following form:

$$\sum_{i=1}^{n} \mathfrak{M}(\mathbf{x}_i;\mathbf{y}) = 0 \ , \tag{1.1}$$

where $\mathbf{x}_i$ are the n critical points of a particular generating family $F_{\mathbf{c},\mathbf{y}}(\mathbf{x})$ with $\mathbf{y}$ fixed (in fact its number of critical points is equal to its index as a Dynkin diagram; i.e., of type A_n $(n \geqslant 2)$, D_n $(n \geqslant 4)$, E_6, E_7, E_8). The key result in Chapters 2 and 3 is Theorem 1, which establishes eqn. (1.1) and provides a geometric explanation for its existence. We will see that this geometric explanation relies upon multi-dimensional residue techniques and the geometry of orbifolds.

1.2 Lensing by Kerr Black Holes

Chapters 4 and 5 develop a unified, analytic framework for gravitational lensing by Kerr black holes. These are rotating black holes, the metrics for which were discovered by Roy Kerr in 1963. Chapter 4 presents a new, general lens equation and magnification formula governing lensing by an arbitrary thin deflector. Our lens equation assumes that the source and observer are in the asymptotically flat region. Furthermore, whereas in all lensing scenarios it is assumed that the bending of the light ray takes place on the plane perpendicular to the line of sight containing the lens (as in Fig. 1.2 above), that assumption is *not* made here. Thus the lens equation

presented in Chapter 4 takes into account the displacement that occurs when the light ray's tangent lines at the source and observer do not meet on the lens plane. Next, restricting to the case when the thin deflector is a Kerr black hole, an explicit expression is given for the displacement when the observer is in the equatorial plane of the Kerr black hole, as well as for the case of spherical symmetry. The reason for deriving these quantities is because the standard gravitational lensing framework assumes that the gravitational field of the lens is weak, so that a Newtonian potential can be applied to model it. This assumption obviously breaks down in the vicinity of a black hole, where the gravity is immense. As a result, one has to go directly to the Kerr metric and its associated geometric invariants, and derive an equation for light bending from first principles. This is the goal of Chapter 4.

Chapter 5 then explores this lens equation; specifically, it develops an analytical theory of quasi-equatorial lensing by Kerr black holes. In this setting the general lens equation (with displacement) is solved perturbatively, going beyond weak-deflection Kerr lensing to second order in the expansion parameter ε, which is the ratio of the angular gravitational radius to the angular Einstein radius. New formulas and results are obtained for the bending angle, image positions, image magnifications, total unsigned magnification, centroid, and time delay, all to second order in ε and including the displacement. For all lensing observables it is shown that the displacement begins to appear only at second order in ε. When there is no spin, new results are obtained on the lensing observables for Schwarzschild lensing with displacement.

1.3 Declaration

This dissertation is the result of my work under the guidance of my adviser Prof. Arlie Petters and two collaborators, Prof. Jeffrey Rabin and Prof. Charles Keeton. The following chapters are based on, or have been excerpted/reproduced from, articles that have either been published or are currently under review for publication:

Chapter 2:

- Aazami, A. B., Petters, A. O., *A universal magnification theorem for higher-order caustic singularities,* J. Math. Phys. **50**, 032501, Copyright 2009, The American Institute of Physics.

- Aazami, A. B., Petters, A. O., *A universal magnification theorem. III. Caustics beyond codimension five,* J. Math. Phys. **51**, 023503, Copyright 2010, The American Institute of Physics.

  This chapter may be downloaded for personal use only.

Chapter 3:

- Aazami, A. B., Petters, A. O., *A universal magnification theorem II. Generic caustics up to codimension five,* J. Math. Phys. **50**, 082501, Copyright 2009, The American Institute of Physics.

- Aazami, A. B., Petters, A. O., *A universal magnification theorem. III. Caustics beyond codimension five,* J. Math. Phys. **51**, 023503, Copyright 2010, The American Institute of Physics.

- Aazami, A. B., Rabin, J. M., and Petters, A. O., *Orbifolds, the A, D, E family of caustic singularities, and gravitational lensing,* J. Math. Phys. **52**, 022501, Copyright 2011, The American Institute of Physics.

  This chapter may be downloaded for personal use only.

Chapter 4:

- Aazami, A. B., Keeton, C. R., and Petters, A. O., *Lensing by Kerr black holes. I. General lens equation and magnification formula,* submitted to J. Math. Phys., Copyright 2011, The American Institute of Physics.

Chapter 5:

- Aazami, A. B., Keeton, C. R., and Petters, A. O., *Lensing by Kerr black holes. II. Analytical study of quasi-equatorial lensing observables,* submitted to J. Math. Phys., Copyright 2011, The American Institute of Physics.

2

Magnification Theorem for Higher-Order Caustic Singularities

2.1 Introduction

One of the key signatures of gravitational lensing is the occurrence of multiple images of lensed sources. The magnifications of the images in turn are also known to obey certain relations. One of the simplest examples of a magnification relation is that due to a single point-mass lens, where the two images of the source have signed magnifications that sum to unity: $\mu_1 + \mu_2 = 1$ (e.g., Petters et al. (2001), p. 191). Witt and Mao (1995) generalized this result to a two point-mass lens. They showed that when the source lies inside the caustic curve, a region which gives rise to five lensed images, the sum of the signed magnifications of these images is also unity: $\sum_i \mu_i = 1$, where μ_i is the signed magnification of image i. This result holds independently of the lens's configuration (in this case, the mass of the point-masses and their positions); it is also true for any source position, so long as the source lies inside the caustic (the region that gives rise to the largest number of images). Further examples of magnification relations, involving other families of lens models (N point-masses, el-

liptical power-law galaxies, etc.), subsequently followed in Rhie (1997), Dalal (1998), Witt and Mao (2000), Dalal and Rabin (2001), and Hunter and Evans (2001). More recently, Werner (2007, 2009) has proposed the application of Lefschetz fixed point theory to a subset of these magnification relations.

Although the above relations are "global" in that they involve all the images of a given source, they are not *universal* because the relations depend on the specific class of lens model used. However, it is well-known that for a source near a fold or cusp caustic, the resulting images close to the critical curve are close doublets and triplets whose signed magnifications always sum to zero (e.g., Blandford and Narayan (1986), Schneider and Weiss (1992), Zakharov (1995)):

$$\begin{aligned} \mu_1 + \mu_2 &= 0 \text{ (fold)} , \\ \mu_1 + \mu_2 + \mu_3 &= 0 \text{ (cusp)} . \end{aligned}$$

These magnification relations (also known as magnification invariants) are "local" and universal. Their locality means that they apply to a subset of the total number of images produced, namely, a close doublet for the fold and close triplet for the cusp, which requires the source to be near the fold and cusp caustics, respectively. Their universality follows from the fact that the relations hold for a generic family of lens models. In addition, the magnification relations for folds and cusps have been shown to provide powerful diagnostic tools for detecting dark substructure on galactic scales using quadruple lensed images of quasars (e.g., Mao and Schneider (1997), Keeton et al. (2003, 2005)).

The aim of this chapter and the next is to show that invariants of the following form also hold universally for lensing maps and general mappings with higher-order caustic singularities:

$$\sum_i \mu_i = 0 .$$

In particular, it is shown that such invariants occur not only for folds and cusps, but also for lensing maps with *elliptic umbilic* and *hyperbolic umbilic* caustics, and for general mappings exhibiting *any* caustic appearing in Vladimir Arnold's A, D, E classification of caustic singularities. As an application, we use the hyperbolic umbilic to show how such magnification relations can be used for substructure studies of four-image lens galaxies. Before stating and proving the main theorem (Theorem 1 in Section 2.3), we begin by reviewing the necessary lensing and singular-theoretic terminologies.

2.2 Basic Concepts

2.2.1 Lensing Theory

The spacetime geometry for gravitational lensing is treated as a perturbation of a Friedmann universe by a "weak field" spacetime. To that end, we regard a gravitational lens as being localized in a very small portion of the sky. Furthermore, we assume that gravity is "weak", so that near the lens it can be described by a Newtonian potential. We also suppose that the lens is static. Respecting these assumptions, the spacetime metric is given by

$$\mathbf{g}_{GL} = -\left(1+\frac{2\phi}{c^2}\right)c^2 d\tau^2 + a(\tau)^2\left(1-\frac{2\phi}{c^2}\right)\left(\frac{dR^2}{1-kR^2} + R^2\left(d\theta^2+\sin^2\theta\, d\varphi^2\right)\right) \ ,$$

where τ is cosmic time, ϕ the time-independent Newtonian potential of the perturbation caused by the lens, k is the curvature constant, and (R, θ, φ) are the coordinates in space. Here terms of order greater than $1/c^2$ are ignored in any calculation involving ϕ.

The above metric is used to derive the time delay function $T_{\mathbf{y}} : L \longrightarrow \mathbb{R}$, which for a single lens plane is given by

$$T_{\mathbf{y}}(\mathbf{x}) = \frac{1}{2}|\mathbf{x}-\mathbf{y}|^2 - \psi(\mathbf{x}) \ ,$$

where $\mathbf{y} = (s_1, s_2) \in S$ is the position of the source on the light source plane $S = \mathbb{R}^2$, $\mathbf{x} = (u, v) \in L$ is the impact position of a light ray on the lens plane $L \subseteq \mathbb{R}^2$, and $\psi : L \longrightarrow \mathbb{R}$ is the gravitational lens potential. As its name suggests, the time delay function gives the time delay of a lensed light ray emitted from a source in S, relative to the arrival time of a light ray emitted from the same source in the absence of lensing. Fermat's principle yields that light rays emitted from a source that reach an observer are realized as critical points of the time delay function. In other words, a *lensed image* of a light source at $\mathbf{y}$ is a solution $\mathbf{x} \in L$ of the equation $(\operatorname{grad} T_{\mathbf{y}})(\mathbf{x}) = \mathbf{0}$, where the gradient is taken with respect to $\mathbf{x}$. When there is no confusion with the mathematical image of a point, we shall follow common practice and sometimes call a lensed image simply an *image*.

The time delay function also induces a *lensing map* $\boldsymbol{\eta} : L \longrightarrow S$, which is defined by

$$\mathbf{x} \longmapsto \boldsymbol{\eta}(\mathbf{x}) = \mathbf{x} - (\operatorname{grad} \psi)(\mathbf{x}) \ .$$

We call $\boldsymbol{\eta}(\mathbf{x}) = \mathbf{y}$ the *lens equation*. Note that $\mathbf{x} \in L$ is a solution of the lens equation if and only if it is a lensed image because $(\operatorname{grad} T_{\mathbf{y}})(\mathbf{x}) = \boldsymbol{\eta}(\mathbf{x}) - \mathbf{y}$. Critical points of the lensing map $\boldsymbol{\eta}$ are those $\mathbf{x} \in L$ for which $\det(\operatorname{Jac} \boldsymbol{\eta})(\mathbf{x}) = 0$. Generically, the locus of critical points of the lensing map form curves called *critical curves*. The value $\boldsymbol{\eta}(\mathbf{x})$ of a critical point $\mathbf{x}$ under $\boldsymbol{\eta}$ is called a *caustic point*. These typically form curves, but could be isolated points. Examples of caustics can be found in Petters et al. (2001). For a generic lensing scenario, the number of lensed images of a given source can change (by ± 2 for generic crossings) if and only if the source crosses a caustic. The *signed magnification* of a lensed image $\mathbf{x} \in L$ of a light source at $\mathbf{y} = \boldsymbol{\eta}(\mathbf{x}) \in S$ is given by

$$\mu(\mathbf{x}) = \frac{1}{\det(\operatorname{Jac} \boldsymbol{\eta})(\mathbf{x})} \ . \tag{2.1}$$

Considering the graph of the time delay function, its principal curvatures coincide with the eigenvalues of $\mathrm{Hess}\, T_{\mathbf{y}}(\mathbf{x})$. In addition, its Gaussian curvature at $(\mathbf{x}, T_{\mathbf{y}}(\mathbf{x}))$ equals $\det(\mathrm{Hess}\, T_{\mathbf{y}})(\mathbf{x})$. In other words, the magnification of an image $\mathbf{x}$ can be expressed as

$$\mu(\mathbf{x}) = \frac{1}{\mathrm{Gauss}(\mathbf{x}, T_{\mathbf{y}}(\mathbf{x}))}\ , \tag{2.2}$$

where $\mathbf{y} = \boldsymbol{\eta}(\mathbf{x})$, $\mathrm{Gauss}(\mathbf{x}, T_{\mathbf{y}}(\mathbf{x}))$ is the Gaussian curvature of the graph of $T_{\mathbf{y}}$ at the point $(\mathbf{x}, T_{\mathbf{y}}(\mathbf{x}))$, and where we have used the fact that $\det(\mathrm{Jac}\, \boldsymbol{\eta}) = \det(\mathrm{Hess}\, \mathrm{T}_{\mathbf{y}})$ for single plane lensing. Therefore, the magnification relations are also *geometric* invariants involving the Gaussian curvature of the graph of $T_{\mathbf{y}}$ at its critical points. Readers are referred to Petters et al. (2001), Chapter 6, for a full treatment of these aspects of lensing.

2.2.2 Higher-Order Caustic Singularities in Lensing

This section briefly reviews those aspects of the theory of singularities that will be needed for our main theorem. It is also worth noting that the terms "universal" and "generic" will be used often. Formally, a property is called *generic* or *universal* if it holds for an open, dense subset of mappings in the given space of mappings. Elements of the open, dense subset are then referred to as being *generic* (or *universal).* See Petters et al. (2001), Chapter 8 for a discussion of genericity.

We saw in the previous section that the time delay function $T_{\mathbf{y}}(\mathbf{x})$, which can be viewed as a two-parameter family of functions with parameter $\mathbf{y}$, gives rise to the lensing map $\boldsymbol{\eta} : L \longrightarrow S$. The set of critical points of $\boldsymbol{\eta}$ consists of all $\mathbf{x} \in L$ such that $\det(\mathrm{Jac}\, \boldsymbol{\eta})(\mathbf{x}) = 0$. In this two-dimensional setting, a generic lensing map will have only two types of generic critical points: folds and cusps (see Petters et al. (2001), Chapter 8). The fold critical points map over to caustic arcs that abut isolated cusp caustic points.

Table 2.1: For the two caustic singularities listed, the second column shows the corresponding universal local forms of the smooth three-parameter family of time delay functions $T_{c,\mathbf{s}}$, along with their one-parameter family of lensing maps $\boldsymbol{\eta}_c$. The parameter c will represent some physical input, such as the source redshift. For a derivation, see Schneider et al. (1992), Chapter 6.

Elliptic umbilic (D_4^-)	$T_{c,\mathbf{s}}(x_1,x_2) = \frac{1}{2}\mathbf{s}^2 - \mathbf{x}\cdot\mathbf{s} + \frac{1}{3}x_1^3 - x_1x_2^2 + 2cx_2^2$ $\boldsymbol{\eta}_c(x_1,x_2) = \left(x_1^2 - x_2^2\ ,\ -2x_1x_2 + 4cx_2\right)$
Hyperbolic umbilic (D_4^+)	$T_{c,\mathbf{s}}(x_1,x_2) = \frac{1}{2}\mathbf{s}^2 - \mathbf{x}\cdot\mathbf{s} + \frac{1}{3}(x_1^3 + x_2^3) + 2cx_1x_2$ $\boldsymbol{\eta}_c(x_1,x_2) = \left(x_1^2 + 2cx_2\ ,\ x_2^2 + 2cx_1\right)$

Now, let $T_{c,\mathbf{y}}(\mathbf{x})$ denote a family of time delay functions parametrized by the source position $\mathbf{y}$ and $c \in \mathbb{R}$. In the context of gravitational lensing, the parameter c may denote external shear, core radius, redshift, or some other physical input. The three-parameter family $T_{c,\mathbf{y}}(\mathbf{x})$ gives rise to a one parameter family of lensing maps $\eta_{\mathbf{c}}$. Varying c causes the caustic curves in the light source plane S to evolve with c. This traces out a caustic surface, called a *big caustic*, in the three-dimensional space $\mathbb{R} \times \mathbb{R}^2 = \{(c, \mathbf{y})\}$; see Schneider et al. (1992), Chapter 6. Beyond folds and cusps, these surfaces form higher-order caustics that are classified into three *universal* or *generic* types for locally stable families $\eta_{\mathbf{c}}$, namely, *swallowtails, elliptic umbilics*, and *hyperbolic umbilics* (e.g., Petters et al. (2001), Chapter 9). Generic c-slices of these big caustics also yield *caustic metamorphoses*.

For the three-parameter family $T_{c,\mathbf{y}}(\mathbf{x})$ of time delay functions, the universal *quantitative* form of the lensing map can be derived locally using *rigid* coordinate transformations and Taylor expansions, along appropriate constraint equations for the caustics (see Schneider et al. (1992), Chapter 6). Table 2.1 summarizes the quantitative forms of $\boldsymbol{\eta}_c$ for the elliptic umbilic and hyperbolic umbilic critical points. Observe that the elliptic and hyperbolic umbilics for $T_{c,\mathbf{y}}$ (or $\boldsymbol{\eta}_c$) do not depend on the lens potential, apart perhaps from c in the event that c is a lens parameter.

2.2.3 Caustic Singularities of the A, D, E family

We can also consider general mappings. Consider a smooth k-parameter family $F_{\mathbf{c},\mathbf{s}}(\mathbf{x})$ of functions on an open subset of $\mathbb{R}^2$ that induces a smooth $(k-2)$-parameter family of mappings $\mathbf{f}_{\mathbf{c}}(\mathbf{x})$ between planes ($k \geqslant 2$). One uses $F_{\mathbf{c},\mathbf{s}}$ to construct a *Lagrangian submanifold* that is projected into the space $\{\mathbf{c}, \mathbf{s}\} = \mathbb{R}^{k-2} \times \mathbb{R}^2$. The caustics of $\mathbf{f}_{\mathbf{c}}$ will then be the critical values of the projection (e.g., Golubitsky and Guillemin (1973), Majthay (1985), Castrigiano and Hayes (2004), and Petters et al. (2001), pp. 276–286). These projections are called *Lagrangian maps*, and they are differentiably equivalent to $\mathbf{f}_{\mathbf{c}}$. As mentioned in Chapter 1, Arnold classified all stable simple Lagrangian map-germs of n-dimensional Lagrangian submanifolds by their generating family $F_{\mathbf{c},\mathbf{s}}$ (Arnold (1973), Arnold et al. (1985), pp. 330–331, and Petters et al. (2001), p. 282). In the process he found a connection between his classification and the Coxeter-Dynkin diagrams of the simple Lie algebras of types A_n $(n \geqslant 2), D_n$ $(n \geqslant 4), E_6, E_7, E_8$. This classification is shown in Table 2.2. (The classification of the elementary catastrophes, for codimension less than 5, was determined by René Thom in the 1960s.)

The $\mathbf{f}_{\mathbf{c}}$ shown in Table 2.2 are obtained from their corresponding $F_{\mathbf{c},\mathbf{s}}$ by taking its gradient with respect to $\mathbf{x}$ and setting it equal to zero: $\text{grad}(F_{\mathbf{c},\mathbf{s}})(\mathbf{x}) = 0$. This equation is then rewritten in the form $\mathbf{f}_{\mathbf{c}}(\mathbf{x}) = \mathbf{s}$. We call $\mathbf{x} \in \mathbb{R}^2$ a *pre-image* of the *target point* $\mathbf{s} \in \mathbb{R}^2$ if $\mathbf{f}_{\mathbf{c}}(\mathbf{x}) = \mathbf{s}$. Equivalently, this will be the case if and only if $\mathbf{x}$ is a critical point of $F_{\mathbf{c},\mathbf{s}}$ (relative to a gradient in $\mathbf{x}$). Next, we define the *magnification* $\mathfrak{M}(\mathbf{x}; \mathbf{s})$ at a critical point $\mathbf{x}$ of the family $F_{\mathbf{c},\mathbf{s}}$ by the reciprocal of the Gaussian curvature at the point $(\mathbf{x}, F_{\mathbf{c},\mathbf{s}}(\mathbf{x}_i))$ in the graph of $F_{\mathbf{c},\mathbf{s}}$:

$$\mathfrak{M}(\mathbf{x}; \mathbf{s}) \equiv \frac{1}{\text{Gauss}(\mathbf{x}, F_{\mathbf{c},\mathbf{s}}(\mathbf{x}))}.$$

Again, this makes it clear that magnification invariants are *geometric* invariants. In

Table 2.2: For each type of Coxeter-Dynkin diagram listed, indexed by n, the second column shows the corresponding universal local forms of the smooth $(n-1)$-parameter family of general functions $F_{\mathbf{c},\mathbf{s}}$, along with their $(n-3)$-parameter family of induced general maps $\mathbf{f_c}$ between planes. This classification is due to Arnold (1973).

$A_n \quad (n \geqslant 2)$	$F_{\mathbf{c},\mathbf{s}}(x,y) = \pm x^{n+1} \pm y^2 + c_{n-1}x^{n-1} + \cdots + c_3x^3 + s_2x^2 - s_1x \pm s_2y$ $\mathbf{f_c}(x,y) = \left(\pm(n+1)x^n + (n-1)c_{n-1}x^{n-2} + \cdots + 3c_3x^2 - 4yx \ , \ \mp 2y\right)$
$D_n \quad (n \geqslant 4)$	$F_{\mathbf{c},\mathbf{s}}(x,y) = x^2y \pm y^{n-1} + c_{n-2}y^{n-2} + \cdots + c_2y^2 - s_2y - s_1x$ $\mathbf{f_c}(x,y) = \left(2xy \ , \ x^2 \pm (n-1)y^{n-2} + (n-2)c_{n-2}y^{n-3} + \cdots + 2c_2y\right)$
E_6	$F_{\mathbf{c},\mathbf{s}}(x,y) = x^3 \pm y^4 + c_3xy^2 + c_2y^2 + c_1xy - s_2y - s_1x$ $\mathbf{f_c}(x,y) = \left(3x^2 + c_3y^2 + c_1y \ , \ \pm 4y^3 + 2c_3xy + 2c_2y + c_1x\right)$
E_7	$F_{\mathbf{c},\mathbf{s}}(x,y) = x^3 + xy^3 + c_4y^4 + c_3y^3 + c_2y^2 + c_1xy - s_2y - s_1x$ $\mathbf{f_c}(x,y) = \left(3x^2 + y^3 + c_1y \ , \ 3xy^2 + 4c_4y^3 + 3c_3y^2 + 2c_2y + c_1x\right)$
E_8	$F_{\mathbf{c},\mathbf{s}}(x,y) = x^3 + y^5 + c_5xy^3 + c_4xy^2 + c_3y^3 + c_2y^2 + c_1xy - s_2y - s_1x$ $\mathbf{f_c}(x,y) = \left(3x^2 + c_5y^3 + c_4y^2 + c_1y \ , \ 5y^4 + 3c_5xy^2 + 2c_4xy + 3c_3y^2 + 2c_2y + c_1x\right)$

addition, since the Gaussian curvature at the point $(\mathbf{x}_i, F_{c,\mathbf{s}}(\mathbf{x}_i))$ in the graph of $F_{c,\mathbf{s}}$ is given by

$$\mathrm{Gauss}(\mathbf{x}_i, F_{c,\mathbf{s}}(\mathbf{x}_i)) = \frac{\det(\mathrm{Hess}\, F_{c,\mathbf{s}})(\mathbf{x}_i)}{1 + |\operatorname{grad} F_{c,\mathbf{s}}(\mathbf{x}_i)|^2} \ ,$$

and since $(\mathbf{x}_i, F_{c,\mathbf{s}}(\mathbf{x}_i))$ is a critical point of the graph, we have that

$$\mathrm{Gauss}(\mathbf{x}_i, F_{\mathbf{c},\mathbf{s}}(\mathbf{x}_i)) = \det(\mathrm{Hess}\, F_{\mathbf{c},\mathbf{s}})(\mathbf{x}_i) \ .$$

Furthermore, a computation shows that for all the $F_{\mathbf{c},\mathbf{s}}$ shown in Table 2.2,

$$\det(\mathrm{Jac}\, \mathbf{f}_c) = \det(\mathrm{Hess}\, F_{c,\mathbf{s}}) \ .$$

Hence we can express the magnification in terms of $\mathbf{f_c}$:

$$\mathfrak{M}(\mathbf{x};\mathbf{s}) = \frac{1}{\det(\mathrm{Jac}\, \mathbf{f_c})(\mathbf{x})}. \tag{2.3}$$

If $\mathbf{s}$ has a total of n pre-images $\mathbf{x}_i$, then the *total signed magnification of* $\mathbf{s}$ is defined to be

$$\mathfrak{M}_{\rm tot}(\mathbf{s}) \equiv \sum_{i=1}^{n} \mathfrak{M}(\mathbf{x}_i; \mathbf{s}). \tag{2.4}$$

Finally, we define the notions of *critical points, caustic points,* and *big caustics* analogously to the lensing case.

In the theorem, the μ-magnification (resp., $\mathfrak{M}$-magnification) relations are *universal* or *generic* in the sense that they hold for an open, dense set of three-parameter families $T_{c,\mathbf{y}}$ (resp., general families $F_{c,\mathbf{s}}$) in the space of such families; see Petters et al. (2001), Chapters 7 and 8.

2.3 The Magnification Theorem

The discovery of this theorem grew out of the four published papers cited:

Theorem 1. *[Aazami and Petters (2009a,b, 2010); Aazami et al. (2011b)] For any of the universal, smooth* $(n-1)$*-parameter families of general functions* $F_{\mathbf{c},\mathbf{s}}$ *(or induced general mappings* $\mathbf{f}_{\mathbf{c}}$*) in Table 2.2, and for any non-caustic target point* $\mathbf{s}$ *in the indicated region, the following results hold for the magnification* $\mathfrak{M}_i \equiv \mathfrak{M}(\mathbf{x}_i; \mathbf{s})$*:*

1. A_n $(n \geqslant 2)$ *obeys the mag. relation in the n-image region:* $\sum_{i=1}^{n} \mathfrak{M}_i = 0$,
2. D_n $(n \geqslant 4)$ *obeys the mag. relation in the n-image region:* $\sum_{i=1}^{n} \mathfrak{M}_i = 0$,
3. E_6 *obeys the magnification relation in the six-image region:* $\sum_{i=1}^{6} \mathfrak{M}_i = 0$,
4. E_7 *obeys the magnification relation in the seven-image region:* $\sum_{i=1}^{7} \mathfrak{M}_i = 0$,
5. E_8 *obeys the magnification relation in the eight-image region:* $\sum_{i=1}^{8} \mathfrak{M}_i = 0$.

In addition, for the two smooth generic three-parameter families of time delay functions $T_{c,\mathbf{y}}$ (or induced lensing maps $\boldsymbol{\eta}_c$) in Table 2.3, and for any non-caustic target point $\mathbf{s}$ *in the indicated region, the following results hold for the magnification* $\mu_i \equiv \mu(\mathbf{x}_i; \mathbf{s})$*:*

1. D_4^- (Elliptic Umbilic) *obeys the magnification relation in four-image region:* $\mu_1 + \mu_2 + \mu_3 + \mu_4 = 0$.

2. D_4^+ (Hyperbolic Umbilic) *obeys the magnification relation in four-image region:* $\mu_1 + \mu_2 + \mu_3 + \mu_4 = 0$.

Remarks. The results of Theorem 1 actually apply even when the non-caustic point $\mathbf{s}$ is not in the maximum number of pre-images region. However, complex pre-images will appear, which are unphysical in gravitational lensing. Note that for $n \geqslant 6$ there are Lagrangian maps that cannot be approximated by stable Lagrangian map-germs Arnold (1973). As mentioned in Section 2.1, the fold (A_2) and cusp (A_3) magnification relations are known (Blandford and Narayan (1986), Schneider and Weiss (1992), Zakharov (1995)), but we restate them in the theorem for completeness.

2.4 Applications

Before discussing the applications, we recall that the magnification μ_i of a lensed image is the flux F_i of the image divided by the flux F_S of the unlensed source (e.g., Petters et al. (2001), pp. 82–85):

$$\mu_i = \pm \frac{F_i}{F_S} \ ,$$

where the "+" choice is for even index images (minima and maxima) and the "−" choice is for odd index images (saddles). Though F_i is an observable, the source's flux F_S is generally unknown. Consequently, the magnification μ_i is not directly

observable and so magnification sums $\sum_i \mu_i$ are also not observable. However, we can construct an observable by introducing the following quantity:

$$R \equiv \frac{\sum_i \mu_i}{\sum_i |\mu_i|} = \frac{\sum_i (\pm) F_i}{\sum_i F_i} \ , \tag{2.5}$$

where the $\pm$ choice is the same as above. This quantity is in terms of the observable image fluxes F_i and image signs, which can be determined for real systems Keeton et al. (2005, 2003).

Now, aside from their natural theoretical interest, the importance of magnification relations in gravitational lensing arises in their applications to detecting dark substructure in galaxies using "anomalous" flux ratios of multiply imaged quasars. The setting consists typically of four images of a quasar lensed by a foreground galaxy. The *smooth* mass density models used for the galaxy lens usually accurately reproduce the number and relative positions of the images, but fail to reproduce the image flux ratios. For the case of a cusp, where a close image triplet appears, Mao and Schneider (1997) showed that the cusp μ-magnification relation fails (i.e., deviates from zero) and argued that it does so since the *smoothness assumption* about the galaxy lens breaks down on the scale of the fold image doublet (this is not the only interpretation; see also Evans and Witt (2003); Congdon and Keeton (2005)). In other words, a violation of the cusp magnification relation in a real lens system may imply a violation of smoothness in the lens, which in turn invokes the presence of substructure or graininess in the galaxy lens on the scale of the image separation. Soon thereafter Metcalf and Madau (2001) and Chiba (2002) showed that dark matter was a plausible candidate for this substructure.

Keeton et al. (2003, 2005) then developed a rigorous theoretical framework showing how the fold and cusp μ-magnification relations provide a diagnostic for detecting substructure on galactic scales. Their analysis employs the R-quantity (2.5) for folds

and cusps:

$$R_{\rm fold} \equiv \frac{\mu_1 + \mu_2}{|\mu_1| + |\mu_2|} = \frac{F_1 - F_2}{F_1 + F_2} \ , \qquad\qquad R_{\rm cusp} \equiv \frac{\mu_1 + \mu_2 + \mu_3}{|\mu_1| + |\mu_2| + |\mu_3|} = \frac{F_1 - F_2 + F_3}{F_1 + F_2 + F_3} \ ,$$

where F_i is the observable flux of image i and image 2 has negative parity. For a source sufficiently close to a fold (resp., cusp) caustic, the images will have a close image pair (resp., close image triplet); see the close doublets and triplets in Figure 2.1(a,b,d,e). Theoretically, these images should have vanishing $R_{\rm fold}$ and $R_{\rm cusp}$ due to the fold and cusp magnification relations and so nontrivial deviations from zero would signal the presence of substructure. In Keeton et al. (2003, 2005), it was shown that 5 of the 12 fold-image systems and 3 of the 4 cusp-image ones showed evidence for substructure.

The study above would look at a multiple-image system and consider subsets of two and three images to analyze $R_{\rm fold}$ and $R_{\rm cusp}$, respectively. Such analyses are then "local" when more than three images occur since only two or three images are studied at a time. Theorem 1 generalizes the above R-quantities from folds and cusps to generic smooth lens systems that exhibit swallowtail, elliptic umbilic, and hyperbolic umbilic singularities. The R-quantities resulting from these higher-order singularities allow one to consider *four* images at a time and so are more global than the fold and cusp relations in terms of how many images are incorporated. The singularity that is most applicable to observed quadruple-images produced by the lensing of quasars is the hyperbolic umbilic (cf. Figure 2.1). The associated R-quantity is

$$R_{\rm h.u.} \equiv \frac{\mu_1 + \mu_2 + \mu_3 + \mu_4}{|\mu_1| + |\mu_2| + |\mu_3| + |\mu_4|} = \frac{F_1 - F_2 + F_3 - F_4}{F_1 + F_2 + F_3 + F_4} \ ,$$

where images 2 and 4 have negative parity.

We now illustrate the hyperbolic umbilic quantity $R_{\rm h.u.}$ using a well-known model for a galaxy lens, namely, a singular isothermal ellipsoid (SIE) lens. The SIE lens

potential and surface mass density are given respectively as follows:

$$\psi(r,\varphi) = rF(\varphi) - \frac{\gamma}{2}r^2\cos 2\varphi, \qquad \kappa(r,\varphi) = \frac{G(\varphi)}{2r},$$

where $F(\varphi)$ and $G(\varphi)$ satisfy $G(\varphi) = F(\varphi) + F''(\varphi)$ by Poisson's equation, and are given explicitly by

$$\begin{aligned} G(\varphi) &= \frac{R_{\rm ein}}{\sqrt{1-\varepsilon\cos 2\varphi}}\ , \\ F(\varphi) &= \frac{R_{\rm ein}}{\sqrt{2\varepsilon}}\left[\cos\varphi\tan^{-1}\left(\frac{\sqrt{2\varepsilon}\cos\varphi}{\sqrt{1-\varepsilon\cos 2\varphi}}\right) + \sin\varphi\tanh^{-1}\left(\frac{\sqrt{2\varepsilon}\sin\varphi}{\sqrt{1-\varepsilon\cos 2\varphi}}\right)\right], \end{aligned}$$

where $R_{\rm ein}$ is the angular Einstein ring radius. The parameter ε is related to the axis ratio q by $\varepsilon = (1-q^2)/(1+q^2)$, and should not be confused with the ellipticity $e = 1-q$. The cusp at $\varphi = 0$ is given by

$$\mathbf{y}_{\rm cusp} = \left(\frac{2\gamma F(0) + (1+\gamma)F''(0)}{1-\gamma}\,,\,0\right)\ . \tag{2.6}$$

Using the *Gravlens* software by Keeton (2001), we now solve the SIE lens equation for sources on the positive horizontal axis in the four-image region of the light source plane, and compute $R_{\rm h.u.}$. Let the SIE have ellipticity $e = 0.35$ and shear $\gamma = 0.05$ oriented along the horizontal axis; both of these values are observationally motivated Keeton et al. (2005, 2003). Figure 2.1(a,b,c) shows three important image configurations for the SIE: the fold, when the source lies close to a fold arc and produces a close pair of images about a critical curve; the cusp, when the source lies close to a cusp caustic and produces a close triplet of images about a critical curve; the cross-like configuration of four images, when the source sits nearer to the center of the astroid-shaped inner caustic curve. Figure 2.1(d,e,f) illustrates how the SIE image configurations are similar to those of the hyperbolic umbilic lensing map $\boldsymbol{\eta}_c$ given in Table 2.2.

We now look at the behavior of R_{fold}, R_{cusp}, and $R_{\text{h.u.}}$ for an SIE. Table 2.3 compares R_{fold} and $R_{\text{h.u.}}$ for a source approaching a fold arc diagonally from the center of the astroid-shaped inner caustic; see Figure 2.1(a). The fold point where the diagonal intersects the fold arc is at

$$\mathbf{y}_{\text{fold}} \approx (0.14055R_{\text{ein}},\ 0.14055R_{\text{ein}}) \ .$$

As the source at $\mathbf{y}$ approaches $\mathbf{y}_{\text{fold}}$ along the diagonal, the values in Table 2.3 show that R_{fold} and $R_{\text{h.u.}}$ each approach the ideal value of 0, and that $R_{\text{h.u.}}$ approaches R_{fold} from *above*. The reason for this is as follows: From Figure 2.1(a) we see that there are two pairs of images in a hyperbolic umbilic configuration: the fold image doublet straddling the critical curve, and whose two images we denote by d_1, d_2, and the pair consisting of the outer two images, which we denote by o_1, o_2. The quantity $R_{\text{h.u.}}$ then becomes

$$R_{\text{h.u.}} = \frac{|\mu_{d_1}| - |\mu_{d_2}| + |\mu_{o_1}| - |\mu_{o_2}|}{|\mu_{d_1}| + |\mu_{d_2}| + |\mu_{o_1}| + |\mu_{o_2}|} \ .$$

As the source approaches $\mathbf{y}_{\text{fold}}$ along the diagonal, Table 2.3 shows that the quantities $|\mu_{d_1}| - |\mu_{d_2}|$ and $|\mu_{o_1}| - |\mu_{o_2}|$ stay roughly constant, though the individual magnifications vary. In addition, near the fold, we see that $|\mu_{d_1}| + |\mu_{d_2}|$ dominates $|\mu_{o_1}| + |\mu_{o_2}|$, causing the denominator of $R_{\text{h.u.}}$ to approach $|\mu_{d_1}| + |\mu_{d_2}|$, which is the denominator of R_{fold}. This leads to

$$R_{\text{h.u.}} \approx \frac{|\mu_{d_1}| - |\mu_{d_2}|}{|\mu_{d_1}| + |\mu_{d_2}|} + \frac{|\mu_{o_3}| - |\mu_{o_4}|}{|\mu_{d_1}| + |\mu_{d_2}|} \geqslant \frac{|\mu_{d_1}| - |\mu_{d_2}|}{|\mu_{d_1}| + |\mu_{d_2}|} = R_{\text{fold}} \ .$$

The net effect is that $R_{\text{h.u.}}$ approaches R_{fold} from above (at least for the path along the diagonal). Furthermore, since the quantity $|\mu_{d_1}| + |\mu_{d_2}|$ diverges, we see that both $R_{\text{h.u.}}$ and R_{fold} approach the magnification relation value of 0.

Table 2.4 compares $R_{\text{h.u.}}$ with R_{cusp} for a source approaching a cusp along the horizontal axis from the center of the astroid-shaped caustic curve; see Figure 2.1(b,c).

Table 2.3: The quantities $R_{\text{h.u.}}$ and R_{fold} for an SIE with $e = 0.35$ and $\gamma = 0.05$ oriented along the horizontal axis. The source approaches the fold point $\mathbf{y}_{\text{fold}} \approx (0.14055R_{\text{ein}},\ 0.14055R_{\text{ein}})$ diagonally from the center of the astroid-shaped inner caustic. The quantity $|\mu_{d_1}| - |\mu_{d_2}|$ is the difference in the magnifications of the images in the close doublet, while $|\mu_{o_1}| - |\mu_{o_2}|$ is the difference for the remaining two outer images; cf. Figure 2.1(a).

Source	R_{fold}	$R_{\text{h.u.}}$	$\lvert\mu_{d_1}\rvert - \lvert\mu_{d_2}\rvert$	$\lvert\mu_{o_1}\rvert - \lvert\mu_{o_2}\rvert$	$\lvert\mu_{d_1}\rvert + \lvert\mu_{d_2}\rvert$	$\lvert\mu_{o_1}\rvert + \lvert\mu_{o_2}\rvert$
$(0.10R_{\text{ein}}, 0.10R_{\text{ein}})$	0.14	0.19	1.22	1.21	8.51	4.35
$(0.11R_{\text{ein}}, 0.11R_{\text{ein}})$	0.13	0.18	1.22	1.22	9.64	4.28
$(0.12R_{\text{ein}}, 0.12R_{\text{ein}})$	0.11	0.15	1.22	1.22	11.55	4.21
$(0.13R_{\text{ein}}, 0.13R_{\text{ein}})$	0.08	0.12	1.22	1.22	15.83	4.15
$(0.14R_{\text{ein}}, 0.14R_{\text{ein}})$	0.02	0.04	1.21	1.23	65.17	4.081
$(0.1405R_{\text{ein}}, 0.1405R_{\text{ein}})$	0.008	0.015	1.21	1.23	156.80	4.078

For these values of the ellipticity and shear, we see from (2.6) that the two cusps on the horizontal axis are located at

$$\mathbf{y}^{\pm}_{\text{cusp}} \approx (\pm 0.48R_{\text{ein}}, 0)\ . \tag{2.7}$$

The table shows that as the source approaches $\mathbf{y}^{+}_{\text{cusp}}$ along the horizontal axis, the quantity $R_{\text{h.u.}}$ approaches R_{fold} from *below*. In other words, $R_{\text{h.u.}}$ is smaller than R_{fold}. To see why this happens, consider the triplet of sub-images in Figure 2.1(b), which we denote by t_1, t_2, t_3, and the extra outer image, denote by o. With this notation,

$$R_{\text{h.u.}} = \frac{|\mu_{t_1}| - |\mu_{t_2}| + |\mu_{t_3}| - |\mu_o|}{|\mu_{t_1}| + |\mu_{t_2}| + |\mu_{t_3}| + |\mu_o|}\ .$$

As the source approaches $\mathbf{y}^{+}_{\text{cusp}}$ along the horizontal axis, the values in Table 2.4 of the cusp relation $|\mu_{t_1}| - |\mu_{t_2}| + |\mu_{t_3}|$ are *positive*. The inclusion of the outer, negative parity magnification μ_o then subtracts from that positive value, yielding

$$(|\mu_{t_1}| - |\mu_{t_2}| + |\mu_{t_3}|) - |\mu_o| \leqslant |\mu_{t_1}| - |\mu_{t_2}| + |\mu_{t_3}|\ ,$$

which implies that

$$R_{\text{h.u.}} \leqslant R_{\text{cusp}}\ .$$

Furthermore, Table 2.4 shows that $|\mu_o|$ grows fainter faster than the value of the signed magnification of the triplet, which yields

$$|\mu_{t_1}| + |\mu_{t_2}| + |\mu_{t_3}| \ \gg |\mu_o|\ .$$

Table 2.4: The quantities $R_{\text{h.u.}}$ and R_{cusp} for an SIE with $e = 0.35$ and $\gamma = 0.05$ oriented along the horizontal axis. The source approaches the cusp point $\mathbf{y}^{+}_{\text{cusp}} \approx (0.48R_{\text{ein}}, 0)$ along the horizontal axis from the center of the astroid-shaped inner caustic. The quantity $|\mu_{t_1}| - |\mu_{t_2}| + |\mu_{t_3}|$ is the signed magnification sum of the cusp triplet, while $|\mu_o|$ is the magnification of the outer image; see Figure 2.1(b).

Source	R_{cusp}	$R_{\text{h.u.}}$	$\lvert\mu_{t_1}\rvert + \lvert\mu_{t_2}\rvert + \lvert\mu_{t_3}\rvert$	$\lvert\mu_{t_1}\rvert - \lvert\mu_{t_2}\rvert + \lvert\mu_{t_3}\rvert$	$\lvert\mu_{o_1}\rvert$
$(0\,,0)$ (center)	0.52	0.23	8.49	4.46	2.02
$(0.10R_{\text{ein}}\,,0)$	0.41	0.22	9.58	3.94	1.49
$(0.15R_{\text{ein}}\,,0)$	0.36	0.21	10.57	3.76	1.29
$(0.20R_{\text{ein}}\,,0)$	0.30	0.19	12.02	3.61	1.12
$(0.25R_{\text{ein}}\,,0)$	0.25	0.17	14.20	3.48	0.98
$(0.30R_{\text{ein}}\,,0)$	0.19	0.14	17.71	3.38	0.85
$(0.35R_{\text{ein}}\,,0)$	0.14	0.10	24.10	3.30	0.74
$(0.40R_{\text{ein}}\,,0)$	0.08	0.07	39.02	3.23	0.64
$(0.45R_{\text{ein}}\,,0)$	0.03	0.02	111.5	3.18	0.55

In other words, as the source approaches $\mathbf{y}^{+}_{\text{cusp}}$ along the horizontal axis, the contribution of the outer image $|\mu_o|$ to the numerator and denominator of $R_{\text{h.u.}}$ becomes negligible. The net effect, at least for the given horizontal axis approach, is that $R_{\text{h.u.}}$ and R_{cusp} converge, with $R_{\text{h.u.}}$ approaching R_{cusp} from below as they both approach the magnification relation value of 0.

Finally, though $R_{\text{h.u.}}$ can approximate R_{fold} and R_{cusp} for fold image doublets and cusp image triplets, resp., *the hyperbolic umbilic magnification relation has a more global reach* in terms of the number of images included. This is because $R_{\text{h.u.}}$ also applies directly to image configurations that are neither close doublets nor triplets; e.g., to cross-like configurations as in Figure 2.1(c). For instance, it was determined in Keeton et al. (2003) that to satisfy the relation $|R_{\text{cusp}}| < 0.1$ at 99% confidence, the opening angle must be $\theta \lesssim 30^{\circ}$. By opening angle we mean the angle of the polygon spanned by the three images in the cusp triplet, measured from the position of the lens galaxy, which in our case, is centered at the origin in the lens plane. For the SIE cross-like configuration shown in Figure 2.1(c), the opening angle is $\theta \approx 140^{\circ}$; a perfect cross, which would be the case if the source were centered inside the astroid-shaped inner caustic, has $\theta = 180^{\circ}$. In other words, to satisfy the cusp relation reasonably well, the cusp triplet must be quite tight as, for example, in the SIE cusp triplet shown in Figure 2.1(b). By contrast, the quantity $R_{\text{h.u.}}$ applies even for values $\theta \gg 30^{\circ}$. (In Table 2.4 note how $R_{\text{h.u.}}$ is smaller than R_{cusp} for source

positions closer to the center $(0, 0)$, which yield more cross-like image configurations.)

A more detailed study of the properties of $R_{\rm h.u.}$ would involve a Monte Carlo analysis similar to that employed in Keeton et al. (2005, 2003) to study $R_{\rm cusp}$ and $R_{\rm fold}$.

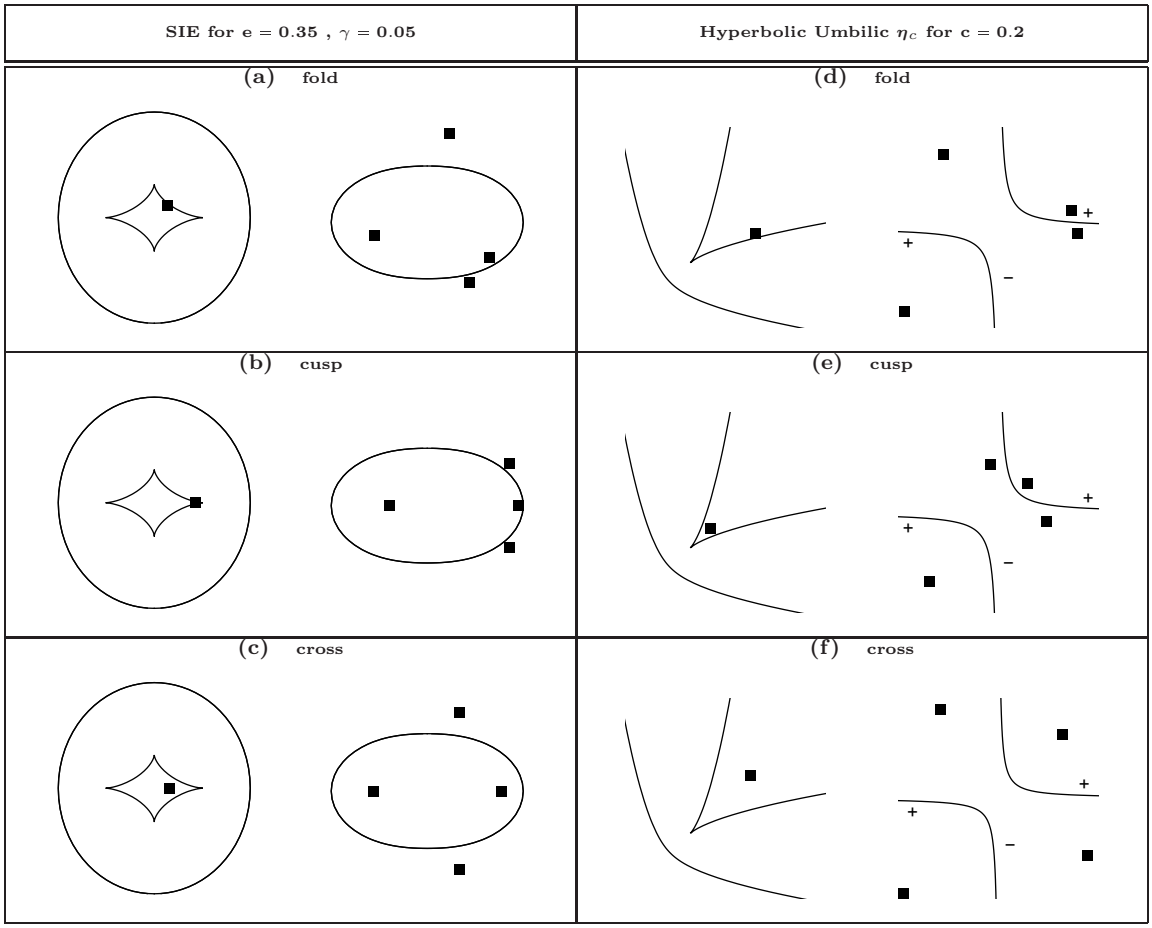

FIGURE 2.1: The first column shows fold, cusp, and cross-like configurations due to an SIE with ellipticity $e = 0.35$ and shear $\gamma = 0.05$ oriented along the horizontal axis (Panels a,b,c). The second column shows the same configurations due to the hyperbolic umbilic lensing map $\boldsymbol{\eta}_c$ in Table 2.2 with parameter value $c = 0.2$ (Panels d,e,f). In each panel, the sub-figure on the left depicts the caustic curves with source position (solid box) in the light source plane, while the sub-figure on the right shows the critical curves with image positions (solid boxes) in the lens plane. For the hyperbolic umbilic, image parities have been indicated through $\pm$ in the given regions. Note that the cross-like configuration shown for the SIE is not a perfect cross, which would be the case if the source were centered inside the astroid-shaped inner caustic. Also, for the SIE fold and cusp configurations, the source is actually located inside (rather than over) the cusped curve of the astroid.

3

Proof of Magnification Theorem

3.1 An Algebraic Proposition

3.1.1 A Recursive Relation for Coefficients of Coset Polynomials

We will make repeated use of the Euler trace formula to prove Theorem 1, by first establishing a proposition about polynomials that will yield the Euler trace formula as a corollary.

We begin with some notation. Let $\mathbb{C}[x]$ be the ring of polynomials over $\mathbb{C}$ and consider a polynomial

$$\varphi(x) = a_n x^n + \cdots + a_1 x + a_0 \in \mathbb{C}[x] \ .$$

Suppose that the n zeros $x_1, \ldots, x_n$ pf $\varphi(x)$ are distinct (generically, the roots of a polynomial are distinct) and let $\varphi'(x)$ be the derivative of $\varphi(x)$. Also, let $R \subset \mathbb{C}(x)$ denote the subring of rational functions that are defined at the roots x_i of $\varphi(x)$:

$$R = \left\{ \frac{p(x)}{q(x)} \ : \ p(x), q(x) \in \mathbb{C}[x] \text{ and } q(x_i) \neq 0 \text{ for all roots } x_i \right\} \ .$$

Let $(\varphi(x))$ be the ideal in R generated by $\varphi(x)$ and denote the cosets of the quotient ring $R/(\varphi(x))$ using an overbar. Below are two basic results that we prove in

Section 3.1.2 below for the convenience of the reader:

- Members of the same coset in $R/(\varphi(x))$ agree on the roots x_i of $\varphi(x)$, that is, if $h_1(x)$ and $h_2(x)$ belong to the same coset, then $h_1(x_i) = h_2(x_i)$.
- Every rational function $h(x) \in R$ has in its coset $\overline{h(x)} \in R/(\varphi(x))$ a unique polynomial representative $h_*(x)$ of degree less than n.

Proposition 2. *Consider any polynomial $\varphi(x) = a_n x^n + \cdots + a_1 x + a_0 \in \mathbb{C}[x]$ with distinct roots and any rational function $h(x) \in R$. Let*

$$h_*(x) = c_{n-1}x^{n-1} + \cdots + c_1 x + c_0$$

be the unique polynomial representative of the coset $\overline{h(x)} \in R/(\varphi(x))$ and let

$$r(x) = b_{n-1}x^{n-1} + \cdots + b_1 x + b_0$$

be the unique polynomial representative of the coset $\overline{\varphi'(x)h(x)} \in R/(\varphi(x))$. Then the coefficients of $r(x)$ are given in terms of the coefficients of $h_*(x)$ and $\varphi(x)$ through the following recursive relation:

$$b_{n-i} = c_{n-1}b_{n-i,n-1} + \cdots + c_1 b_{n-i,1} + c_0 b_{n-i,0} \qquad i = 1, \ldots, n \ , \tag{3.1}$$

with

$$\begin{cases} b_{n-i,0} = (n-(i-1))\, a_{n-(i-1)} \ , & i = 1, \ldots, n \ , \\ b_{n-i,k} = -\dfrac{a_{n-i}}{a_n}\, b_{n-1,k-1} + b_{n-(i+1),k-1} \ , & i = 1, \ldots, n \ , \quad k = 1, \ldots, n-1 \ , \end{cases} \tag{3.2}$$

where $b_{-1,k-1} \equiv 0$.

By Proposition 2, if $r_k(x)$ is the unique polynomial representative of the coset $\overline{\varphi'(x)x^k} \in R/(\varphi(x))$, then

$$r_k(x) = b_{n-1,k}x^{n-1} + \cdots + b_{1,k}x + b_{0,k} \ , \qquad k = 0, 1, \ldots, n-1 \ , \tag{3.3}$$

where its coefficients are given in terms of the coefficients of $\varphi(x)$ through (3.2).

Corollary 3. *Assume the hypotheses and notation of Proposition 2. Given the distinct roots $x_1, \ldots, x_n$ of $\varphi(x)$, the Newton sums $N_k \equiv \sum_{i=1}^{n} (x_i)^k$ satisfy:*

$$N_k = \frac{b_{n-1,k}}{a_n} \ , \qquad\qquad k = 0, 1, \ldots, n-1 \ . \tag{3.4}$$

In other words, the quantity $a_n N_k$ equals the $(n-1)$st coefficient of the unique polynomial representative (3.3) of the coset $\overline{\varphi'(x)x^k}$ in $R/(\varphi(x))$.

Proof. Note that for $k = 0$, eqn. (3.2) in Proposition 2 yields

$$b_{n-1,0} = na_n = N_0 a_n \ .$$

For $1 \leqslant k \leqslant n-1$, there is a known recursive relation for N_k, in terms of $N_1, \ldots, N_{k-1}$; see, e.g., Barbeau (2003), p. 203. It is given by

$$ka_{n-k} + a_{n-k+1}N_1 + a_{n-k+2}N_2 + \cdots + a_{n-1}N_{k-1} + a_n N_k = 0 \ . \tag{3.5}$$

We proceed by induction on k for $1 \leqslant k \leqslant n-1$. For $k = 1$, eqn. (3.5) implies $N_1 = -\frac{a_{n-1}}{a_n}$, while eqn. (3.2) gives $b_{n-1,1} = -a_{n-1} = a_n N_1$, which agrees with eqn. (3.4). Now assume that $b_{n-1,j} = a_n N_j$ for $j = 1, \ldots, k-1$. To establish the result

for $j = k$, we shall repeatedly apply Proposition 2:

$$\begin{aligned}
b_{n-1,k} &= -\frac{a_{n-1}}{a_n}\, b_{n-1,k-1} + b_{n-2,k-1} \\
&= -\frac{a_{n-1}}{a_n}\, b_{n-1,k-1} + \left[-\frac{a_{n-2}}{a_n}\, b_{n-1,k-2} + b_{n-3,k-2} \right] \\
&= -\frac{a_{n-1}}{a_n}\, b_{n-1,k-1} - \frac{a_{n-2}}{a_n}\, b_{n-1,k-2} + \left[-\frac{a_{n-3}}{a_n}\, b_{n-1,k-3} + b_{n-4,k-3} \right] \\
&\vdots \\
&= -\frac{a_{n-1}}{a_n}\, b_{n-1,k-1} - \frac{a_{n-2}}{a_n}\, b_{n-1,k-2} - \frac{a_{n-3}}{a_n}\, b_{n-1,k-3} \\
&\qquad - \cdots - \frac{a_{n-(k-1)}}{a_n}\, b_{n-1,1} - \frac{a_{n-k}}{a_n} b_{n-1,0} + b_{n-(k+1),0} \ . \\
&= -\left(a_{n-1}N_{k-1} + a_{n-2}N_{k-2} + a_{n-3}N_{k-3} + \cdots + a_{n-(k-1)}N_1 + k a_{n-k} \right) \\
&= a_n N_k \ ,
\end{aligned}$$

where $b_{n-1,0} = n a_n$ and $b_{n-(k+1),0} = (n-k)a_{n-k}$ follow from eqn. (3.2) in Proposition 2, and the last equality is due to (3.5). $\square$

Corollary 4 (Euler Trace Formula)**.** *Assume the hypotheses and notation of Proposition 2. For any rational function $h(x) \in R$, the following holds:*

$$\sum_{i=1}^{n} h(x_i) = \frac{b_{n-1}}{a_n} \ , \tag{3.6}$$

where b_{n-1} is the $(n-1)$st coefficient of the unique polynomial representative $r(x)$ of the coset $\overline{\varphi'(x)\, h(x)} \in R/(\varphi(x))$ and a_n the nth coefficient of $\varphi(x)$.

Proof. Let $h_*(x)$ be the unique polynomial representative of the coset $\overline{h(x)} \in R/(\varphi(x))$. First note that, since $h(x)$ and $h_*(x)$ belong to the same coset, we have $h(x_i) = h_*(x_i)$. The Euler trace formula now proceeds from a simple application of

Propositon 2 and Corollary 3:

$$\begin{aligned}
\sum_{i=1}^{n} h(x_i) &= \sum_{i=1}^{n} h_*(x_i) = \sum_{i=1}^{n}\sum_{j=0}^{n-1} c_j \cdot (x_i)^j = \sum_{j=0}^{n-1} c_j \sum_{i=1}^{n} (x_i)^j = \sum_{j=0}^{n-1} c_j N_j \\
&= c_{n-1}N_{n-1} + \cdots + c_1 N_1 + c_0 N_0 \\
&= c_{n-1}\left(\frac{b_{n-1,n-1}}{a_n}\right) + \cdots + c_1\left(\frac{b_{n-1,1}}{a_n}\right) + c_0\left(\frac{b_{n-1,0}}{a_n}\right) \qquad \text{(by Cor. 3)} \\
&= \frac{c_{n-1}b_{n-1,n-1} + \cdots + c_1 b_{n-1,1} + c_0 b_{n-1,0}}{a_n} \\
&= \frac{b_{n-1}}{a_n} \cdot \qquad \text{(by Proposition 2)} \quad \square
\end{aligned}$$

Remark. Dalal and Rabin (2001) gave a different proof of the Euler trace formula, one employing residues.

3.1.2 Proof of Proposition 2

We begin with some preliminaries about quotient rings to make the proof more self-contained. Let $\mathbb{C}[x]$ be the ring of polynomials over $\mathbb{C}$ and let $\mathbb{C}(x)$ be the field of rational functions formed from quotients of polynomials in $\mathbb{C}[x]$. The n zeros $x_1, \ldots, x_n$ of $\varphi(x) = a_n x^n + \cdots + a_1 x + a_0 \in \mathbb{C}[x]$ are assumed to be distinct (generically, the roots of a polynomial are distinct). Let $(\varphi(x))$ denote the ideal in $\mathbb{C}[x]$ generated by $\varphi(x)$, and consider the quotient ring $\mathbb{C}[x]/(\varphi(x))$, whose cosets we denote by $\overline{g(x)}$. This quotient ring has two important properties:

- *Property 1:* If $\overline{g_1(x)} = \overline{g_2(x)}$, then by definition $g_1(x) - g_2(x) = h(x)\varphi(x)$ for some $h(x) \in \mathbb{C}[x]$, from which it follows that $g_1(x_i) = g_2(x_i)$ for all n roots x_i of $\varphi(x)$. Thus members of the same coset must agree on the roots of $\varphi(x)$, so that, in particular, $\sum_{i=1}^{n} g_1(x_i) = \sum_{i=1}^{n} g_2(x_i)$.

- *Property 2:* Each coset $\overline{g(x)}$ has a *unique* representative of degree at most $n-1$, as follows: by the division algorithm in $\mathbb{C}[x]$, there exist polynomials $q(x)$ and $r(x)$ such that

$$g(x) = q(x)\varphi(x) + r(x) \ ,$$

where deg $r <$ deg $\varphi = n$. Passing to the quotient ring $\mathbb{C}[x]/(\varphi(x))$, we see that $\overline{g(x)} = \overline{r(x)}$. Suppose now that there exists another polynomial $p(x)$ of degree less than n with $\overline{g(x)} = \overline{p(x)}$. Then $\overline{p(x)} = \overline{r(x)}$, so that

$$p(x) - r(x) = h(x)\varphi(x)$$

for some $h(x) \in \mathbb{C}[x]$. If $h(x) \not\equiv 0$, then deg $h\,\varphi \geqslant n$, while the degree of the left-hand side is less than n. We must therefore have $h(x) \equiv 0$ and $p(x) = r(x)$. We may thus represent every coset by its unique polynomial representative of degree less than n, which in turn implies that $\mathbb{C}[x]/(\varphi(x))$ is a vector space of dimension n, with basis $\left\{\overline{1}, \overline{x}, \overline{x^2} \ldots, \overline{x^{n-1}}\right\}$.

The next result will be used to show that Properties 1 and 2 also hold for a certain subset of rational functions in $\mathbb{C}(x)$ (see Claim 2 below).

Claim 1. Let $x_1, \ldots, x_n \in \mathbb{C}$ be distinct. Let $c_1, \ldots, c_n \in \mathbb{C}$, not necessarily distinct. Then there exists a unique polynomial $H(x) \in \mathbb{C}[x]$ with deg $h < n$ such that $H(x_i) = c_i$.

Proof (Claim 1). Induction on n. For $n = 1$, define $H(x) \equiv c_1$. Now assume that the result is true for $n-1$, and consider a set of n distinct complex numbers $x_1, \ldots, x_n$. By the induction hypothesis, there exists a polynomial $h(x) \in \mathbb{C}[x]$ with deg $h < n-1$ such that $h(x_i) = c_i$ for $i = 1, \ldots, n-1$. Now define

$$H(x) = h(x) + \frac{(x-x_1)(x-x_2)\cdots(x-x_{n-1})}{(x_n-x_1)(x_n-x_2)\cdots(x_n-x_{n-1})}\ (c_n - h(x_n)) \ .$$

It follows that $H(x) \in \mathbb{C}[x]$ has degree less than n, and $H(x_i) = c_i$ for all $i = 1, \ldots, n$. (As a simple example to show that $H(x)$ need not be unique if the $x_1, \ldots, x_n$ are not distinct, consider the numbers $2, 2, 3, 3$ all being mapped to 0. Then the polynomials $H_1(x) = (x-2)^2(x-3)$, $H_2(x) = (x-2)(x-3)^2$, and $H_3(x) = (x-2)(x-3)$ all satisfy the assumptions of the lemma.) Suppose that there exist two polynomials $H_1(x)$ and $H_2(x)$ with $H_1(x_i) = c_i = H_2(x_i)$. By the division algorithm in $\mathbb{C}[x]$, there are unique polynomials $q(x)$ and $r(x)$ such that

$$H_1(x) - H_2(x) = q(x)\left[(x-x_1)(x-x_2)\cdots(x-x_n)\right] + r(x) \ ,$$

where $\deg r < n$. If $q(x) \not\equiv 0$, then the degree of the polynomial on the right-hand side is at least n, whereas $H_1(x) - H_2(x)$ has degree less than n. We must therefore have $q(x) \equiv 0$. Moreover, if $r(x) \not\equiv 0$, then $H_1(x_i) = H_2(x_i)$ gives that $r(x_i) = 0$ for all $x_1, \ldots, x_n$. This implies, however, that $r(x)$ has n distinct zeros and so must have degree n, a contradiction. Thus $H_1(x) = H_2(x)$. $\square$ (Claim 1)

Let $R \subset \mathbb{C}(x)$ denote the subring of rational functions that are defined at the roots x_i of $\varphi(x)$,

$$R = \left\{ \frac{p(x)}{q(x)} \ : \ p(x), q(x) \in \mathbb{C}[x] \text{ and } q(x_i) \neq 0 \text{ for all roots } x_i \right\} \ ,$$

and consider the quotient ring $R/(\varphi(x))$. The next claim states that the ring $R/(\varphi(x))$ satisfies Properties 1 and 2.

Claim 2. Members of the same coset in $R/(\varphi(x))$ agree on the roots x_i of $\varphi(x)$, that is, if $g_1(x)$ and $g_2(x)$ belong to the same coset, then $g_1(x_i) = g_2(x_i)$, and so $\sum_{i=1}^n g_1(x_i) = \sum_{i=1}^n g_2(x_i)$. In addition, any rational function $h(x) \in R$ will have in its coset $\overline{h(x)} \in R/(\varphi(x))$ a unique polynomial representative $r(x)$ of degree less than n.

Proof (Claim 2). Notice that, if $\overline{h_1(x)} = \overline{h_2(x)} \in R/(\varphi(x))$, then by definition there exists a rational function $h(x) \in R$ such that

$$h_1(x) - h_2(x) = h(x)\varphi(x) \ ,$$

so that $h_1(x_i) = h_2(x_i)$ for all the zeros x_i of $\varphi(x)$. In other words, $R/(\varphi(x))$ also satisfies Property 1. It turns out that when the zeros $x_1, \ldots, x_n$ of $\varphi(x)$ are distinct, as we are assuming they are, then $R/(\varphi(x))$ also satisfies Property 2 (in fact $R/(\varphi(x))$ and $\mathbb{C}[x]/(\varphi(x))$ will be isomorphic as rings). For given a coset $\overline{h(x)} \in R/(\varphi(x))$, Claim 1 shows that there is a unique polynomial $g(x) \in \mathbb{C}[x]$ of degree less than n whose values at the n roots x_i are $h(x_i)$. Then the rational function $g(x) - h(x) \in R$ vanishes at every x_i, and a simple application of the division algorithm applied to the numerator of $g(x) - h(x)$ shows that $\overline{g(x)} = \overline{h(x)} \in R/(\varphi(x))$. Thus any rational function $h(x) \in R$ will have in its coset $\overline{h(x)} \in R/(\varphi(x))$ a unique polynomial representative $r(x)$ of degree less than n. $\square$ (Claim 2)

We now begin the proof of the Proposition by establishing the following Lemma:

Lemma. Let $\varphi(x) = a_n x^n + \cdots + a_1 x + a_0$ and consider the quotient ring $R/(\varphi(x))$. For any $1 \leqslant k \leqslant n-1$, let

$$r_k(x) \equiv b_{n-1,k}\, x^{n-1} + \cdots + b_{1,k}\, x + b_{0,k}$$

be the unique polynomial representative in the coset $\overline{\varphi'(x)x^k}$. Then the following recursive relation holds:

$$\begin{cases} b_{n-i,0} = (n-(i-1))\, a_{n-(i-1)} \ , & i = 1, \ldots, n \ , \\ b_{n-i,k} = -\dfrac{a_{n-i}}{a_n}\, b_{n-1,k-1} + b_{n-(i+1),k-1} \ , & i = 1, \ldots, n \ , \quad k = 1, \ldots, n-1 \ , \end{cases} \tag{3.7}$$

where $b_{-1,k-1} \equiv 0$.

Proof of Lemma. The existence and uniqueness of the polynomial

$$r_k(x) = b_{n-1,k}\, x^{n-1} + \cdots + b_{n-i,k}\, x^{n-i} + \cdots + b_{1,k}\, x + b_{0,k}\, 1 \ ,$$

where

$$\overline{\varphi'(x)\, x^k} = \overline{r_k(x)} = b_{n-1,k}\, \overline{x^{n-1}} + \cdots + b_{n-i,k}\, \overline{x^{n-i}} + \cdots + b_{1,k}\overline{x} + b_{0,k}\, \overline{1} \ , \qquad (3.8)$$

were established in Claim 2. Also, note that since $\overline{\varphi(x)} = \overline{0} \in R/(\varphi(x))$, we have

$$\overline{x^n} = -\frac{a_{n-1}}{a_n}\overline{x^{n-1}} - \cdots - \frac{a_1}{a_n}\overline{x} - \frac{a_0}{a_n}\overline{1} \ . \qquad (3.9)$$

Case $k = 0$: By (3.8), we get

$$\overline{\varphi'(x)x^0} = \overline{r_0(x)} = b_{n-1,0}\, \overline{x^{n-1}} + \cdots + b_{n-i,0}\, \overline{x^{n-i}} + \cdots + b_{1,0}\, \overline{x} + b_{0,0}\, \overline{1} \ .$$

However,

$$\overline{\varphi'(x)x^0} = \overline{\varphi'(x)} = na_n\, \overline{x^{n-1}} + \cdots + (n-(i-1))a_{n-(i-1)}\, \overline{x^{n-i}} + \cdots + 2a_2\, \overline{x} + a_1\, \overline{1} \ .$$

Consequently,

$$b_{n-i,0} = (n-(i-1))\, a_{n-(i-1)} \ , \qquad i = 1, \ldots, n \ . \qquad (3.10)$$

Case $k = 1, \ldots, n-1$: Equations (3.8) and (3.9) yield

$$\begin{aligned}
\overline{\varphi'(x)\, x^k} &= b_{n-1,k}\, \overline{x^{n-1}} + \cdots + b_{n-i,k}\, \overline{x^{n-i}} + \cdots + b_{1,k}\, \overline{x} + b_{0,k}\, \overline{1} \\
&= \overline{x\, \varphi'(x)\, x^{k-1}} \\
&= \overline{x}\left[b_{n-1,k-1}\, \overline{x^{n-1}} + b_{n-2,k-1}\, \overline{x^{n-2}} + \cdots + b_{1,k-1}\, \overline{x} + b_{0,k-1}\, \overline{1}\right] \\
&= b_{n-1,k-1}\, \overline{x^n} + b_{n-2,k-1}\, \overline{x^{n-1}} + \cdots + b_{1,k-1}\, \overline{x^2} + b_{0,k-1}\, \overline{x} \\
&= b_{n-1,k-1}\left[-\frac{a_{n-1}}{a_n}\, \overline{x^{n-1}} - \cdots - \frac{a_1}{a_n}\, \overline{x} - \frac{a_0}{a_n}\, \overline{1}\right] \\
&\quad + b_{n-2,k-1}\, \overline{x^{n-1}} + \cdots + b_{1,k-1}\, \overline{x^2} + b_{0,k-1}\, \overline{x} \\
&= \sum_{i=1}^{n}\left[-\frac{a_{n-i}}{a_n}\, b_{n-1,k-1} + b_{n-(i+1),k-1}\right]\, \overline{x^{n-i}} \ .
\end{aligned}$$

The coefficients of (3.8) are then related to the coefficients of a_i of $\varphi(x)$ as follows:

$$b_{n-i,k} = -\frac{a_{n-i}}{a_n}\, b_{n-1,k-1} + b_{n-(i+1),k-1} \ , \qquad i = 1, \ldots, n \ , \qquad k = 1, \ldots, n-1 \ ,$$

where the coeffiencients $b_{n-i,0}$ are given by (3.10). Note that $b_{n,k} = 0$ since the unique polynomial goes up to degree $n-1$. $\square$ (Lemma)

We now complete the proof of the Proposition. If $h_{1,*}(x)$ and $h_{2,*}(x)$ are the unique polynomial representatives of the cosets $\overline{h_1(x)}$ and $\overline{h_2(x)}$, respectively, then by uniqueness, the sum $h_{1,*}(x) + h_{2,*}(x)$ is the unique polynomial representative of the coset $\overline{h_1(x) + h_2(x)}$. With that said, we note that, since $\overline{h(x)} = \overline{h_*(x)}$, it follows that $\overline{r(x)} = \overline{\varphi'(x)h(x)} = \overline{\varphi'(x)h_*(x)}$. We thus have

$$\begin{aligned}
\overline{r(x)} &= \overline{\varphi'(x)h_*(x)} \\
&= \overline{c_{n-1}\varphi'(x)x^{n-1}} + \cdots + \overline{c_1\varphi'(x)x} + \overline{c_0\varphi'(x)} \\
&= \overline{c_{n-1}r_{n-1}(x)} + \cdots + \overline{c_1 r_1(x)} + \overline{c_0 r_0(x)} \\
&= c_{n-1}\sum_{i=1}^{n} b_{n-i,n-1}\overline{x^{n-i}} + \cdots + c_1\sum_{i=1}^{n} b_{n-i,1}\overline{x^{n-i}} + c_0\sum_{i=1}^{n} b_{n-i,0}\overline{x^{n-i}} \\
&= \sum_{i=1}^{n} \left(c_{n-1}b_{n-i,n-1} + \cdots + c_1 b_{n-i,1} + c_0 b_{n-i,0}\right)\overline{x^{n-i}} \\
&= \sum_{i=1}^{n} b_{n-i}\overline{x^{n-i}} \ . \qquad \square \text{ (Proposition)}
\end{aligned}$$

3.2 Algebraic Proof of Magnification Theorem

We are now ready to prove our Main Theorem. We begin by establishing some preliminaries before starting the computational part of the proof.

Recall from Section 2.2.3 that given a family of functions $F_{\mathbf{c},\mathbf{s}}$, a parameter vector $(\mathbf{c}_0, \mathbf{s}_0)$ is called a *caustic point* of the family if there is at least one critical point $\mathbf{x}_0$ of $F_{\mathbf{c}_0,\mathbf{s}_0}$ (i.e., $\mathbf{x}_0$ satifies $\text{grad}(F_{\mathbf{c}_0,\mathbf{s}_0})(\mathbf{x}_0) = \mathbf{0}$) such that the Gaussian curvature at

$(\mathbf{x}_0, F_{\mathbf{c},\mathbf{s}}(\mathbf{x}_0))$ in the graph of $F_{\mathbf{c},\mathbf{s}}$ vanishes. Equivalently, $(\mathbf{c}_0, \mathbf{s}_0)$ will be a caustic point if $\det(\mathrm{Jac}\,\mathbf{f}_\mathbf{c})(\mathbf{x}_0)$ vanishes, since

$$\mathrm{Gauss}(\mathbf{x}_0, F_{\mathbf{c},\mathbf{s}}(\mathbf{x}_0)) = \det(\mathrm{Jac}\,\mathbf{f}_\mathbf{c})(\mathbf{x}_0) \ .$$

Now, given an induced mapping $\mathbf{f}_\mathbf{c}$ and a target point $\mathbf{s} = (s_1, s_2)$, we can use the pair of equations

$$(s_1, s_2) = \mathbf{f}_\mathbf{c}(x, y) \equiv (f_\mathbf{c}^{(1)}(x, y), f_\mathbf{c}^{(2)}(x, y))$$

to solve for (x, y) in terms of (s_1, s_2), which will give the pre-images $\mathbf{x}_i = (x_i, y_i)$ of $\mathbf{s}$ under $\mathbf{f}_\mathbf{c}$. For the singularities in Table 2.2, we shall see that the pre-images can be determined from solutions of a polynomial in one variable, which is obtained by eliminating one of the pre-image coordinates, say y. In doing so we obtain a polynomial $\varphi(x) \in \mathbb{C}[x]$ whose roots will be the x-coordinates x_i of the different pre-images under $\mathbf{f}_\mathbf{c}$:

$$\varphi(x) = a_n x^n + \cdots + a_1 x + a_0 \ .$$

Generically, we can assume that the roots of $\varphi(x)$ are distinct, an assumption made throughout the paper.

We would then be able to express the magnification $\mathfrak{M}(x, y; \mathbf{s})$ at a general pre-image point (x, y) as a function of one variable, in this case x, so that

$$\mathfrak{M}(x, y(x); \mathbf{s}) = \frac{1}{J(x, y(x))} \equiv \frac{1}{J(x)} \equiv \mathfrak{M}(x) \ ,$$

where $J \equiv \det(\mathrm{Jac}\,\mathbf{f}_\mathbf{c})$ and the explicit notational dependence on $\mathbf{s}$ is dropped for simplicity (recall eqn. (2.3) in Section 2.2.3). Since we shall consider only non-caustic target points $\mathbf{s}$ giving rise to pre-images $(x_i, y(x_i))$, we know that $J(x_i) \neq 0$. Furthermore, we shall only consider non-caustic points that yield the maximum number of pre-images. In addition, for the singularities in Table 2.2, the rational function $\mathfrak{M}(x)$ is defined at the roots of $\varphi(x)$, i.e., $\mathfrak{M}(x) \in R$. Now, denote by $\mathfrak{m}(x)$

the unique polynomial representative in the coset $\overline{\varphi'(x)\,\mathfrak{M}(x)} \in R/(\varphi(x))$, and let b_{n-1} be its $(n-1)$st coefficient. In the notation of Proposition 2, we have $h(x) \equiv \mathfrak{M}(x)$ and $r(x) \equiv \mathfrak{m}(x)$. Euler's trace formula (Corollary 3.6) then tells us immediately that the total signed magnification satisfies

$$\sum_i \mathfrak{M}_i = \frac{b_{n-1}}{a_n} \ . \tag{3.11}$$

It therefore remains to determine the coefficient b_{n-1} for each caustic singularity in Table 2.2. Next to each singularity below we indicate the value of $n-1$, which is the codimension of the singularity.

Finally, we mention that the full theorem is not a direct consequence of the Euler-Jacobi formula, of multi-dimensional residue integral methods, or of Lefschetz fixed point theory, because some of the singularities have fixed points at infinity. We will address these issues in greater detail in our geometric proof of Main Theorem in Section 3.3 below. We now begin the proof of Theorem 1.

Consider first the singularities of type A_n. Since the cases $n = 2, 3$ are known, we will consider $n \geqslant 4$ here. The $(n-1)$-parameter family of general functions F^{A_n} is given in Arnold (1973) by

$$F^{A_n}(x,y) = \pm x^{n+1} \pm y^2 + c_{n-1}x^{n-1} + c_{n-2}x^{n-2} + \cdots + c_3x^3 + c_2x^2 + c_1x. \tag{3.12}$$

To convert this into the form shown in Table 2.2, we use the following coordinate transformation on the domain $\{(x,y)\} = \mathbb{R}^2$:

$$(x,y) \longmapsto \left(x, y + \frac{c_2}{2}\right). \tag{3.13}$$

This transforms eqn. (3.12) to

$$F^{A_n}_{\mathbf{c},\mathbf{s}}(x,y) = \pm x^{n+1} \pm y^2 + c_{n-1}x^{n-1} + \cdots + c_3x^3 + s_2x^2 - s_1x \pm s_2y \ , \tag{3.14}$$

where $c_1 \equiv -s_1$ and $c_2 \equiv s_2$. The parameters s_1, s_2 are to be interpreted in the context of gravitational lensing as the rectangular coordinates on the source plane $S = \mathbb{R}^2$. Note that we omitted the constant term from eqn. (3.14) since it will not affect any of our results below. Note also that

$$\det\big(\mathrm{Hess}\, F^{A_n}\big) = \det\big(\mathrm{Hess}\, F^{A_n}_{\mathbf{c},\mathbf{s}}\big)\ ,$$

so that the magnification (as defined in eqn. (2.3)) is unaltered. We will work with the form of $F^{A_n}_{\mathbf{c},\mathbf{s}}$ in eqn. (3.14). The corresponding $(n-3)$-parameter family of general mappings $\mathbf{f}^{A_n}_{\mathbf{c}}\colon\ \mathbb{R}^2 \longrightarrow \mathbb{R}^2$ is

$$\mathbf{f}^{A_n}_{\mathbf{c}}(x,y) = \big(\pm(n+1)x^n + (n-1)c_{n-1}x^{n-2} + \cdots + 3c_3x^2 \mp 4yx\ ,\ \ \mp 2y\big) = (s_1, s_2).$$

Here $\mathbf{s} = (s_1, s_2)$ is a non-caustic target point lying in the region with the maximum number of lensed images. Since $s_2 = \pm 2y$, we can eliminate y to obtain a polynomial in the variable x:

$$\varphi_{A_n}(x) \equiv \pm(n+1)x^n + (n-1)c_{n-1}x^{n-2} + \cdots + 3c_3x^2 + 2s_2x - s_1\ , \qquad (3.15)$$

whose n roots are the x-coordinates of the lensed images $\mathbf{x}_i$ of $\mathbf{s}$. The Jacobian determinant of $\mathbf{f}^{A_n}_{\mathbf{c}}$ expressed in the single variable x is

$$\det\left(\mathrm{Jac}\,\mathbf{f}^{A_n}_{\mathbf{c}}\right) = \mp 2\left[\pm n(n+1)x^{n-1} + (n-2)(n-1)c_{n-1}x^{n-3} + \cdots + 6c_3x + 2s_2\right]. \qquad (3.16)$$

A comparison of eqns. (3.15) and (3.16) then shows that

$$\pm 2\varphi'_{A_n}(x) = \det\left(\mathrm{Jac}\,\mathbf{f}^{A_n}_{\mathbf{c}}\right)(x) = \frac{1}{\mathfrak{M}(x)}\cdot$$

We thus have

$$\varphi'_{A_n}(x)\mathfrak{M}(x) = \pm\frac{1}{2}\cdot$$

Thus the unique polynomial representative of the coset $\overline{\varphi'_{A_n}(x)\mathfrak{M}(x)}$ is the polynomial $\mathfrak{m}(x) \equiv \pm 1/2$, whose $(n-1)$st coefficient is $b_{n-1} = 0$ for all $n \geqslant 4$. Euler's trace formula in the form of eqn. (3.11) then tells us that the total signed magnification is

$$\sum_{i=1}^{n} \mathfrak{M}_i = 0 \ , \quad (A_n,\ n \geqslant 2).$$

For type D_n, $n \geqslant 4$, the corresponding $(n-3)$-parameter family of induced general maps $\mathbf{f}_{\mathbf{c}}^{D_n^{\pm}} \colon \mathbb{R}^2 \longrightarrow \mathbb{R}^2$ is shown in Table 2.2:

$$\begin{aligned} \mathbf{f}_{\mathbf{c}}^{D_n^{\pm}}(x,y) &= \big(2xy \ , \ x^2 \pm (n-1)y^{n-2} + \cdots + (n-i)c_{n-i}y^{n-(i+1)} + \cdots + 2c_2 y\big) \\ &= (s_1, s_2). \end{aligned} \tag{3.17}$$

Once again the point $\mathbf{s} = (s_1, s_2)$ is a non-caustic target point lying in the region with the maximum number of lensed images. This time, however, we eliminate x to obtain a polynomial in the variable y:

$$\begin{aligned} \varphi_{D_n^{\pm}}(y) \ \equiv \ & \pm 4(n-1)y^n + 4(n-2)c_{n-2}y^{n-1} + \cdots \\ & + 4(n-i)c_{n-i}y^{n-(i-1)} + \cdots + 8c_2y^3 - 4s_2y^2 + s_1^2 \ , \end{aligned}$$

whose n roots are the y-coordinates of the n lensed images $\mathbf{x}_i$ of $\mathbf{s}$. The derivative of $\varphi_{D_n^{\pm}}(y)$ is

$$\begin{aligned} \varphi'_{D_n^{\pm}}(y) &= \pm 4n(n-1)y^{n-1} + 4(n-1)(n-2)c_{n-2}y^{n-2} \\ &\quad + \cdots + 4(n-(i-1))(n-i)c_{n-i}y^{n-i} + \cdots + 24c_2y^2 - 8s_2y \ , \end{aligned} \tag{3.18}$$

while the Jacobian determinant of $\mathbf{f}_{\mathbf{c}}^{D_n^{\pm}}$ is

$$\begin{aligned} \det\Big(\operatorname{Jac}\mathbf{f}_{\mathbf{c}}^{D_n^{\pm}}\Big) &= \det\begin{bmatrix} 2y & 2x \\ 2x & \pm(n-2)(n-1)y^{n-3} + (n-3)(n-2)c_{n-2}y^{n-4} + \cdots + 2c_2 \end{bmatrix} \\ &= \pm 2(n-2)(n-1)y^{n-2} + 2(n-3)(n-2)c_{n-2}y^{n-3} + \cdots \\ &\quad \cdots + 2(n-(i+1))(n-i)c_{n-i}y^{n-(i+1)} + \cdots + 4c_2y - 4x^2. \end{aligned}$$

We can use eqn. (3.17) to eliminate x as follows:

$$
\begin{aligned}
&= \pm 2(n-2)(n-1)y^{n-2} + 2(n-3)(n-2)c_{n-2}y^{n-3} \\
&\quad + \cdots + 2(n-(i+1))(n-i)c_{n-i}y^{n-(i+1)} + \cdots + 4c_2 y \\
&\quad + 4\underbrace{\left(\pm(n-1)y^{n-2} + (n-2)c_{n-2}y^{n-3} + \cdots + (n-i)c_{n-i}y^{n-(i+1)} + \cdots + 2c_2 y - s_2\right)}_{= -x^2 \quad \text{(by eqn. (3.17))}} \\
&= \pm 2n(n-1)y^{n-2} + 2(n-1)(n-2)c_{n-2}y^{n-3} \\
&\qquad + \cdots + 2(n-(i-1))(n-i)c_{n-i}y^{n-(i+1)} + \cdots + 12c_2 y - 4s_2 \\
&= \det\left(\mathrm{Jac}\,\mathbf{f}_{\mathbf{c}}^{D_n^{\pm}}\right)(y) = \mathfrak{M}(y)^{-1}.
\end{aligned}
$$

A comparison with eqn. (3.18) then shows that

$$\varphi'_{D_n^{\pm}}(y)\mathfrak{M}(y) = 2y.$$

The unique polynomial representative of the coset $\overline{\varphi'_{D_n^{\pm}}(y)\mathfrak{M}(y)}$ is therefore the polynomial $\mathfrak{m}(y) \equiv 2y$, whose $(n-1)$st coefficient is $b_{n-1} = 0$ for all $n \geqslant 7$. Eqn. (3.11) then tells us that the total signed magnification is

$$\sum_{i=1}^{n} \mathfrak{M}_i = 0\ , \quad (D_n,\ n \geqslant 4).$$

The proofs for types E_6, E_7, E_8, as well as for the quantitative forms for the elliptic and hyperbolic umbilics, are identical to the proofs presented here, and can be found in Aazami and Petters (2009b, 2010). □

3.3 Orbifolds and Multi-Dimensional Residues

The proof just given was algebraic, making repeated use of the Euler trace formula. We now give a *geometric* explanation for the existence of such relations. We do so by generalizing the multi-dimensional residue technique developed by

Dalal and Rabin (2001). Their procedure was as follows. Each caustic singularity appearing in Arnold's classification gives rise (through its gradient) to a mapping between planes. Complexifying, and using homogeneous coordinates, one can extend these mappings to the complex projective plane $\mathbb{CP}^2$. Next, the magnifications $\mathfrak{M}_i$ are realized as residues of a certain meromorphic two-form. By the Global Residue Theorem (Griffiths and Harris, 1978, p. 656), the sum of these residues, which reside in affine space, is precisely equal to minus the sum of the residues at infinity. A magnification relation is thus transformed into a statement about the behavior of these (extended) mappings at infinity in $\mathbb{CP}^2$.

Ideally, if the right-hand side of a magnification relation is identically zero, one would like for there to be *no* residues at infinity. For the A_n $(n \geqslant 2), D_n$ $(n \geqslant 4), E_6, E_7, E_8$ family of caustic singularities, however, this is not always the case. The way around this is to consider extensions into spaces other than $\mathbb{CP}^2$, namely, the so-called weighted projective spaces $\mathbb{WP}(a_0, a_1, a_2)$. These are compact orbifolds which have recently come into prominence in string theory (see, e.g., Adem et al. (2007)). We show that one can extend each mapping associated to a caustic singularity to a particular weighted projective space such that there will be *no* residues at infinity. Magnification relations are then immediately explained.

3.3.1 Weighted Projective Space as a Compact Orbifold

In this section we provide a brief overview of orbifolds and of weighted projective space in particular, for the benefit of readers who may be unfamiliar with them. Complex projective n-space $\mathbb{CP}^n$ is the set of 1-dimensional complex-linear subspaces of $\mathbb{C}^{n+1}$, with smooth quotient map $\pi\colon\ \mathbb{C}^{n+1} \setminus \{0\} \longrightarrow \mathbb{CP}^n$. It is compact because the restriction of π to the compact embedded submanifold $\mathbb{S}^{2n+1} \subset \mathbb{C}^{n+1}$ is surjective. We can also view $\mathbb{CP}^n$ as being obtained by the following smooth action of $\mathbb{S}^1 \subset \mathbb{C}$

on $\mathbb{S}^{2n+1}$:

$$z \cdot (w_0, \ldots, w_n) = (zw_0, \ldots, zw_n). \tag{3.19}$$

This action is *proper*. This means by definition that the map $\rho\colon\ \mathbb{S}^1 \times \mathbb{S}^{2n+1} \longrightarrow \mathbb{S}^{2n+1} \times \mathbb{S}^{2n+1}$ defined by $z \cdot (w_0, \ldots, w_n) = ((zw_0, \ldots, zw_n), (w_0, \ldots, w_n))$ is proper; i.e., for any compact set $K \subset \mathbb{S}^{2n+1} \times \mathbb{S}^{2n+1}$, its pre-image $\rho^{-1}(K) \subset \mathbb{S}^1 \times \mathbb{S}^{2n+1}$ is compact. Smooth actions are automatically proper if the Lie group is compact, as with $\mathbb{S}^1$. The action in eqn. (3.19) is also *free*, because the stabilizer group

$$\mathbb{S}^1_w \equiv \{z \in \mathbb{S}^1 \ :\ z \cdot w = w\} = \{1\}$$

for every $w \in \mathbb{S}^{2n+1}$. Being smooth, proper, and free guarantees that the resulting quotient space $\mathbb{S}^{2n+1}/\mathbb{S}^1$ is a smooth manifold, which is clearly diffeomorphic to $\mathbb{CP}^n$ (see, e.g., Lee (2003), Chapter 9).

Now consider generalizing the action defined by eqn. (3.19), as follows:

$$z \cdot (w_0, \ldots, w_n) = (z^{a_0} w_0, \ldots, z^{a_n} w_n), \tag{3.20}$$

where the a_i are coprime positive integers. This action is still smooth and proper, but it is no longer free: elements in $\mathbb{S}^{2n+1}$ of the form $(0, \ldots, 0, w_i, 0, \ldots, 0)$ have stabilizer groups isomorphic to $\mathbb{Z}/a_i\mathbb{Z}$, because they are fixed by a_ith roots of unity. Thus the action defined by eqn. (3.20) is *almost free:* although the stabilizer group $\mathbb{S}^1_w$ is not necessarily trivial for every $w \in \mathbb{S}^{2n+1}$, it is always *finite*. The resulting quotient space $\mathbb{S}^{2n+1}/\mathbb{S}^1 \equiv \mathbb{WP}(a_0, \ldots, a_n)$ is known as *weighted projective space*, and it is not in general a manifold. It is an example of an *orbifold,* which we now define. Consult Satake (1956), Moerdijk and Pronk (1997), and Adem et al. (2007), Chapter 1, for a more detailed discussion of the material presented here.

Let X be a paracompact Hausdorff space, and define the following:

1. An *n-dimensional orbifold chart* is a connected open subset $\widetilde{U} \subset \mathbb{R}^n$ and a continuous mapping $\phi\colon\ \widetilde{U} \longrightarrow \phi(\widetilde{U}) \equiv U \subset X$, together with a finite group

G of smooth automorphisms of $\widetilde{U}$ that satisfies the following condition: ϕ is G-invariant ($\phi \circ g = \phi$ for all $g \in G$) and induces a homeomorphism $\widetilde{U}/G \cong U$. Let us clarify two points about this definition:

(a) Here $\widetilde{U}/G$ is the quotient space defined by the usual quotient map $\pi\colon\ \widetilde{U} \longrightarrow \widetilde{U}/G$ (which is an open map because each $g\colon\ \widetilde{U} \longrightarrow \widetilde{U}$ is a diffeomorphism). Because ϕ is G-invariant, it is constant on the fibers of π, so by the universal property of quotient maps it induces a unique continuous map $\varphi\colon\ \widetilde{U}/G \longrightarrow U$ satisfying $\varphi \circ \pi = \phi$. In the definition of an orbifold chart we are therefore assuming that this map is a homeomorphism.

(b) Any finite group is a compact zero-dimensional Lie group. G acts smoothly on $\widetilde{U}$ by hypothesis, and the action is proper because G is compact. If the action were also free, which we are *not* assuming, then the quotient space $\widetilde{U}/G$ would be a smooth manifold and the quotient map π a smooth submersion.

We write an orbifold chart as $(\widetilde{U}, G, \phi)$.

2. Given two such charts $(\widetilde{U}, G, \phi)$ and $(\widetilde{V}, H, \psi)$, an *embedding* between them is a smooth embedding $\lambda\colon\ \widetilde{U} \hookrightarrow \widetilde{V}$ satisfying $\psi \circ \lambda = \phi$.

3. Two orbifold charts $(\widetilde{U}, G, \phi)$ and $(\widetilde{V}, H, \psi)$ are *locally compatible* if every point $x \in U \cap V \subset X$ has an open neighborhood $W \subset U \cap V$ and an orbifold chart $(\widetilde{W}, K, \mu)$ with embeddings $(\widetilde{W}, K, \mu) \hookrightarrow (\widetilde{U}, G, \phi)$ and $(\widetilde{W}, K, \mu) \hookrightarrow (\widetilde{V}, H, \psi)$.

We say that X is an *n-dimensional orbifold* if it has a maximal atlas of locally compatible n-dimensional orbifold charts. Thus we see that an orbifold is locally

modeled on quotients of open subsets of $\mathbb{R}^n$ by finite group actions, and not simply open subsets of $\mathbb{R}^n$ as with manifolds. In general, therefore, orbifolds are not manifolds, though of course all manifolds are orbifolds. However, if the finite group actions on the orbifold charts are all free, then X is a smooth manifold by (1) and (3).

Now let X be an orbifold. For any $x \in X$, pick an orbifold chart $(\widetilde{U}, G, \phi)$ containing it and pick a point y in the fiber $\phi^{-1}(x) \subset \widetilde{U} \subset \mathbb{R}^n$. Define the *local group of x at y* to be

$$G_y = \{g \in G : g(y) = y\}.$$

If we instead choose another point $y' \in \phi^{-1}(x)$, then by (1a) above there is a (not necessarily unique) $g \in G$ such that $g(y) = y'$, and thus $G_{y'} = gG_yg^{-1}$. If $(\widetilde{V}, H, \psi)$ is another orbifold chart containing x, and if $\tilde{y} \in \psi^{-1}(x) \subset \widetilde{V}$ is any point in its fiber, then in fact $H_{\tilde{y}}$ and G_y are also conjugate to each other (this fact is not trivial; it follows from the fact that an orbifold embedding $(\widetilde{U}, G, \phi) \hookrightarrow (\widetilde{V}, H, \psi)$ induces an injective group homomorphism $G \hookrightarrow H$; see Moerdijk and Pronk (1997)). Thus the local group of x, which we now denote simply by G_x, is uniquely determined up to conjugacy. If $G_x = 1$, then x is said to be *regular;* if $G_x \neq 1$, then it is *singular*. If X has no singular points, then the local actions are all free, so X is a smooth manifold.

The most common types of orbifolds are those that arise as quotient of manifolds by compact Lie groups. In particular, if a compact Lie group G acts smoothly, effectively (an action is *effective* if $g \cdot p = p$ for all $p \in M$ implies that $g = 1$), and almost freely on a smooth manifold M, then it can be shown that the resulting quotient space M/G will be an orbifold; see Moerdijk and Pronk (1997); Adem et al. (2007) for the details. In particular, weighted projective space $\mathbb{WP}(a_0, \ldots, a_n) \equiv \mathbb{S}^{2n+1}/\mathbb{S}^1$, with the action defined by eqn. (3.20), is a $2n$-dimensional orbifold.

3.3.2 Multi-Dimensional Residue Theorem on Compact Orbifolds

The essence of the residue method developed in Dalal and Rabin (2001) is to express the magnification $\mathfrak{M}(\mathbf{x};\mathbf{s})$ in eqn. (2.3) as the residue of a meromorphic two-form defined on compact projective space $\mathbb{CP}^2$. We summarize the procedure here, in the context of the general mappings $\mathbf{f_c}$ shown in Table 2.2; consult Dalal and Rabin (2001) for a detailed treatment, including applications to realistic lens models in gravitational lensing.

Let $\mathbf{f_c}$ be any mapping shown in Table 2.2, with a given pre-image $\mathbf{x} = (x, y)$ of a non-caustic target point $\mathbf{s} = (s_1, s_2)$. Let $f_{\mathbf{c}}^{(1)}(x, y)$ and $f_{\mathbf{c}}^{(2)}(x, y)$ denote the two components of $\mathbf{f_c}$, with degrees d_1 and d_2, respectively. We can then express the pre-image $\mathbf{x}$ as a common root of the following two polynomials:

$$P_1(x, y) \equiv f_{\mathbf{c}}^{(1)}(x, y) - s_1 \quad , \quad P_2(x, y) \equiv f_{\mathbf{c}}^{(2)}(x, y) - s_2. \tag{3.21}$$

Note that

$$J(\mathbf{x}) \equiv \det\begin{bmatrix} \partial_x P_1 & \partial_y P_1 \\ \partial_x P_2 & \partial_y P_2 \end{bmatrix} = \mathfrak{M}(\mathbf{x};\mathbf{s})^{-1}.$$

In particular, $J(\mathbf{x}) \neq 0$ because $\mathbf{s}$ is a non-caustic target point. Now treat the pre-image coordinates $\mathbf{x} = (x, y)$ as complex variables, so that $\mathbf{x} \in \mathbb{C}^2$ and $\mathbf{f_c} \colon\ \mathbb{C}^2 \longrightarrow \mathbb{C}^2$, and consider the following meromorphic two-form defined on $\mathbb{C}^2$:

$$\omega = \frac{dx\, dy}{P_1(x, y) P_2(x, y)}.$$

At points where $J \neq 0$, the residue of ω is given by

$$\operatorname{Res} \omega = \frac{1}{J(x, y)} = \mathfrak{M}(\mathbf{x};\mathbf{s}). \tag{3.22}$$

Thus we have expressed the magnification $\mathfrak{M}(\mathbf{x};\mathbf{s})$ as the residue of a meromorphic two-form defined on $\mathbb{C}^2$. Next, since $\mathbb{C}^2$ can be viewed as the affine piece of $\mathbb{CP}^2$,

changing to homogeneous coordinates $[X : Y : U]$ with $x = X/U$ and $y = Y/U$ extends the mapping $\mathbf{f_c}$ to $\mathbb{CP}^2$, so that $\mathbf{f_c}\colon\ \mathbb{CP}^2 \longrightarrow \mathbb{CP}^2$. In homogeneous coordinates the two polynomials $P_i(x, y)$ are now expressed as follows:

$$\begin{cases} P_1(X, Y, U)_{\text{hom}} \equiv U^{d_1} f_{\mathbf{c}}^{(1)}(X/U, Y/U) - s_1 U^{d_1} \ , \\ P_2(X, Y, U)_{\text{hom}} \equiv U^{d_2} f_{\mathbf{c}}^{(2)}(X/U, Y/U) - s_2 U^{d_2} \ . \end{cases} \tag{3.23}$$

Homogeneous coordinates express the local form of a mapping on $\mathbb{CP}^2$ both in affine space ($U = 1$) and at infinity ($U = 0$). We can similarly extend ω to a form on $\mathbb{CP}^2$, still denoted ω, that is homogeneous of degree zero:

$$\omega = \frac{d(X/U)d(Y/U)}{P_1(X/U, Y/U)P_2(X/U, Y/U)} = \frac{U^{d_1+d_2-3}(UdXdY - XdUdY - YdXdU)}{P_1(X, Y, U)_{\text{hom}} P_2(X, Y, U)_{\text{hom}}}. \tag{3.24}$$

Since $\mathbb{CP}^2$ is a compact smooth manifold, the Global Residue Theorem states that the sum of the residues of any meromorphic form, such as ω, on $\mathbb{CP}^2$, is identically zero. Since all the poles of ω in affine space correspond to pre-images of $\mathbf{f_c}$ and vice-versa, the sum of their residues is the total signed magnification $\mathfrak{M}_{\text{tot}}(\mathbf{s})$ given by eqn. (2.4). The Global Residue Theorem thus states that $\mathfrak{M}_{\text{tot}}(\mathbf{s})$ is precisely equal to minus the sum of the residues of ω at infinity ($U = 0$). This is the fundamental explanation of magnification relations established in Dalal and Rabin (2001): *the total signed magnification corresponding to a non-caustic target point of a mapping* $\mathbf{f_c}$ *reflects the behavior of* $\mathbf{f_c}$ *at infinity when it is extended to* $\mathbb{CP}^2$. So in particular, if the homogeneous polynomials in eqn. (3.23) have *no* common roots at infinity, then ω has no poles at infinity and thus no residues at infinity, and we can immediately conclude that $\mathfrak{M}_{\text{tot}}(\mathbf{s}) = 0$. If there *are* common roots at infinity, then ω will have poles at infinity and their residues will have to be computed. In Dalal and Rabin (2001) a procedure for doing this was outlined and used to uncover magnification

relations corresponding to a variety of lens models in gravitational lensing. Such residues in general cannot be computed via eqn. (3.22), because zeros at infinity may not satisfy $J \neq 0$. Instead they are computed using the Leray residue formula, details of which can be found in Dalal and Rabin (2001). Note in any case that the mappings are always extended to the compact smooth manifold $\mathbb{CP}^2$. It is precisely this extension that we generalize here.

Given the simple form of the magnification relations

$$\mathfrak{M}_{\rm tot}(\mathbf{s}) = \sum_{i=1}^{n} \mathfrak{M}_i = 0,$$

one would expect there to be *no* common roots at infinity and thus no residue to calculate. This, however, is not the case for some of the induced general mappings $\mathbf{f_c}$ shown in Table 2.2. Take for example the D_5 caustic singularity (the parabolic umbilic), whose mapping is

$$\mathbf{f_c}(x,y) = \left(2xy\ ,\ x^2 \pm 4y^3 + 3c_3y^2 + 2c_2y\right) = (s_1, s_2), \tag{3.25}$$

where once again (s_1, s_2) is a non-caustic target point. Extending this mapping via homogeneous coordinates into $\mathbb{CP}^2$ leads to the following two polynomials, as in eqn. (3.23):

$$\mathbf{f_c} \text{ homog. in } \mathbb{CP}^2 \implies \begin{cases} 2XY - s_1U^2 \\ X^2U \pm 4Y^3 + 3c_3Y^2U + 2c_2YU^2 - s_2U^3. \end{cases} \tag{3.26}$$

In affine space ($U = 1$) we recover eqn. (3.25). At infinity ($U = 0$), however, there is one nonzero common root, namely the point $[1:0:0]$ (recall that in homogeneous coordinates $[X:Y:U] = [X':Y':U'] \iff$ there is a nonzero $\lambda \in \mathbb{C}$ with $X = \lambda X',\ Y = \lambda Y',\ U = \lambda U'$; recall also that $[0:0:0] \notin \mathbb{CP}^2$). The residue of ω at this point will therefore have to be computed. This is not difficult, and the residue will be zero (as expected). Nevertheless, this leads to the following question: can

we find an extension of eqn. (3.25) to a compact space *other* than $\mathbb{CP}^2$ that ensures there will be *no* common roots at infinity? The answer is yes: consider the weighted projective space $\mathbb{WP}(3,2,1)$ (see Section 3.3.1). In homogeneous coordinates, the difference between $\mathbb{WP}(3,2,1)$ and $\mathbb{CP}^2$ is the following: because of the action given by eqn. (3.20),

$$z \cdot (w_0, w_1, w_2) = (z^3 w_0, z^2\, w_1, z\, w_2),$$

the variables w_0, w_1 in $\mathbb{WP}(3,2,1)$ now have *weights* associated with them. As a result, the relationship between homogeneous and affine coordinates is now given by

$$x = \frac{X}{U^3} \quad , \quad y = \frac{Y}{U^2}.$$

Extending eqn. (3.25) to $\mathbb{WP}(3,2,1)$ thus gives the following two polynomials, which are different from those in eqn. (3.26):

$$\mathbf{f_c} \text{ homog. in } \mathbb{WP}(3,2,1) \implies \begin{cases} 2XY - s_1 U^5 \\ X^2 \pm 4Y^3 + 3c_3 Y^2 U^2 + 2c_2 Y U^4 - s_2 U^6. \end{cases} \quad (3.27)$$

Once again in affine space ($U = 1$) we recover eqn. (3.25). The situation at infinity ($U = 0$), however, is now decidedly better, because the only common root of eqn. (3.27) at infinity is the point $[0:0:0]$, which of course is not a point in $\mathbb{WP}(3,2,1)$. We have therefore found an extension in which there are no roots at infinity. Moreover, the only singularities of the orbifold $\mathbb{WP}(3,2,1)$ occur at infinity, because U has weight 1. In other words, the only $z \in \mathbb{S}^1$ that satisfies $z\, w_2 = w_2$ for $w_2 \neq 0$ is $z = 1$. In fact the only singular points of $\mathbb{WP}(3,2,1)$ are $[1:0:0]$ and $[0:1:0]$, with local groups isomorphic to $\mathbb{Z}/3\mathbb{Z}$ and $\mathbb{Z}/2\mathbb{Z}$, respectively. Thus there are no singular points in affine space, where the pre-images reside.

As we will see in Appendix 3.4, an extension such as that in eqn. (3.27), in which there are no common roots at infinity, can be obtained for *all* the caustic singularities of the A, D, E family. Each such weighted projective space will be of

the form $\mathbb{WP}(a_0, a_1, 1)$, so it will have no singular points in affine space. The common roots lie in the affine subset $U = 1$ which is nonsingular and simply $\mathbb{C}^2$. The vanishing of the total magnification in $\mathbb{C}^2$ then follows from the orbifold version of the Global Residue Theorem.

The Global Residue Theorem as presented in Griffiths and Harris (1978) applies to compact smooth manifolds only. The extension to compact orbifolds is Remark 4.10 of Cattani et al. (1997b). However, Cattani et al. (1997a) give a useful statement adapted to our context of weighted projective spaces (Corollary 1.18). Consider a generalization of the form ω in $\mathbb{C}^2$,

$$\omega = \frac{h(x, y)\, dx\, dy}{P_1(x, y) P_2(x, y)}, \tag{3.28}$$

where $h(x, y)$ is a polynomial. Such a form can occur in the computation of total magnification when x, y are non-rectangular coordinates for the pre-images, or more generally in computing moments of the magnification. Then ω has no residue at infinity in $\mathbb{WP}(a_0, a_1, 1)$ whenever it has negative degree, that is, when

$$\deg h < \deg P_1 + \deg P_2 - a_0 - a_1. \tag{3.29}$$

In this statement it is understood that all degrees are weighted, so that $\deg x = a_0$ and $\deg y = a_1$. When the degree of ω is nonnegative, a simple algorithm is given in Cattani et al. (1997a) to compute the residue at infinity.

3.4 Geometric Proof of Magnification Theorem

3.4.1 Singularities of Type A_n

From Table 2.2 we have

$$\begin{aligned} \mathbf{f}_{\mathbf{c}}^{A_n}(x, y) &= \left(\pm(n+1)x^n + (n-1)c_{n-1}x^{n-2} + \cdots + 3c_3x^2 - 4xy\ ,\ -2y\right) \\ &= (s_1, s_2), \end{aligned} \tag{3.30}$$

whose pre-images (x_i, y_i) have magnification

$$\big(\det\big(\mathrm{Jac}\,\mathbf{f}_{\mathbf{c}}^{A_n}\big)\big)^{-1}(x_i,y_i) = \det\big(\mathrm{Hess}\,F_{\mathbf{c},\mathbf{s}}^{A_n}\big)^{-1}(x_i,y_i) \equiv \mathfrak{M}_i\ .$$

The simple form of the leading order terms in eqn. (3.30) suggests that we extend $\mathbf{f}_{\mathbf{c}}^{A_n}$ to $\mathbb{WP}(1,1,1) = \mathbb{CP}^2$. Indeed, in homogeneous coordinates $[X : Y : U]$, the solutions of eqn. (3.30) are the common roots in affine space ($U = 1$) of the following two homogeneous polynomials in $\mathbb{WP}(1,1,1)$:

$$\mathbf{f}^{A_n} \text{ homog. in } \mathbb{WP}(1,1,1) \implies \tag{3.31}$$

$$\begin{cases} \pm(n+1)X^n + (n-1)c_{n-1}X^{n-2}U^2 + \cdots + 3c_3X^2U^{n-2} - 4XYU^{n-2} - s_1U^n \\ -2Y - s_2U. \end{cases}$$

The common roots at infinity are obtained by setting $U = 0$, which yields only the root $[0:0:0] \notin \mathbb{WP}(1,1,1)$. Moreover, since $\mathbb{WP}(1,1,1) = \mathbb{CP}^2$ is a (compact) smooth manifold, it has no singular points. The Global Residue Theorem then tells us that the sum of the residues in affine space is minus the sum of the residues at infinity. Since there are no residues at infinity, the magnification theorem immediately follows.

3.4.2 Singularities of Type D_n

For type D_n, $n \geqslant 4$, the corresponding $(n-3)$-parameter family of induced general maps $\mathbf{f}_{\mathbf{c}}^{D_n^{\pm}}$ is shown in Table 2.2:

$$\mathbf{f}_{\mathbf{c}}^{D_n^{\pm}}(x,y) = \big(2xy\ ,\ x^2 \pm (n-1)y^{n-2} + (n-2)c_{n-2}y^{n-3} + \cdots + 2c_2y\big) = (s_1,s_2). \tag{3.32}$$

We now extend eqn. (3.32) to the weighted projective space $\mathbb{WP}(n-2,2,1)$, so that the affine coordinates x, y are related to the homogeneous coordinates $[X : Y : U]$ by

$$x = \frac{X}{U^{n-2}} \qquad , \qquad y = \frac{Y}{U^2}. \tag{3.33}$$

The solutions of eqn. (3.32) are the common roots in affine space ($U = 1$) of the following two homogeneous polynomials in $\mathbb{WP}(n-2,2,1)$:

$$\mathbf{f}_{\mathbf{c}}^{D_n^{\pm}} \text{ homogenized in } \mathbb{WP}(n-2,2,1) \implies \tag{3.34}$$

$$\begin{cases} 2XY - s_1 U^n \\ X^2 \pm (n-1)Y^{n-2} + (n-2)c_{n-2}Y^{n-3}U^2 + \cdots + 2c_2 YU^{2n-6} - s_2 U^{2n-4}. \end{cases}$$

(Note that these polynomials *are* homogeneous, since X and Y now have weights $n-2$ and 2, respectively; the degree of the term $2XY$, for example, is $(n-2)+2 = n$.) At infinity ($U = 0$), the only common root is $[0:0:0] \notin \mathbb{WP}(n-2,2,1)$. Note that the singular points of $\mathbb{WP}(n-2,2,1)$ occur at infinity.

3.4.3 Singularities of Type E_n

The 5-parameter family of induced general maps $\mathbf{f}_{\mathbf{c}}^{E_6}$ corresponding to type E_6 is shown in Table 2.2:

$$\mathbf{f}_{\mathbf{c}}^{E_6}(x,y) = \left(3x^2 + c_3y^2 + c_1y \ , \ \pm 4y^3 + 2c_3xy + 2c_2y + c_1x\right) = (s_1, s_2). \tag{3.35}$$

As with A_n, we can extend eqn. (3.35) to $\mathbb{WP}(1,1,1) = \mathbb{CP}^2$, with corresponding homogeneous polynomials

$$\mathbf{f}_{\mathbf{c}}^{E_6} \text{ homogenized in } \mathbb{WP}(1,1,1) \implies \begin{cases} 3X^2 + c_3Y^2 + c_1YU - s_1U^2 \\ \pm 4Y^3 + 2c_3XYU + 2c_2YU^2 + c_1XU^2 - s_2U^3. \end{cases}$$

The only common root at infinity ($U = 0$) is $[0:0:0] \notin \mathbb{WP}(1,1,1)$.

For type E_7, Table 2.2 gives the corresponding 4-parameter family of induced general maps $\mathbf{f}_{\mathbf{c}}^{E_7}$:

$$\mathbf{f}_{\mathbf{c}}^{E_7}(x,y) = \left(3x^2 + y^3 + c_1y \ , \ 3xy^2 + 4c_4y^3 + 3c_3y^2 + 2c_2y + c_1x\right) = (s_1, s_2). \tag{3.36}$$

We extend eqn. (3.36) to $\mathbb{WP}(3,2,1)$, with homogeneous coordinates

$$x = \frac{X}{U^3} \quad , \quad y = \frac{Y}{U^2}$$

and corresponding homogeneous polynomials

$$\mathbf{f}_{\mathbf{c}}^{E_7} \text{ homogenized in } \mathbb{WP}(3,2,1) \implies \tag{3.37}$$

$$\begin{cases} 3X^2 + Y^3 + c_1 YU^4 - s_1 U^6 \\ 3XY^2 + 4c_4 Y^3 U + 3c_3 Y^2 U^3 + 2c_2 YU^5 + c_1 XU^4 - s_2 U^7, \end{cases}$$

whose common roots in affine space ($U = 1$) are precisely the solutions to eqn. (3.36). The only common root at infinity ($U = 0$) is $[0:0:0] \notin \mathbb{WP}(3,2,1)$.

The polynomials in this case have weighted degrees 6 and 7. As an example of the vanishing criterion quoted in eqn. (3.29), a form ω as in eqn. (3.28) would have vanishing sum of residues in $\mathbb{C}^2$ when $\deg h < 6 + 7 - 3 - 2 = 8$.

Finally, Table 2.2 gives the 5-parameter family of induced general mappings $\mathbf{f}_{\mathbf{c}}^{E_8}$ corresponding to type E_8:

$$\begin{aligned} \mathbf{f}_{\mathbf{c}}^{E_8}(x,y) &= \left(3x^2 + c_5 y^3 + c_4 y^2 + c_1 y \ , \ 5y^4 + 3c_5 xy^2 + 2c_4 xy + 3c_3 y^2 + 2c_2 y + c_1 x\right) \\ &= (s_1, s_2). \end{aligned}$$

Once again we will use $\mathbb{WP}(3,2,1)$. This time the corresponding homogeneous polynomials are

$$\mathbf{f}_{\mathbf{c}}^{E_8} \text{ homogenized in } \mathbb{WP}(3,2,1) \implies \tag{3.38}$$

$$\begin{cases} 3X^2 + c_5 Y^3 + c_4 Y^2 U^2 + c_1 YU^4 - s_1 U^6 \\ 5Y^4 + 3c_5 XY^2 U + 2c_4 XYU^3 + 3c_3 Y^2 U^4 + 2c_2 YU^6 + c_1 XU^5 - s_2 U^8. \end{cases}$$

And, of course, the only common root at infinity ($U = 0$) is $[0:0:0]$.

3.4.4 Quantitative Forms for the Elliptic and Hyperbolic Umbilics

Elliptic and Hyperbolic Umbilics: Table 2.3 gives the universal, quantitative form of a lensing map in the neighborhood of either an elliptic umbilic (D_4^-) or hyperbolic umbilic (D_4^+) caustic. These are both one-parameter maps $\boldsymbol{\eta}_c$ induced by

a three-parameter time delay family $T_{c,\mathbf{s}}$. (In the context of gravitational lensing, c will represent some physical input, such as the source redshift.) For the elliptic umbilic, this induced mapping is

$$\boldsymbol{\eta}_{c,\text{ell}}(x,y) = \left(x^2 - y^2\ ,\ -2xy + 4cy\right) = (s_1, s_2),$$

while for the hyperbolic umbilic, it is

$$\boldsymbol{\eta}_{c,\text{hyp}}(x,y) = \left(x^2 + 2cy\ ,\ y^2 + 2cx\right) = (s_1, s_2).$$

The desired extension in both cases is to $\mathbb{WP}(1,1,1) = \mathbb{CP}^2$, with corresponding homogeneous polynomials

$$\boldsymbol{\eta}_{c,\text{ell}} \text{ homogenized in } \mathbb{WP}(1,1,1) \implies \begin{cases} X^2 - Y^2 - s_1U^2 \\ -2XY + 4cYU - s_2U^2 \end{cases}$$

and

$$\boldsymbol{\eta}_{c,\text{hyp}} \text{ homogenized in } \mathbb{WP}(1,1,1) \implies \begin{cases} X^2 + 2cYU - s_1U^2 \\ Y^2 + 2cXU - s_2U^2. \end{cases}$$

The only common root at infinity ($U = 0$) in either case is $[0:0:0] \notin \mathbb{WP}(1,1,1)$. $\square$

4

A Lens Equation for Equatorial Kerr Black Hole Lensing

4.1 Introduction

We now switch gears and address gravitational lensing in the setting of one of the most important non-spherically symmetric and non-static solutions of the Einstein equations, namely, Kerr black holes. This has already been the focus of many studies. Indeed, several authors have explored the Kerr's caustic structure, as well as Kerr black hole lensing in the strong deflection limit, focusing on leading order effects in light passing close to the region of photon capture (e.g., Rauch and Blandford (1994), Bozza (2003, 2008a,b), Vazquez and Esteban (2003), Bozza et al. (2005), Bozza et al. (2006), and Bozza and Scarpetta (2007)).

Studies of Kerr lensing have also been undertaken in the weak deflection limit. In particular, Sereno and De Luca (2006, 2008) gave an analytic treatment of caustics and two lensing observables for Kerr lensing in the weak deflection limit, while Iyer and Hansen (2009a,b) found an asymptotic expression for the equatorial bending angle. Werner and Petters (2007) used magnification relations for weak-deflection

Kerr lensing to address the issue of Cosmic Censorship (for lensing and Cosmic Censorship in the spherically symmetric case, see Virbhadra and Ellis (2002)).

This chapter and the next develops a comprehensive analytic framework for Kerr black hole lensing, with a focus on regimes beyond the weak deflection limit (but not restricted to the strong deflection limit). This chapter begins by presenting a new, general lens equation and magnification formula governing lensing by a thin deflector. This lens equation is applicable for non-equatorial observers and assume that the source and observer are in the asymptotically flat region. In addition, it incorporates the displacement for a general setting that Bozza and Sereno (2006) introduced for the case of a spherically symmetric deflector. This occurs when the light ray's tangent lines at the source and observer do not intersect on the lens plane. An explicit expression is given for this displacement when the observer is in the equatorial plane of a Kerr black hole as well as for the case of spherical symmetry. In Chapter 5 this lens equation is solved perturbatively to obtain analytic expressions for five lensing observables (image positions, magnifications, total unsigned magnification, centroid, and time delay) for the regime of quasi-equatorial lensing.

4.2 General Lens Equation with Displacement

4.2.1 Angular Coordinates on the Observer's Sky

We assume that our deflector is a "thin lens," by which we mean that its spatial extent is much less than its distances to the source and observer. Let us define Cartesian coordinates (x, y, z) centered on the thin lens and oriented such that the observer lies on the positive x-axis.

Assume that the observer in the asymptotically flat region is at rest relative to the (x, y, z) coordinates. *All equations derived in this section are relative to the asymptotically flat geometry of such an observer.* The natural coordinates for the observer to use in gravitational lensing are angles on the sky. To describe these angles,

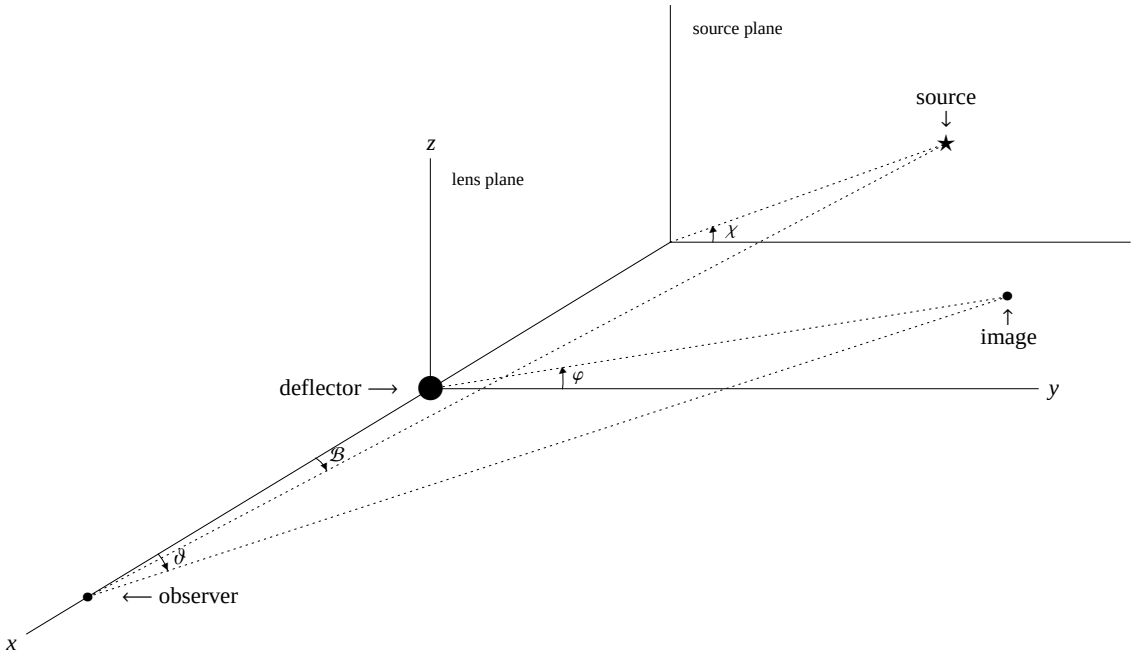

FIGURE 4.1: Angles on the observer's sky. An image's position is determined by (ϑ, φ). The source's position is given by $(\mathcal{B}, \chi)$.

we introduce "spherical polar" coordinates defined with respect to the observer and the optical axis (from the observer to the lens), and the yz-planes at the deflector and the light source. The vector to the image position is then described by the angle ϑ it makes with the optical axis, and an azimuthal angle φ. Similarly, the vector to the source position is described by the angle $\mathcal{B}$ it makes with the optical axis and by an azimuthal angle χ. These angles are shown in Fig. 4.1. Note that the optical axis is the x-axis. We adopt the usual convention for spherical polar coordinates: the image position has $\vartheta > 0$ and $0 \leqslant \varphi < 2\pi$, while the source position has $\mathcal{B} \geqslant 0$ and $0 \leqslant \chi < 2\pi$. In fact, since we only need to consider the "forward" hemisphere from the observer we can limit ϑ to the interval $(0, \pi/2)$ and $\mathcal{B}$ to the interval $[0, \pi/2)$.

The "lens plane" is the plane perpendicular to the optical axis containing the lens, and the "source plane" is the plane perpendicular to the optical axis containing

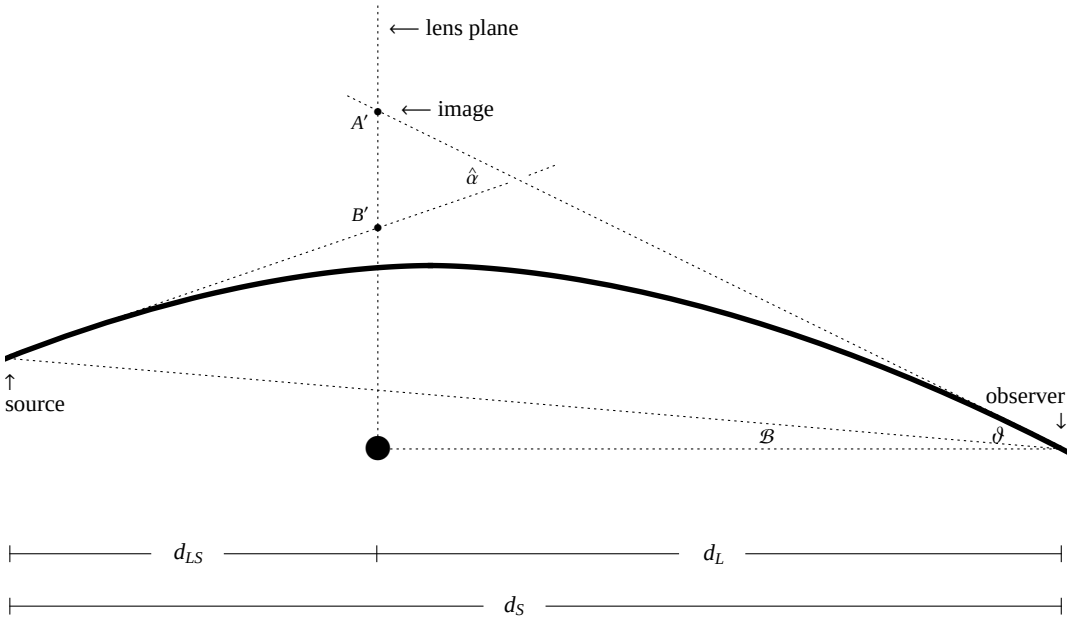

FIGURE 4.2: A lensing scenario demonstrating that the tangent line to the segment of the ray arriving at the observer and the tangent line of the ray at the source need not intersect on the lens plane; i.e., $A' \neq B'$ in general. The angles $\mathcal{B}$ and ϑ are as in Fig. 4.1 (or rather, they are their projections onto the xz-plane), $\hat{\alpha}$ is the "bending angle," and d_L, d_S, and d_{LS} are the perpendicular distances between the lens plane and observer, the source plane and observer, and the lens and source planes, respectively.

the source; these are also shown in Fig. 4.1. Define the distances d_L and d_S to be the perpendicular distances from the observer to the lens plane and source plane, respectively, while d_{LS} is the perpendicular distance from the lens plane to the source plane. Some investigators define d_S to be the distance from the observer to the source itself, as opposed to the shortest distance to the source plane. We shall comment on this distinction in Section 4.3.3.

4.2.2 General Lens Equation via Asymptotically Flat Geometry

Consider the lensing geometry shown in Fig. 4.2. With respect to the light ray being lensed, there are two tangent lines of interest: the tangent line to the segment of the ray arriving at the observer and the tangent line to the ray emanating from the source. As first emphasized in Bozza and Sereno (2006), *it is important to realize*

that these two tangent lines need not intersect. If they do intersect (as for a spherical lens, since in that case the tangent lines are coplanar), the intersection point need not lie in the lens plane. This effect has often been neglected, and while it may be small in the weak deflection limit (see Section 4.3.3 below) we should include it for greater generality. A simple way to capture this displacement is to consider the points where the two tangent lines cross the lens plane, namely, the points A' and B' in Fig. 4.2. If the tangent lines do intersect in the lens plane, then $A' = B'$. Otherwise, as can be seen in greater detail in Fig. 4.3, there is a displacement on the lens plane that we quantify by defining

$$\mathtt{d}_y = B'_y - A'_y\,, \qquad \mathtt{d}_z = B'_z - A'_z\,. \tag{4.1}$$

Note from Fig. 4.3 that the tangent line to the segment of the ray arriving at the observer is determined by (ϑ, φ). The tangent line to the ray emanating from the source can likewise be described by the angles (ϑ_S, φ_S), where $-\pi/2 < \vartheta_S < \pi/2$ and $0 \leqslant \varphi_S < 2\pi$. As shown in Fig. 4.3, ϑ_S has vertex B' and is measured from the line joining the points B' and B'', which runs parallel to the optical axis. We adopt the following sign convention for ϑ_S: if ϑ_S goes *toward* the optical axis, then it will be positive; otherwise it is negative (e.g., the ϑ_S shown in Fig. 4.3 is positive). We will obtain the general lens equation by considering the coordinates of the points A' and B' in Fig. 4.3. Using the asymptotically flat geometry of the observer, we have

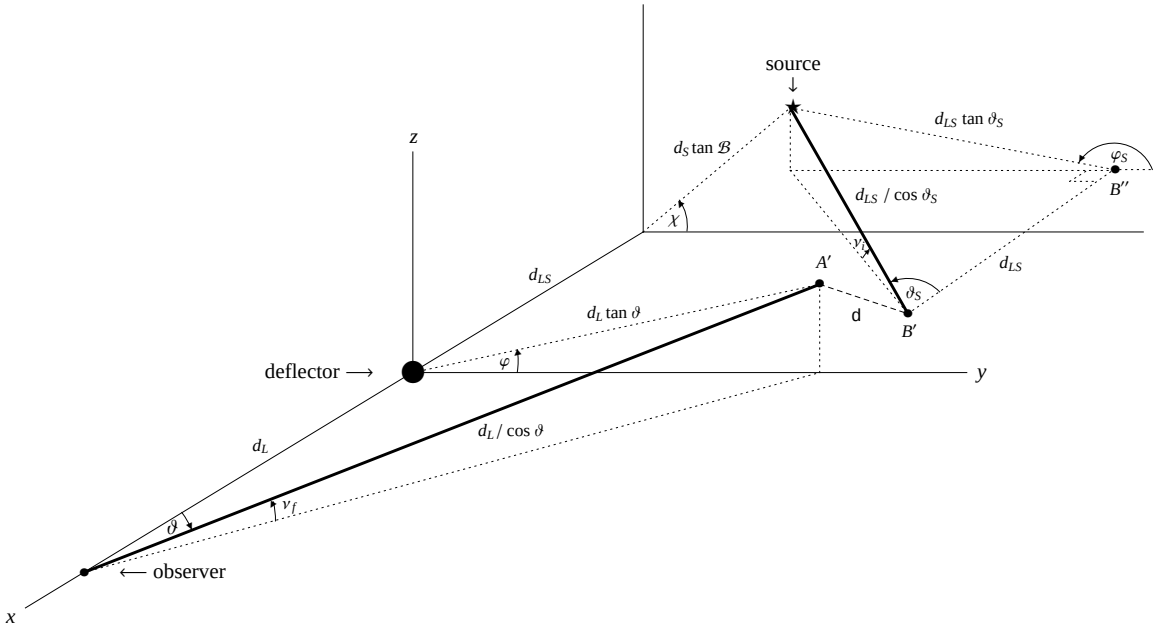

FIGURE 4.3: A detailed diagram of lensing with displacement. The tangent line to the segment of the ray arriving at the observer is determined by (ϑ, φ) and intersects the lens plane at A', while the tangent line to the ray emanating from the source is determined by (ϑ_S, φ_S) and intersects the lens plane at B'. The distance between these two points is quantified by the displacement amplitude $\mathtt{d}$, whose horizontal and vertical components we denote by $\mathtt{d}_y$ and $\mathtt{d}_z$, respectively. The deflector could be a Kerr black hole and the light ray may dip below the xy-plane.

$$
\begin{aligned}
A'_x &= 0\,, \\
A'_y &= d_L \tan\vartheta\, \cos\varphi\,, && (4.2)\\
A'_z &= d_L \tan\vartheta\, \sin\varphi\,, && (4.3)\\
B'_x &= 0\,, \\
B'_y &= d_S \tan\mathcal{B}\, \cos\chi + d_{LS} \tan\vartheta_S\, \cos(\pi - \varphi_S)\,, && (4.4)\\
B'_z &= d_S \tan\mathcal{B}\, \sin\chi - d_{LS}\, \tan\vartheta_S\, \sin(\pi - \varphi_S)\,. && (4.5)
\end{aligned}
$$

Substituting eqns. (4.2)–(4.5) into eqn. (4.1) yields

$$d_S \tan\mathcal{B} \cos\chi \;=\; d_L \tan\vartheta \cos\varphi \;+\; d_{LS} \tan\vartheta_S \cos\varphi_S \;+\; \mathtt{d}_y \,, \tag{4.6}$$

$$d_S \tan\mathcal{B} \sin\chi \;=\; d_L \tan\vartheta \sin\varphi \;+\; d_{LS} \tan\vartheta_S \sin\varphi_S \;+\; \mathtt{d}_z \,. \tag{4.7}$$

The left-hand sides involve only the source position, while the right-hand sides involve only the image position. In other words, *this pair of equations is the general form of the gravitational lens equation for source and observer in the asymptotically flat region, for a general isolated thin lens.* Note that apart from the asymptotic flatness assumption, these equations use no properties specific to Kerr black holes; and if the deflector was a Kerr black hole, then neither the observer nor the source was assumed to be equatorial. We shall refer to eqns. (4.6) and (4.7), respectively, as the "horizonal" and "vertical" components of the lens equation due to the cosine/sine dependence on χ.

Consider now the case when the light ray and its tangent lines lie in a plane which contains the optical axis. This forces $\chi = \varphi$ or $\chi = \varphi + \pi$ depending on whether the source is on the same or opposite side of the lens as the image. To distinguish these two cases, it is useful to define $\mathtt{q} = \cos(\chi - \varphi)$ to be a sign that indicates whether the source is on the same side of the lens as the image ($\mathtt{q} = +1$) or on the opposite side ($\mathtt{q} = -1$). The condition $A' \neq B'$ will still hold in general, but the line in the lens plane from the origin to the point B' will now make the same angle with respect to the y-axis as the point A', namely, the angle φ (see Fig. 4.3). As a result, the line in the source plane from the origin to the point B'' will also make the angle φ with respect to the y-axis. Thus we will have $\varphi_S = \varphi + \pi$. Given these conditions, eqns. (4.6) and (4.7) reduce to the single lens equation

$$d_S\, \mathtt{q} \tan\mathcal{B} = d_L \tan\vartheta - d_{LS} \tan(\hat{\alpha} - \vartheta) + \mathtt{d} \,, \tag{4.8}$$

where the displacement amplitude is $\mathtt{d} = \mathtt{d}_y/\cos\varphi = \mathtt{d}_z/\sin\varphi$ (in the case of planar rays), and to connect with traditional descriptions of gravitational lensing we have

introduced the light bending angle $\hat{\alpha} \equiv \vartheta + \vartheta_S$. (If desired, the sign $\mathtt{q}$ can be incorporated into the tangent so that the left-hand side is written as $\tan(\mathtt{q}\mathcal{B})$, where we think of $\mathtt{q}\mathcal{B}$ as the signed source position.) *Eqn. (4.8) is the general form of the lens equation in the case of planar rays.* If the displacement $\mathtt{d}$ is ignored, then eqn. (4.8) matches the spherical lens equation given by Virbhadra and Ellis (2000). We consider the displacement term in Section 4.3.3.

4.2.3 General Magnification Formula

The magnification of a small source is given by the ratio of the solid angle subtended by the image to the solid angle subtended by the source, since lensing conserves surface brightness (e.g., Petters et al. (2001), p. 82). As measured by the observer, if ℓ is the distance to the image (as opposed to the perpendicular distance), then the small solid angle subtended by the image is

$$d\Omega_I = \frac{|(\ell\, d\vartheta)\,(\ell \sin\vartheta\, d\varphi)|}{\ell^2} = |\sin\vartheta\; d\vartheta\; d\varphi| = |d(\cos\vartheta)\; d\varphi|.$$

Similarly, the small solid angle subtended by the source is

$$d\Omega_S = |\sin\mathcal{B}\; d\mathcal{B}\; d\chi| = |d(\cos\mathcal{B})\; d\chi|.$$

We then have the absolute magnification

$$|\mu| = \frac{d\Omega_I}{d\Omega_S} = |\det J|^{-1},$$

where J is the Jacobian matrix

$$J = \frac{\partial(\cos\mathcal{B}, \chi)}{\partial(\cos\vartheta, \varphi)} = \begin{bmatrix} \frac{\partial\cos\mathcal{B}}{\partial\cos\vartheta} & \frac{\partial\cos\mathcal{B}}{\partial\varphi} \\ \frac{\partial\chi}{\partial\cos\vartheta} & \frac{\partial\chi}{\partial\varphi} \end{bmatrix}$$

Writing out the determinant and dropping the absolute value in order to obtain the signed magnification, we get

$$\mu = \left[\frac{\sin\mathcal{B}}{\sin\vartheta}\left(\frac{\partial\mathcal{B}}{\partial\vartheta}\,\frac{\partial\chi}{\partial\varphi} - \frac{\partial\mathcal{B}}{\partial\varphi}\,\frac{\partial\chi}{\partial\vartheta}\right)\right]^{-1}. \tag{4.9}$$

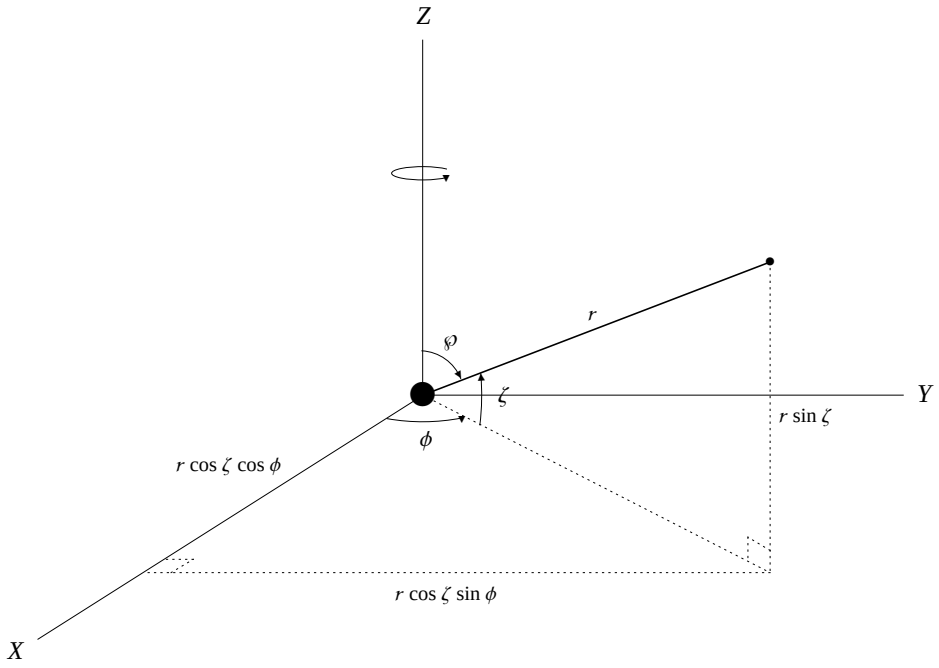

FIGURE 4.4: Cartesian (X, Y, Z) and spherical polar (r, ζ, ϕ) coordinates centered on the black hole, where $\zeta = \pi/2 - \wp$ with $\wp$ the polar angle; note that $-\pi/2 \leqslant \zeta \leqslant \pi/2$. The black hole spins about the Z-axis, which corresponds to $\zeta = \pi/2$, in the direction of increasing ϕ. The equatorial plane of the black hole corresponds to $\zeta = 0$ or the (X, Y)-plane.

In the case of spherical symmetry, the image and source lie in the same plane, so $\partial\mathcal{B}/\partial\varphi = 0$ and $\partial\chi/\partial\varphi = 1$, recovering the familiar result

$$\mu = \left(\frac{\sin \mathcal{B}}{\sin \vartheta} \, \frac{\partial \mathcal{B}}{\partial \vartheta} \right)^{-1} .$$

4.3 Lens Equation for Kerr Black Holes

4.3.1 Kerr Metric

Now let the deflector in Fig. 4.3 be a Kerr black hole. The Kerr metric is the unique axisymmetric, stationary, asymptotically flat, vacuum solution of the Einstein equations describing a stationary black hole with mass $\mathcal{M}_\bullet$ and spin angular momentum $\mathcal{J}_\bullet$ (see, e.g., Wald (1984), p. 322–324). Consider the Kerr metric in Boyer-Lindquist

coordinates $(t, r, \wp, \phi)$, where $\wp$ is the polar angle and ϕ the azimuthal angle. For our purposes, it is convenient to transform $\wp$ to $\zeta = \pi/2 - \wp$ and work with the slightly modified Boyer-Lindquist coordinates (t, r, ζ, ϕ); note that $-\pi/2 \leqslant \zeta \leqslant \pi/2$. The spatial coordinates are shown in Fig. 4.4.

The metric takes the form

$$ds^2 = g_{tt}\,dt^2 + g_{rr}\,dr^2 + g_{\zeta\zeta}\,d\zeta^2 + g_{\phi\phi}\,d\phi^2 + 2\,g_{t\phi}\,dt\,d\phi\,,$$

where $t = c\mathtt{t}$ with $\mathtt{t}$ being physical time. The metric coefficients are

$$g_{tt} = -\frac{r(r-2\mathsf{m}_\bullet) + \mathsf{a}^2\sin^2\zeta}{r^2 + \mathsf{a}^2\sin^2\zeta}\,, \tag{4.10}$$

$$g_{rr} = \frac{r^2 + \mathsf{a}^2\sin^2\zeta}{r(r-2\mathsf{m}_\bullet) + \mathsf{a}^2}\,, \tag{4.11}$$

$$g_{\zeta\zeta} = r^2 + \mathsf{a}^2\sin^2\zeta\,, \tag{4.12}$$

$$g_{\phi\phi} = \frac{(r^2+\mathsf{a}^2)^2 - \mathsf{a}^2(\mathsf{a}^2 + r(r-2\mathsf{m}_\bullet))\cos^2\zeta}{r^2 + \mathsf{a}^2\sin^2\zeta}\,\cos^2\zeta\,, \tag{4.13}$$

$$g_{t\phi} = -\frac{2\mathsf{m}_\bullet\mathsf{a}\,r\cos^2\zeta}{r^2 + \mathsf{a}^2\sin^2\zeta}\,. \tag{4.14}$$

The parameter $\mathsf{m}_\bullet$ is the gravitational radius, and a is the angular momentum per unit mass:

$$\mathsf{m}_\bullet = \frac{G\mathcal{M}_\bullet}{c^2}\,, \qquad \mathsf{a} = \frac{\mathcal{J}_\bullet}{c\mathcal{M}_\bullet}\,.$$

Note that both $\mathsf{m}_\bullet$ and a have dimensions of length. It is convenient to define a dimensionless spin parameter:

$$\hat{a} = \frac{\mathsf{a}}{\mathsf{m}_\bullet}\,.$$

Unless stated to the contrary, the black hole's spin is subcritical; i.e., $\hat{a}^2 < 1$.

4.3.2 Lens Equation for an Equatorial Observer

We now specialize to the case when the observer lies in the equatorial plane of the Kerr black hole, so the coordinates (x, y, z) in Fig. 4.2 coincide with the coordinates (X, Y, Z) in Fig. 4.4. Note that we still consider general source positions.

In Appendix 4.4 we carefully analyze null geodesics seen by an observer in the equatorial plane. By considering constants of the motion, we derive the following lens equation:

$$d_S \tan\mathcal{B} \cos\chi \;=\; d_{LS} \tan\vartheta_S \cos\varphi_S \;+\; d_L \,\frac{\sin\vartheta\cos\varphi}{\cos\vartheta_S}\;, \tag{4.15}$$

$$d_S \tan\mathcal{B} \sin\chi \;=\; d_{LS} \tan\vartheta_S \sin\varphi_S \;+\; \frac{d_L \sin\vartheta}{1-\sin^2\vartheta_S \sin^2\varphi_S} \times \tag{4.16}$$

$$\left[\cos\varphi \sin\vartheta_S \tan\vartheta_S \sin\varphi_S \cos\varphi_S + \left(\sin^2\varphi - \sin^2\vartheta_S \sin^2\varphi_S\right)^{1/2}\right].$$

This is the general form of the lens equation for an equatorial observer in the Kerr metric for observer and source in the asymptotically flat region. It is valid for all light rays, whether they loop around the black hole or not, as long as they lie outside the region of photon capture. No small-angle approximation is required.

Note that eqns. (4.6) and (4.7) represent the general form of the lens equation, with the displacement terms explicitly written, while eqns. (5.3) and (5.4) give the exact lens equation for an equatorial Kerr observer, with the displacement terms implicitly included. Demanding that these two pairs of equations be equivalent allows us to identify the displacement terms for an equatorial Kerr observer:

$$\mathtt{d}_y \;=\; d_L \sin\vartheta\cos\varphi \left(\frac{1}{\cos\vartheta_S} - \frac{1}{\cos\vartheta}\right), \tag{4.17}$$

$$\mathtt{d}_z \;=\; -d_L \tan\vartheta \sin\varphi \;+\; \frac{d_L \sin\vartheta}{1-\sin^2\vartheta_S \sin^2\varphi_S} \times$$

$$\left[\cos\varphi \sin\vartheta_S \tan\vartheta_S \sin\varphi_S \cos\varphi_S + \left(\sin^2\varphi - \sin^2\vartheta_S \sin^2\varphi_S\right)^{1/2}\right]. \tag{4.18}$$

4.3.3 Schwarzschild Case

In the case of a spherically symmetric lens we have $\varphi_S = \varphi + \pi$, and either $\chi = \varphi$ or $\chi = \varphi + \pi$, depending on whether the source lies on the same or opposite side of the lens as the image. Once again, we define $\mathtt{q} = \cos(\chi - \varphi)$ to be a sign that distinguishes these two cases. With these conditions eqns. (5.3) and (5.4) combine to form the single lens equation with displacement for a Schwarzschild black hole:

$$d_S\, \mathtt{q}\, \tan\mathcal{B} = d_L\, \frac{\sin\vartheta}{\cos\vartheta_S}\; -\; d_{LS}\, \tan\vartheta_S\,. \tag{4.19}$$

Two comments are in order. First, our spherical lens equation (4.19) is equivalent to the spherical lens equation recently derived by Bozza and Sereno (2006) (up to the sign $\mathtt{q}$, which was not discussed explicitly in Bozza and Sereno (2006)); see also Bozza (2008a). The second comment refers to the amplitude of the displacement. By comparing our general planar-ray lens equation (4.8) with eqn. (4.19), we can identify the displacement

$$\mathtt{d} = d_L \sin\vartheta \left[\frac{1}{\cos(\alpha - \vartheta)} - \frac{1}{\cos\vartheta}\right], \tag{4.20}$$

where we have switched from ϑ_S to the bending angle $\alpha = \vartheta + \vartheta_S$. Now let $\delta\alpha = \alpha \bmod 2\pi$, and assume that ϑ and $\delta\alpha$ are small. (Note that we need not assume α itself is small, only that $\delta\alpha$ is small. This means that our analysis applies to all light rays, including those that loop around the lens.) Taylor expanding the displacement in ϑ and α yields

$$\mathtt{d} = \frac{d_L}{2}\,(\vartheta\;\delta\alpha)(\delta\alpha - 2\vartheta)\;+\;\mathcal{O}(4).$$

4.4 Exact Kerr Null Geodesics for Equatorial Observers

In this section we determine the equations of motion governing light rays seen by equatorial observers in the Kerr metric. We obtain the exact equations of motion by

considering constants of the motion.

4.4.1 Equations of Motion for Null Geodesics

We first study the equations of motion for a general Kerr null geodesic $\mathcal{C}(\lambda) = (t(\lambda), r(\lambda), \zeta(\lambda), \phi(\lambda))$, where λ is an affine parameter. The geodesic is assumed to be outside the region of photon capture. Two immediate constants of the motion for Kerr geodesics are the energy $\mathcal{E}$ and the orbital angular momentum $\mathcal{L}$. They yield two equations of motion (see, e.g., O'Neill (1995), p. 180):

$$\begin{aligned} \dot{t} &= \frac{g_{\phi\phi}\mathcal{E} + g_{t\phi}\mathcal{L}}{g_{t\phi}^2 - g_{tt}g_{\phi\phi}}\,, \\ \dot{\phi} &= \frac{g_{t\phi}\mathcal{E} + g_{tt}\mathcal{L}}{g_{tt}g_{\phi\phi} - g_{t\phi}^2}\,, \end{aligned}$$

where the dot denotes differentiation relative to the affine parameter λ. Since we only consider unbound light rays, we may assume $\mathcal{E} > 0$. With a suitable fixed choice of affine parameter λ, we henceforth assume that $\mathcal{E}\,\lambda$ has dimension of length. The dimension of the ratio $\mathcal{L}/\mathcal{E}$ is also length. A third constant of motion is nullity, which yields

$$\dot{r} = \pm\left(\frac{-g_{tt}\dot{t}^2 - g_{\zeta\zeta}\dot{\zeta}^2 - g_{\phi\phi}\dot{\phi}^2 - 2g_{t\phi}\dot{t}\dot{\phi}}{g_{rr}}\right)^{1/2}.$$

A fourth constant of motion $\mathcal{Q}$ is the Carter constant, which comes from separating the Hamilton-Jacobi equation (Carter (1968)). We henceforth assume that $\mathcal{Q} \geqslant 0$; i.e., that the light ray either crosses the equatorial plane or asymptotically approaches it (see, e.g., O'Neill (1995), p. 204–205). Employing the notation

$$\hat{\lambda} = \mathcal{E}\,\lambda\,, \qquad \hat{\dot{x}} = \frac{dx}{d\hat{\lambda}}\,, \qquad \hat{\mathcal{L}} = \frac{\mathcal{L}}{\mathcal{E}}\,, \qquad \hat{\mathcal{Q}} = \frac{\mathcal{Q}}{\mathcal{E}^2}\,,$$

the fourth equation of motion can be written

$$\hat{\dot{\zeta}} = \frac{d\zeta}{d\hat{\lambda}} = \pm\frac{(\hat{\mathcal{Q}} + \mathsf{a}^2\sin^2\zeta - \hat{\mathcal{L}}^2\tan^2\zeta)^{1/2}}{r^2 + \mathsf{a}^2\sin^2\zeta} \ . \tag{4.21}$$

Using the metric coefficients (4.10)–(4.14) shown in Section 4.3.1, the null geodesic equations of motion become

$$\hat{\dot{t}} = 1 + \frac{2\mathsf{m}_\bullet r(\mathsf{a}^2 - \mathsf{a}\hat{\mathcal{L}} + r^2)}{[\mathsf{a}^2 + r(r - 2\mathsf{m}_\bullet)](r^2 + \mathsf{a}^2\sin^2\zeta)} \ , \tag{4.22}$$

$$\hat{\dot{r}} = \pm\frac{[r^4 - (\hat{\mathcal{Q}} + \hat{\mathcal{L}}^2 - \mathsf{a}^2)r^2 + 2\mathsf{m}_\bullet((\hat{\mathcal{L}} - \mathsf{a})^2 + \hat{\mathcal{Q}})r - \mathsf{a}^2\hat{\mathcal{Q}}]^{1/2}}{r^2 + \mathsf{a}^2\sin^2\zeta} \ , \tag{4.23}$$

$$\hat{\dot{\phi}} = \frac{2\mathsf{a}\mathsf{m}_\bullet r + \hat{\mathcal{L}}r(r - 2\mathsf{m}_\bullet)\sec^2\zeta + \mathsf{a}^2\hat{\mathcal{L}}\tan^2\zeta}{[\mathsf{a}^2 + r(r - 2\mathsf{m}_\bullet)](r^2 + \mathsf{a}^2\sin^2\zeta)} \ . \tag{4.24}$$

Eqns. (4.21)–(4.24) form the set of equations of motion that we must solve in order to describe null geodesics in the Kerr metric.

4.4.2 Exact Lens Equation for Equatorial Observers

Assuming that the source and equatorial observer are in the asymptotically flat region, we consider now the constants of motion $\hat{\mathcal{L}}$ and $\hat{\mathcal{Q}}$. We can find them by examining the equations of motion in the asymptotically flat region of the spacetime far from the black hole. Formally, this means taking the limits $\mathsf{a}, \mathsf{m}_\bullet \to 0$, in which case the equations of motion reduce to

$$\hat{\dot{t}} = 1 \ , \quad \hat{\dot{r}} = \pm\frac{(r^2 - \hat{\mathcal{Q}} - \hat{\mathcal{L}}^2)^{1/2}}{r} \ , \quad \hat{\dot{\zeta}} = \pm\frac{(\hat{\mathcal{Q}} - \hat{\mathcal{L}}^2\tan^2\zeta)^{1/2}}{r^2} \ , \quad \hat{\dot{\phi}} = \frac{\hat{\mathcal{L}}}{r^2\cos^2\zeta} \ . \tag{4.25}$$

At the position of the observer, the light ray is a straight line described by the angles ϑ and φ. For an equatorial observer, we see from Fig. 4.3 that the three Cartesian

components of the line can be written as

$$\begin{aligned} x(\hat{\lambda}) &= d_L + (\hat{\lambda} - \hat{\lambda}_O)\cos\vartheta\,, \\ y(\hat{\lambda}) &= -(\hat{\lambda} - \hat{\lambda}_O)\sin\vartheta\cos\varphi\,, \\ z(\hat{\lambda}) &= -(\hat{\lambda} - \hat{\lambda}_O)\sin\vartheta\sin\varphi\,, \end{aligned}$$

where $\hat{\lambda}_O$ is the value of the affine parameter at the position of the observer, and the affine parameter range for the line segment is $-d_L/\cos\vartheta + \hat{\lambda}_O \leqslant \hat{\lambda} \leqslant \hat{\lambda}_O$ (recall that $0 < \vartheta < \pi/2$ and that $\hat{\lambda}$ has dimension of length). Next, we convert to spherical coordinates (r, ζ, ϕ) and evaluate r, ζ, $\hat{\dot{r}}$, and $\hat{\dot{\phi}}$ at $\hat{\lambda} = \hat{\lambda}_O$:

$$r(\hat{\lambda}_O) = d_L\ , \quad \zeta(\hat{\lambda}_O) = 0\ , \quad \hat{\dot{r}}\,(\hat{\lambda}_O) = \cos\vartheta\ , \quad \hat{\dot{\phi}}\,(\hat{\lambda}_O) = -\frac{\sin\vartheta\cos\varphi}{d_L}\ . \tag{4.26}$$

Finally, we substitute eqn. (4.26) into eqn. (4.25) to solve for $\hat{\mathcal{L}}$ and $\hat{\mathcal{Q}}$ when $\hat{\lambda} = \hat{\lambda}_O$:

$$\hat{\mathcal{L}}_O = \hat{\dot{\phi}}\, r^2\cos^2\zeta\,\Big|_{\hat{\lambda}=\hat{\lambda}_O} = -d_L\sin\vartheta\cos\varphi\,, \tag{4.27}$$

$$\hat{\mathcal{Q}}_O = \left[r^2\left(1 - \hat{\dot{r}}^{\,2}\right) - \hat{\mathcal{L}}^2\right]\Big|_{\hat{\lambda}=\hat{\lambda}_O} = d_L^2\sin^2\vartheta\sin^2\varphi\,. \tag{4.28}$$

(To be clear, we have labeled these constants of motion with "O" for observer. Note that $\hat{\mathcal{Q}}_O \geqslant 0$. Note also that we could just as well have used $\hat{\dot{r}}$ and $\hat{\dot{\zeta}}$, or $\hat{\dot{\zeta}}$ and $\hat{\dot{\phi}}$, to solve for $\hat{\mathcal{L}}$ and $\hat{\mathcal{Q}}$.) Going further, we define

$$b \equiv \left(\hat{\mathcal{Q}} + \hat{\mathcal{L}}^2\right)^{1/2} = d_L\sin\vartheta \tag{4.29}$$

to be the (absolute) impact parameter of the light ray (since $0 < \vartheta < \pi/2$, $\sin\vartheta$ is positive.) This is clearly a constant of the motion.

We could equally well express the constants of motion in terms of the light ray at the position of the source. To be clear, we write these constants as $\hat{\mathcal{L}}_S$ and $\hat{\mathcal{Q}}_S$. Recall that the position of the source is defined by the angles $(\mathcal{B}, \chi)$, while the direction of

the light ray at the source is defined by the angles (ϑ_S, φ_S). So the three Cartesian components of the light ray at the source can be written as

$$\begin{aligned} x(\hat{\lambda}) &= -d_{LS} + (\hat{\lambda} - \hat{\lambda}_S)\cos\vartheta_S\,, \\ y(\hat{\lambda}) &= d_S\, Y_{\rm src} - (\hat{\lambda} - \hat{\lambda}_S)\sin\vartheta_S\cos\varphi_S\,, \\ z(\hat{\lambda}) &= d_S\, Z_{\rm src} - (\hat{\lambda} - \hat{\lambda}_S)\sin\vartheta_S\sin\varphi_S\,, \end{aligned}$$

where $\hat{\lambda}_S$ is the value of the affine parameter at the position of the source, and the affine parameter range for the line segment is $\hat{\lambda}_S \leqslant \hat{\lambda} \leqslant d_{LS}/\cos\vartheta_S + \hat{\lambda}_S$ (recall that $0 \leqslant \vartheta_S < \pi/2$). Note that for simplicity we have defined

$$Y_{\rm src} \equiv \tan\mathcal{B}\cos\chi\,, \qquad Z_{\rm src} \equiv \tan\mathcal{B}\sin\chi\,.$$

By a computation identical to those in eqns. (4.26) and (4.28), we solve eqn. (4.25) for $\hat{\mathcal{L}}$ and $\hat{\mathcal{Q}}$ when $\hat{\lambda} = \hat{\lambda}_S$ to obtain

$$\hat{\mathcal{L}}_S = -d_S\, Y_{\rm src}\cos\vartheta_S + d_{LS}\sin\vartheta_S\cos\varphi_S\,, \tag{4.30}$$

$$\begin{aligned} \hat{\mathcal{Q}}_S &= d_S^2 Z_{\rm src}^2(\cos^2\vartheta_S + \sin^2\vartheta_S\cos^2\varphi_S) \\ &\quad -2\, d_S\, Z_{\rm src}\,\sin\vartheta_S\sin\varphi_S(d_{LS}\cos\vartheta_S + d_S\, Y_{\rm src}\sin\vartheta_S\cos\varphi_S) \\ &\quad +(d_S^2 Y_{\rm src}^2 + d_{LS}^2)\sin^2\vartheta_S\sin^2\varphi_S\,. \end{aligned} \tag{4.31}$$

Since we are discussing constants of the motion, we must have $\hat{\mathcal{L}}_O = \hat{\mathcal{L}}_S$ and $\hat{\mathcal{Q}}_O = \hat{\mathcal{Q}}_S$. Using eqns. (4.27) and (4.30), the condition $\hat{\mathcal{L}}_O = \hat{\mathcal{L}}_S$ is a trivial linear equation for $Y_{\rm src}$, which yields

$$d_S\tan\mathcal{B}\cos\chi = d_{LS}\tan\vartheta_S\cos\varphi_S \;+\; d_L\,\frac{\sin\vartheta\cos\varphi}{\cos\vartheta_S}\,. \tag{4.32}$$

Using eqns. (4.28) and (4.31), the condition $\hat{\mathcal{Q}}_O = \hat{\mathcal{Q}}_S$ is a quadratic equation in $Z_{\rm src}$,

which yields the following two roots:

$$Z_{\rm src} = \frac{d_{LS}\tan\vartheta_S\sin\varphi_S}{d_S} + \frac{d_L\sin\vartheta}{d_S\left(1-\sin^2\vartheta_S\sin^2\varphi_S\right)}\times \tag{4.33}$$
$$\left[\cos\varphi\sin\vartheta_S\tan\vartheta_S\sin\varphi_S\cos\varphi_S \pm \left(\sin^2\varphi-\sin^2\vartheta_S\sin^2\varphi_S\right)^{1/2}\right].$$

We will take the positive root in eqn. (4.33) because in the case of spherical symmetry only the positive root, taken together with eqn. (4.32), will combine to form eqn. (4.19) in Section 4.3.3. We thus have

$$d_S\tan\mathcal{B}\sin\chi = d_{LS}\tan\vartheta_S\sin\varphi_S + \frac{d_L\sin\vartheta}{1-\sin^2\vartheta_S\sin^2\varphi_S}\times \tag{4.34}$$
$$\left[\cos\varphi\sin\vartheta_S\tan\vartheta_S\sin\varphi_S\cos\varphi_S + \left(\sin^2\varphi-\sin^2\vartheta_S\sin^2\varphi_S\right)^{1/2}\right].$$

Eqns. (4.32) and (4.34) thus constitute the two components of the general lens equation for an equatorial observer in the Kerr metric.

5

Quasi-Equatorial Lensing Observables

5.1 Introduction

This last chapter addresses lensing observables in the regime of quasi-equatorial lensing by a Kerr black hole. First, the full light bending angle is obtained with "horizontal" and "vertical" components for an equatorial observer and light rays that are quasi-equatorial. Next, the lens equation of Chapter 5 is solved perturbatively to second order in ε, which is the ratio of the angular gravitational radius to the angular Einstein radius, to obtain formulas for the lensing observables: image position, image magnification, total unsigned magnification, centroid, and time delay. It is shown that the displacement begins to affect the lensing observables only at second order in ε, and so can safely be ignored for studies of first-order corrections to weak-deflection quasi-equatorial Kerr lensing. The findings presented here also yield new results on the lensing observables in Schwarzschild lensing with displacement.

5.2 Definitions and Assumptions

We work under the following assumptions:

1. The Kerr black hole and the light source are not at cosmological distances, so that $d_S = d_L + d_{LS}$, where d_S and d_L are the perpendicular distances from the observer to the source and lens planes, respectively, and d_{LS} is the perpendicular distance from the lens plane to the source plane;

2. Both the source and observer are in the asymptotically flat region of the Kerr spacetime, and the observer lies in the equatorial plane of the Kerr black hole. This last condition implies that the coordinates (x, y, z) coincide with the Boyer-Lindquist coordinates (X, Y, Z) centered on the black hole (see Fig. 4.4);

3. The source is not required to be incrementally close to the optical axis and can be either on the equatorial plane or slightly off it, so that $\chi = \chi_0 + \delta\chi$, where $\chi_0 = 0$ or π. Similarly, the lift of the light ray off the equatorial plane is small, so that $\varphi = \varphi_0 + \delta\varphi$ and $\varphi_S = \varphi_0 + \pi + \delta\varphi_S$, where $\varphi_0 = 0$ (retrograde motion) or π (prograde motion), and where $\delta\varphi$ and $\delta\varphi_S$ are small and considered only to linear order. We henceforth refer to this as the *quasi-equatorial regime*.

In Chapter 4 we derived the following general lens equation governing lensing by a thin deflector, for source and observer in the asymptotically flat region:

$$d_S \tan\mathcal{B} \cos\chi = d_L \tan\vartheta \cos\varphi + d_{LS} \tan\vartheta_S \cos\varphi_S + \mathtt{d}_y\,, \tag{5.1}$$

$$d_S \tan\mathcal{B} \sin\chi = d_L \tan\vartheta \sin\varphi + d_{LS} \tan\vartheta_S \sin\varphi_S + \mathtt{d}_z\,. \tag{5.2}$$

Here the displacements are shown explicitly; note that $\left(\mathtt{d}_y^2 + \mathtt{d}_z^2\right)^{1/2} = \mathtt{d}$ in Fig. 4.3.

Specializing to the case of an equatorial observer in the Kerr metric, we also derived in Chapter 4 the following lens equation with the displacements implicitly

included:

$$d_S \tan\mathcal{B} \cos\chi \;=\; d_{LS} \tan\vartheta_S \cos\varphi_S \;+\; d_L \,\frac{\sin\vartheta\cos\varphi}{\cos\vartheta_S}\;, \tag{5.3}$$

$$d_S \tan\mathcal{B} \sin\chi \;=\; d_{LS} \tan\vartheta_S \sin\varphi_S \;+\; \frac{d_L \sin\vartheta}{1-\sin^2\vartheta_S \sin^2\varphi_S} \times \tag{5.4}$$

$$\left[\cos\varphi \sin\vartheta_S \tan\vartheta_S \sin\varphi_S \cos\varphi_S + \left(\sin^2\varphi - \sin^2\vartheta_S \sin^2\varphi_S\right)^{1/2}\right].$$

This is valid for all light rays, whether they loop around the black hole or not, as long as they lie outside the region of photon capture. No small-angle approximation is required. Comparing our two lens equations allowed us to extract the displacement terms:

$$\mathtt{d}_y \;=\; d_L \sin\vartheta\cos\varphi \left(\frac{1}{\cos\vartheta_S} - \frac{1}{\cos\vartheta}\right), \tag{5.5}$$

$$\mathtt{d}_z \;=\; -d_L \tan\vartheta \sin\varphi \;+\; \frac{d_L \sin\vartheta}{1-\sin^2\vartheta_S \sin^2\varphi_S} \times$$

$$\left[\cos\varphi \sin\vartheta_S \tan\vartheta_S \sin\varphi_S \cos\varphi_S + \left(\sin^2\varphi - \sin^2\vartheta_S \sin^2\varphi_S\right)^{1/2}\right]. \tag{5.6}$$

5.3 Quasi-Equatorial Kerr Light Bending

With that as background, we begin by calculating the component of the bending angle in the equatorial plane, which is the xy-plane in Fig. 4.3; we call this the "horizontal" component. Due to the technical nature of the calculations, we quote the key results here and refer to Section 5.7 for the detailed treatment. Note from Fig. 4.3 that according to the way the angles ϑ and ϑ_S are defined, they may lift off the xy-plane. Let us define $\hat{\vartheta}$ and $\hat{\vartheta}_S$ to be their projections onto the xy-plane, respectively. Without loss of generality, we choose the same sign conventions for $\hat{\vartheta}$ and $\hat{\vartheta}_S$ as we chose for ϑ and ϑ_S, in which case we can unambiguously write the "horizontal" component of the bending angle as

$$\hat{\alpha}_{\rm hor} = \hat{\vartheta} + \hat{\vartheta}_S \;. \tag{5.7}$$

Note that the positivity of $\hat{\vartheta}$ and the fact that the bending angle is nonnegative forces the condition

$$\hat{\vartheta}_S \geqslant -\hat{\vartheta} \ .$$

(Indeed, with our signs conventions the condition $\hat{\vartheta}_S < -\hat{\vartheta}$ would be equivalent to repulsion of the light ray.) Writing $\hat{\vartheta}$ and $\hat{\vartheta}_S$ in terms of the angles $\vartheta, \varphi, \vartheta_S, \varphi_S$, we have

$$\hat{\vartheta} \ = \ \tan^{-1}(\tan\vartheta\cos\varphi) \ , \tag{5.8}$$

$$\hat{\vartheta}_S \ = \ \tan^{-1}(\tan\vartheta_S\cos(\pi-\varphi_S)) \ . \tag{5.9}$$

As stated in assumption (3) above, in the quasi-equatorial regime we have

$$\varphi = \varphi_0 + \delta\varphi \, , \qquad \varphi_S = \varphi_0 + \pi + \delta\varphi_S \, , \tag{5.10}$$

where φ_0 is either 0 (retrograde motion) or π (prograde motion), while $\delta\varphi$ and $\delta\varphi_S$ are small and considered only to linear order. In this regime eqns. (5.8) and (5.9) simplify to

$$\hat{\vartheta} \ \approx \ \pm\vartheta \ ,$$

$$\hat{\vartheta}_S \ \approx \ \pm\vartheta_S \ .$$

Since $\hat{\vartheta}$ and $\hat{\vartheta}_S$ have the same signs as ϑ and ϑ_S, respectively, we discard the negative solutions, so that eqn. (5.7) reduces to

$$\hat{\alpha}_{\rm hor} \approx \vartheta + \vartheta_S \ , \quad \vartheta_S \geqslant -\vartheta \, . \tag{5.11}$$

Thus in the quasi-equatorial regime we may use the full angles ϑ and ϑ_S in place of their respective projections onto the xy-plane. With that said, we show in eqn. (5.70) of Section 5.7 that the "horizontal" bending of light has the following invariant series expansion:

$$\hat{\alpha}_{\rm hor}(b) \ = \ A_1\left(\frac{\mathsf{m}_\bullet}{b}\right) \ + \ A_2\left(\frac{\mathsf{m}_\bullet}{b}\right)^2 \ + \ A_3\left(\frac{\mathsf{m}_\bullet}{b}\right)^3 \ + \ A_4\left(\frac{\mathsf{m}_\bullet}{b}\right)^4 \ + \ \mathcal{O}\left(\frac{\mathsf{m}_\bullet}{b}\right)^5 , \tag{5.12}$$

where

$$A_1 = 4 \,, \tag{5.13}$$

$$A_2 = \frac{15\pi}{4} - 4\,\mathsf{s}\,\hat{a} \,, \tag{5.14}$$

$$A_3 = \frac{128}{3} - 10\,\pi\,\mathsf{s}\,\hat{a} + 4\,\hat{a}^2 \,, \tag{5.15}$$

$$A_4 = \frac{3465\pi}{64} - 192\,\mathsf{s}\,\hat{a} + \frac{285\pi\,\hat{a}^2}{16} - 4\,\mathsf{s}\,\hat{a}^3 \,. \tag{5.16}$$

The variable s equals ± 1 depending on whether the light ray undergoes prograde $(+1)$ or retrograde (-1) motion (see eqn. (5.57) in Section 5.7 below). Note that eqns. (5.12)–(5.16) are consistent with the bending angle obtained by Iyer & Hansen Iyer and Hansen (2009a) by a different means—note also that their bending angle is consistent with the exact bending angle Iyer and Hansen (2009a,b). We remind the reader of our conventions in Chapter 4. The parameter $\mathsf{m}_\bullet$ is the gravitational radius and a is the angular momentum per unit mass,

$$\mathsf{m}_\bullet = \frac{G\mathcal{M}_\bullet}{c^2} \,, \qquad \mathsf{a} = \frac{\mathcal{J}_\bullet}{c\mathcal{M}_\bullet} \,, \tag{5.17}$$

where $\mathcal{M}_\bullet$ is the mass of the black hole and $\mathcal{J}_\bullet$ its spin angular momentum (see, e.g., Wald (1984), pp. 322–324). Note that both $\mathsf{m}_\bullet$ and a have dimensions of length. The quantity $\hat{a}$ is a dimensionless spin parameter:

$$\hat{a} = \frac{\mathsf{a}}{\mathsf{m}_\bullet} \,.$$

Unless stated to the contrary, the black hole's spin is subcritical; i.e., $\hat{a}^2 < 1$. Finally, $b = d_L \sin\vartheta$ is the impact parameter (see eqn. (4.29) in Chapter 4), which is a constant of the motion.

When there is no spin, the coefficients reduce to $A_1 = 4$, $A_2 = 15\pi/4$, $A_3 = 128/3$, $A_4 = 3465\pi/64$ and recover the Schwarzschild bending angle in Keeton and Petters

(2006b). Also, eqn. (5.12) shows that in the weak-deflection limit (at first order in $\mathtt{m}_\bullet/b$) the Kerr bending angle agrees with the Schwarzschild bending angle. The spin enters only in higher-order correction terms. The sign is such that the spin makes the bending angle *larger* for light rays that follow retrograde motion ($\mathtt{s} = -1$). This makes sense intuitively because retrograde rays spend more time in the presence of the black hole's gravitational pull.

5.4 Observable Properties of Lensed Images

In this section we derive asymptotic formulas for image position, image magnification, total unsigned magnification, centroid, and time delay for quasi-equatorial Kerr lensing with displacement.

5.4.1 Quasi-Equatorial Lens Equation

We begin with our general lens equation (5.18)–(5.19) and insert a bookkeeping parameter ξ to monitor the displacement in either $\mathtt{d}_y$ or $\mathtt{d}_z$:

$$d_S \tan\mathcal{B} \cos\chi \;=\; d_L \tan\vartheta \cos\varphi \;+\; d_{LS} \tan\vartheta_S \cos\varphi_S \;+\; \xi\, \mathtt{d}_y \,, \tag{5.18}$$

$$d_S \tan\mathcal{B} \sin\chi \;=\; d_L \tan\vartheta \sin\varphi \;+\; d_{LS} \tan\vartheta_S \sin\varphi_S \;+\; \xi\, \mathtt{d}_z \,. \tag{5.19}$$

(The displacements $\mathtt{d}_y$ and $\mathtt{d}_z$ are given by eqns. (5.5) and (5.6).) We can take $\xi = 1$ to include the displacements properly, or choose $\xi = 0$ if we wish to ignore the displacements (in order to connect with work in Keeton and Petters (2006b,a)).

Beginning with eqn. (5.18), we substitute eqn. (5.5) in place of $\mathtt{d}_y$ and Taylor expand in the small angles $\delta\varphi$, $\delta\varphi_S$, and $\delta\chi$, to obtain

$$\begin{aligned} \mathtt{q} \tan\mathcal{B} \;=\; & (1-D)\tan\vartheta \;-\; D\tan\vartheta_S \;+\; \xi(1-D)\sin\vartheta \left(\frac{1}{\cos\vartheta_S} - \frac{1}{\cos\vartheta} \right) \\ & +\; \mathcal{O}(2) \,, \end{aligned} \tag{5.20}$$

where $\mathsf{q} = \cos(\chi_0 - \varphi_0)$, $D = d_{LS}/d_S$, and $\mathcal{O}(2)$ indicates terms that are second order in $\delta\varphi$, $\delta\varphi_S$, and/or $\delta\chi$. (Below, we incorporate the sign q into the tangent so that the left-hand side is written as $\tan(\mathsf{q}\mathcal{B})$ and we think of $\mathsf{q}\mathcal{B}$ as the signed source position.) This is the "horizontal" component of the lens equation. Recall that ξ identifies terms associated with the displacement. Including the displacement by setting $\xi = 1$ in eqn. (5.20) yields

$$\mathsf{q}\,\tan\mathcal{B} = (1-D)\frac{\sin\vartheta}{\cos\vartheta_S} - D\tan\vartheta_S \;+\; \mathcal{O}(2)\,.$$

Thus, to lowest order in out-of-plane motion we recover the same lens equation as in the Schwarzschild case (see eqn. (4.19) in Chapter 4).

We use $\vartheta_S = \hat{\alpha}_{\rm hor} - \vartheta$, taking $\hat{\alpha}_{\rm hor}$ from eqn. (5.12), and introduce scaled angular variables:

$$\beta = \frac{\mathsf{q}\mathcal{B}}{\vartheta_E}\;, \quad \theta = \frac{\vartheta}{\vartheta_E}\;, \quad \vartheta_\bullet = \tan^{-1}\left(\frac{\mathsf{m}_\bullet}{d_L}\right)\;, \quad \varepsilon = \frac{\vartheta_\bullet}{\vartheta_E} = \frac{\vartheta_E}{4\,D}\;. \tag{5.21}$$

Here the natural angular scale is given by the angular Einstein ring radius:

$$\vartheta_E = \sqrt{\frac{4G\mathcal{M}_\bullet d_{LS}}{c^2 d_L d_S}} = \sqrt{\frac{4\mathsf{m}_\bullet D}{d_L}}\;. \tag{5.22}$$

Note that we have defined the scaled source position β to be a signed quantity, with a sign that indicates whether the source is on the same or opposite side of the lens as the image. In eqn. (5.12) we wrote the bending angle $\hat{\alpha}_{\rm hor}$ as a series expansion in $\mathsf{m}_\bullet/b$. For analyzing the observable image positions, ε is the more natural expansion parameter. To convert $\hat{\alpha}_{\rm hor}$ into a series expansion in ε, note that according to eqns. (5.21) and (5.22) and the fact that $b = d_L \sin\vartheta$, we have

$$\frac{\mathsf{m}_\bullet}{b} = \frac{4D\,\varepsilon^2}{\sin(4D\,\varepsilon\,\theta)} = \frac{1}{\theta}\,\varepsilon + \frac{8D^2\,\theta}{3}\,\varepsilon^3 + \mathcal{O}(\varepsilon)^5\;. \tag{5.23}$$

As in Keeton and Petters (2006b,a, 2005), we postulate that the solution of the "horizontal" lens equation (5.20) can be written as a series expansion of the form

$$\theta = \theta_0 \, + \, \theta_1 \, \varepsilon \, + \, \theta_2 \, \varepsilon^2 \, + \, \mathcal{O}\left(\varepsilon\right)^3 . \tag{5.24}$$

Converting now to our scaled angular variables (5.21)–(5.24), our quasi-equatorial "horizontal" lens equation (5.20) takes the form

$$\begin{aligned}
\beta \;\; = \;\; & \left[\theta_0 - \frac{1}{\theta_0}\right] \, + \, \frac{1}{\theta_0^2}\left[\mathtt{s}\,\hat{a} - \frac{15\pi}{16} + (1+\theta_0^2)\,\theta_1\right]\,\varepsilon \\
& + \, \frac{1}{24\,\theta_0^3}\Bigg[12\,\mathtt{s}\,\hat{a}\,(5\pi - 4\theta_1) - 24\,\hat{a}^2 - 384 + 3\,\theta_1\,(15\pi - 8\theta_1) + 24\,\theta_0\,\theta_2\,(1+\theta_0^2) \\
& + \, 8\,\theta_0\left(48\,D\,\theta_0 + 8D^2\,\theta_0^2(-2\beta^3 - 7\theta_0 + 2\theta_0^3)\right) + 192\theta_0^2\,(1-D)(1-2\,D\,\theta_0^2)\,\xi\Bigg]\,\varepsilon^2 \\
& + \, \mathcal{O}\left(\varepsilon\right)^3 .
\end{aligned} \tag{5.25}$$

Note that displacement terms (indicated by ξ) only begin to appear at second order. Also, since we are simultaneously expanding $\tan \mathtt{q}\mathcal{B} = \tan(4\,\beta\,D\,\varepsilon)$, note the occurrence of β^3 in the ε^2 term.

Now we turn to the "vertical" component of the lens equation, namely, eqn. (5.19). Substituting eqn. (5.6) in place of $\mathtt{d}_z$ and Taylor expanding in the small angles $\delta\varphi$, $\delta\varphi_S$, and $\delta\chi$, we obtain

$$\begin{aligned}
(\delta\chi)\,(\mathtt{q}\tan\mathcal{B}) \;\; = \;\; & (\delta\varphi)\,(1-\xi)(1-D)\tan\vartheta \;\; - \;\; (\delta\varphi_S)\,D\tan\vartheta_S \\
& + \, \xi(1-D)\sin\vartheta\left\{(\delta\varphi_S\sin\vartheta_S\tan\vartheta_S + \left[(\delta\varphi)^2 - (\delta\varphi_S)^2\sin^2\vartheta_S\right]^{1/2}\right\} \\
& + \, \mathcal{O}\left(2\right).
\end{aligned} \tag{5.26}$$

Next, we use eqn. (5.79) in Section 5.7 to write $(\delta\varphi_S)\,\sin\vartheta_S = (\delta\varphi)\,W(\vartheta)$:

$$\begin{aligned}
(\delta\chi)\,(\mathtt{q}\tan\mathcal{B}) \;\; = \;\; & \delta\varphi\,(1-\xi)(1-D)\tan\vartheta + \delta\varphi\,D\,W(\vartheta)(\cos\vartheta_S)^{-1} \\
& + \;\; \xi(1-D)\sin\vartheta\{\delta\varphi\,W(\vartheta)\tan\vartheta_S + \delta\varphi\left[1 - W(\vartheta)^2\right]^{1/2}\} \; .
\end{aligned} \tag{5.27}$$

(In Section 5.7 we show that $1-W(\vartheta)^2 > 0$, so this equation is never complex-valued.) Finally, we convert to our scaled angular variables (5.21)–(5.24) and expand in ε, obtaining

$$\begin{aligned}
&\left(\beta + \frac{16}{3} D^2 \beta^3 \varepsilon^2 + \mathcal{O}(\varepsilon)^4\right) \delta\chi = \\
&\delta\varphi \left\{ \left[\theta_0 - \frac{1}{\theta_0}\right] + \frac{1}{\theta_0^2}\left[2\,\mathtt{s}\,\hat{a} - \frac{15\pi}{16} + (1+\theta_0^2)\,\theta_1\right]\varepsilon \right. \\
&+ \frac{1}{24\,\theta_0^3}\Big[\mathtt{s}\,\hat{a}\,(90\pi - 96\theta_1) + 2\hat{a}^2 + 45\pi\theta_1 - 24(16+\theta_1^2) + 8\theta_0\left(8D^2\theta_0^3(-7+2\theta_0^2+6\xi)\right. \\
&\left.\left. + \; 3(\theta_2 + \theta_0^2\theta_2 + 8\theta_0\xi) - 24D\theta_0(-2+\xi+2\theta_0^2\xi)\right)\Big]\varepsilon^2 + \; \mathcal{O}(\varepsilon)^3 \right\}. \qquad (5.28)
\end{aligned}$$

This is the "vertical" component of the lens equation. We will use it to obtain a relation between the small angles $\delta\chi$ and $\delta\varphi$. To that end, we divide eqn. (5.28) by eqn. (5.25) to eliminate β:

$$\begin{aligned}
\delta\chi \;\; = \;\; \delta\varphi \; &\left\{ 1 \; + \; \frac{\mathtt{s}\,\hat{a}}{\theta_0(\theta_0^2-1)}\,\varepsilon \right. \qquad (5.29) \\
&+ \frac{\hat{a}}{16\theta_0^2(\theta_0^2-1)^2}\Big[\mathtt{s}\,(-5\pi + 4\theta_0^2(5\pi - 12\theta_1) + 16\theta_1) + 16\hat{a}(1-2\theta_0^2)\Big]\varepsilon^2 \\
&\left. + \mathcal{O}(\varepsilon)^3 \right\}.
\end{aligned}$$

Observe that in general $\delta\chi \neq \delta\varphi$ in the regime of quasi-equatorial lensing. *Thus when $\hat{a} \neq 0$, the light ray's trajectory cannot lie in a plane other than the equatorial plane (in which case $\delta\varphi = \delta\chi = 0$).*

5.4.2 Image Positions

We now solve our "horizontal" lens equation (5.25) term by term to find $\theta_0, \theta_1, \theta_2$, and θ_3. The zeroth-order term is the familiar weak-deflection lens equation for the

Schwarzschild metric,

$$\beta = \theta_0 - \frac{1}{\theta_0} \ , \tag{5.30}$$

which yields the weak-deflection image position

$$\theta_0 = \frac{1}{2}\left(\sqrt{\beta^2+4} + \beta\right) . \tag{5.31}$$

We neglect the negative solution because we have explicitly specified that angles describing image positions are positive. For a source with $\beta > 0$, the negative-parity image is obtained by plugging $-\beta$ in eqn. (5.31); note that eqn. (5.31) will still be positive. (Note also that we are solving for quasi-equatorial images; there may be additional images in the general case.)

Requiring that the first-order term in eqn. (5.25) vanishes yields

$$\theta_1 = \frac{15\pi - 16\,\mathbf{s}\,\hat{a}}{16(\theta_0^2+1)} \ . \tag{5.32}$$

Likewise with the vanishing of the second-order term,

$$\begin{aligned}\theta_2 \ = \ & \frac{1}{24\,\theta_0\,(\theta_0^2+1)}\Bigg[64\left(6 - D(2D + 6(1-D)\theta_0^2 - D\theta_0^4)\right) + 24\hat{a}^2 - 12\,\mathbf{s}\,\hat{a}(5\pi - 4\theta_1) \\ & -3\theta_1(15\pi - 8\theta_1) - 192\theta_0^2(1-D)(1-2D\theta_0^2)\,\xi\Bigg],\end{aligned} \tag{5.33}$$

where we have used eqn. (5.30) to substitute for β in terms of θ_0. Note that the displacement only affects θ_2, not θ_0 and θ_1.

In terms of the source position β, we can write the terms for the positive- and negative-parity images as

$$\begin{aligned}\theta_0^{\pm} \ &= \ \frac{1}{2}\left(\sqrt{\beta^2+4} \pm |\beta|\right), \\ \theta_1^{\pm} \ &= \ \left(1 \mp \frac{|\beta|}{\sqrt{\beta^2+4}}\right)\frac{15\pi - 16\,\mathbf{s}^{\pm}\,\hat{a}}{32} \ ,\end{aligned}$$

where we have written $\mathtt{s}^{\pm}$ to remind ourselves that the two images have different respective values of the prograde/retrograde sign parameter. In fact, we have $\mathtt{s}^{-} = -\mathtt{s}^{+}$. The terms $\theta_2^{\pm}$ as functions of β are similarly obtained, but are too lengthy to be written here. Now thinking of the universal relations studied in Keeton and Petters (2006a), we observe that the zeroth-order terms obey

$$\theta_0^+ \; - \; \theta_0^- = |\beta|, \qquad \theta_0^+ \, \theta_0^- = 1,$$

which are identical to the zeroth-order position relations obeyed by PPN models (see Keeton and Petters (2006a)). The first-order terms have

$$\theta_1^+ \; + \; \theta_1^- = \frac{15\pi}{16} \; + \; \frac{\mathtt{s}^+ \, \hat{a} \, |\beta|}{\sqrt{\beta^2 + 4}} \; .$$

In Keeton and Petters (2006a) it was shown that $\theta_1^+ + \theta_1^-$ is independent of source position for static, spherical black holes in all theories of gravity that can be expressed in the PPN framework. However, as first shown in Werner and Petters (2007), we see that in the presence of spin, $\theta_1^+ + \theta_1^-$ is no longer independent of source position. This is a direct consequence of the fact that one image corresponds to a light ray that follows prograde motion, while the other has retrograde motion. The difference between the second-order components is (cf. Keeton and Petters (2006a))

$$\begin{aligned} \theta_2^+ \; - \; \theta_2^- = \; & - \; 2\hat{a}^2 \sqrt{4+\beta^2} \; + \; \frac{\hat{a}|\beta|(16\hat{a} + 15\pi\mathtt{s}^+)\sqrt{4+\beta^2}}{8(4+\beta^2)^{3/2}} \\ & + \; \frac{-30\pi\mathtt{s}^+\hat{a} + \hat{a}(48\hat{a} + 15\pi\mathtt{s}^+)\,(4+\beta^2)}{8\,(4+\beta^2)^{3/2}} \; + \; \frac{|\beta|\,\mathtt{I}}{256}, \end{aligned}$$

where

$$\mathtt{I} = -4096 + 225\pi^2 + 2048D^2 + 160\pi\mathtt{s}^+\hat{a} - 512\hat{a}^2 + 4096D(1-D)\xi.$$

Plots of the image correction terms θ_1 and θ_2 as functions of the source position β are shown in Fig. 5.1, for a positive-parity image undergoing either prograde ($\mathtt{s} = +1$) or retrograde ($\mathtt{s} = -1$) motion.

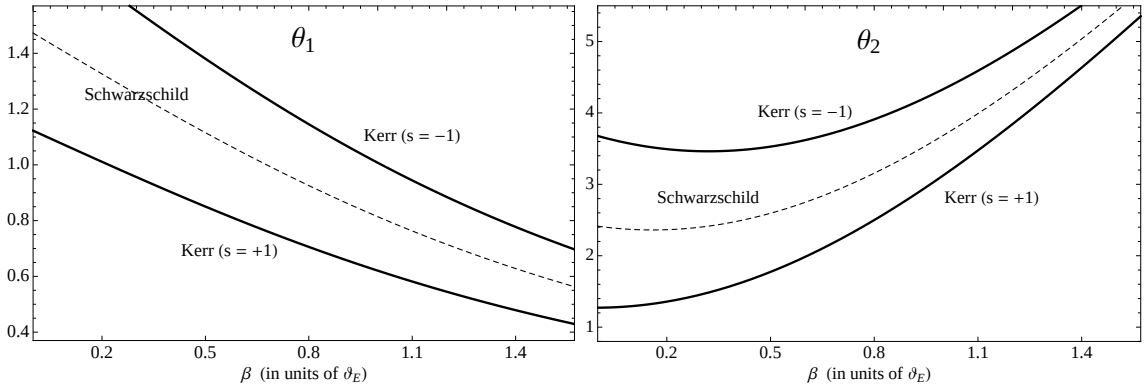

FIGURE 5.1: First- and second- order angular image correction terms as functions of the angular source position β, for a positive-parity image undergoing either prograde ($\mathtt{s} = +1$) or retrograde ($\mathtt{s} = -1$) motion near the equatorial plane of a Kerr black hole. The solid curves represent a Kerr black hole with spin parameter $\hat{a} = 0.7$. When $\hat{a} = 0$, we recover Schwarzschild lensing (dashed curves). For the second- and third- order image corrections, the displacement parameter $\xi = 1$ and $D = d_{LS}/d_S = 0.5$. (Note that θ_1 and θ_2 are dimensionless, but have factors of ε and ε^2, respectively. Note also that d_{LS} and d_S are the perpendicular distances between the lens and source planes and the observer and source plane, respectively.) These results hold for a black hole with sufficiently small ϑ_E.

5.4.3 Magnifications

In Chapter 4 we derived the following general magnification formula:

$$\mu = \left[\frac{\sin \mathcal{B}}{\sin \vartheta} \left(\frac{\partial \mathcal{B}}{\partial \vartheta} \, \frac{\partial \chi}{\partial \varphi} - \frac{\partial \mathcal{B}}{\partial \varphi} \, \frac{\partial \chi}{\partial \vartheta} \right) \right]^{-1} . \tag{5.34}$$

To compute $\partial \mathcal{B}/\partial \vartheta$, we employ the same techniques that led to eqn. (5.25). For $\partial \chi/\partial \varphi$, we use eqn. (5.29). (Note that $\partial \mathcal{B}/\partial \varphi = 0$ for quasi-equatorial lensing.) The result is the following series expansion:

$$\mu = \mu_0 \; + \; \mu_1 \, \varepsilon \; + \; \mu_2 \, \varepsilon^2 \; + \; \mathcal{O}\left(\varepsilon\right)^3 , \tag{5.35}$$

where

$$\mu_0 = \frac{\theta_0^4}{\theta_0^4 - 1} , \tag{5.36}$$

$$\mu_1 = -\frac{[15\pi(\theta_0^2-1)^2 + 64\,\mathtt{s}\,\hat{a}\,\theta_0^2]\,\theta_0^3}{16\,(\theta_0^2-1)^2(\theta_0^2+1)^3} , \tag{5.37}$$

$$\begin{aligned}\mu_2 = \frac{\theta_0^2}{384(\theta_0^2-1)^3(\theta_0^2+1)^5}\Bigg[& 768\,\hat{a}^2\theta_0^4(5-2\theta_0^2+5\theta_0^4) \\ & + 120\pi\mathtt{s}^+\hat{a}(1+16\theta_0^2-34\theta_0^4+44\theta_0^6-39\theta_0^8+12\theta_0^{10}) \\ & + \theta_0^2(\theta_0^2-1)^2\left(-12288D(\theta_0+\ \theta_0^3)^2+1024D^2(1+\theta_0^2)^2(\theta_0^4+16\theta_0^2+1)\right. \\ & \left. - 3\,\theta_0^2\left(4096+\theta_0^2(-675\pi^2+4096(\theta_0^2+2))\right)\right) \\ & - 6144(D-1)\left(\theta_0-\theta_0^5\right)^2(-1+2D\theta_0^2(2+\theta_0^2))\,\xi\Bigg] .\end{aligned} \tag{5.38}$$

Note that displacement terms (indicated by ξ) begin to appear only at second order in ε. In terms of the source position β, we can write the terms for the positive- and negative-parity images as

$$\mu_0^\pm = \frac{1}{2} \pm \frac{\beta^2+2}{2\,|\beta|\sqrt{\beta^2+4}} ,$$

$$\mu_1^\pm = -\frac{15\pi\,\beta^2 + 64\,\mathtt{s}^\pm\,\hat{a}}{16\,\beta^2\,(\beta^2+4)^{3/2}} ,$$

$$\begin{aligned}\mu_2^\pm = & \pm\frac{2025\pi^2 - 1024(\beta^2+4)(12+D(12-(\beta^2+18)D))}{384\,|\beta|\,(\beta^2+4)^{5/2}} \\ & + \frac{5\pi\,\mathtt{s}^\pm\,\hat{a}}{32\,\beta^2}\left[-1 \pm \frac{|\beta|\,(\beta^4+34\beta^2+48)}{(\beta^2+4)^{5/2}}\right] \ \pm\ 2\,\hat{a}^2\,\frac{5\beta^2+8}{|\beta|^3(\beta^2+4)^{5/2}} \\ & + 16\,\xi\,(1-D)\left[D \pm \frac{D(\beta^4+6\beta^2+6)-1}{|\beta|\,(\beta^2+4)^{3/2}}\right].\end{aligned}$$

Observe that

$$
\begin{aligned}
\mu_0^+ \;+\; \mu_0^- \;&=\; 1\,, \\
\mu_0^+ \;-\; \mu_0^- \;&=\; \frac{\beta^2+2}{|\beta|\,(\beta^2+4)^{1/2}}\,, \\
\mu_1^+ \;+\; \mu_1^- \;&=\; -\frac{15\pi}{8(\beta^2+4)^{3/2}}\,, \\
\mu_1^+ \;-\; \mu_1^- \;&=\; -\frac{8\,\mathtt{s}^+\,\hat{a}}{\beta^2(\beta^2+4)^{3/2}}\,, \\
\mu_2^+ \;+\; \mu_2^- \;&=\; \frac{5\pi\,\mathtt{s}^+\,\hat{a}}{16}\frac{|\beta|\,(\beta^4+34\beta^2+48)}{\beta^2(\beta^2+4)^{5/2}} \;+\; 32\,\xi\,D(1-D)\,, \\
\mu_2^+ \;-\; \mu_2^- \;&=\; -\,\frac{5\pi\,\mathtt{s}^+\,\hat{a}}{16\,\beta^2} \;+\; 4\,\hat{a}^2\,\frac{5\beta^2+8}{|\beta|^3(\beta^2+4)^{5/2}} \\
&\quad +\,32\,\xi\,(1-D)\left[\frac{D(\beta^4+6\beta^2+6)-1}{|\beta|\,(\beta^2+4)^{3/2}}\right] \\
&\quad +\,\frac{2025\pi^2-1024(\beta^2+4)(12+D(12-(\beta^2+18)D))}{192\,|\beta|\,(\beta^2+4)^{5/2}}\,.
\end{aligned}
\tag{5.39}
$$

The zeroth-order sum relation is the same as the universal relation found for static, spherical PPN models in Keeton and Petters (2006a). Notice that the zeroth-order difference relation is independent of spin. In the first-order difference relation, the right-hand side is zero for PPN models, but nonzero in the presence of spin (see also Werner and Petters (2007)). In the second-order sum relation, the right-hand side is not zero even in the absence of spin. This is a consequence of the displacement (indicated by ξ).

5.4.4 Critical and Caustic Points

To determine the set of critical points, we set $\mu^{-1} = 0$, the reciprocal of the series expansion given by eqn. (5.35) in Section 5.4.3, and solve for $\theta_0, \theta_1, \theta_2$, and θ_3 (see Aazami et al. (2011a) for a derivation of the third-order term θ_3). This yields the

following θ-components:

$$\theta_{0\,\mathtt{critical}}^{\pm} = 1 \,, \tag{5.40}$$

$$\theta_{1\,\mathtt{critical}}^{\pm} = -\mathtt{s}\,\hat{a} + \frac{15\pi}{32} \,, \tag{5.41}$$

$$\theta_{2\,\mathtt{critical}}^{\pm} = 8 - \frac{15\pi\,\mathtt{s}\,\hat{a}}{32} - \frac{675\pi^2}{2048} + D^2\left(\frac{20}{3} - 8\,\xi\right) + 4D(3\,\xi - 2) - 4\xi \,, \tag{5.42}$$

$$\begin{aligned}\theta_{3\,\mathtt{critical}}^{\pm} = {} & -\mathtt{s}\,\hat{a}\left(\frac{225\pi^2}{256} - 8D^2\,(1-\xi) - 8D\,\xi - 8\right) - \frac{15\pi\,\hat{a}^2}{64} \\ & - \frac{15\pi(400 - 225\pi^2 - 4096D^2(1-\xi) + 2048\,\xi - 2048D(-2+3\,\xi))}{8192} \,,\end{aligned} \tag{5.43}$$

where " $\pm$ " corresponds to the two values $\mathtt{s} = \pm 1$. Note that since we are in the regime of quasi-equatorial Kerr lensing ($\varphi = \varphi_0 + \delta\varphi$ with $\varphi_0 = 0$ (retrograde motion) or π (prograde motion)), eqns. (5.40)–(5.43) do not define a circle on the lens plane, but are to be interpreted (by eqn. (5.58)) as four points $(\theta^{+}_{\mathrm{crit}}, \pi \pm \delta\varphi), (\theta^{-}_{\mathrm{crit}}, \pm\delta\varphi)$ on the lens plane, for a given $\delta\varphi$. We now insert these into the "horizontal" lens equation (5.25) to third order in ε and solve for β. This yields the β-components of the caustic points, which we express here as a series expansion in ε to third order:

$$\begin{aligned}\beta_{\mathtt{caustic}}^{\pm} = {} & -\mathtt{s}\,\hat{a}\,\varepsilon - \frac{5\pi\,\mathtt{s}\,\hat{a}}{16}\,\varepsilon^2 \\ & + \frac{\hat{a}}{512}\Big[1136\pi\,\hat{a} + \mathtt{s}\left(225\pi^2 - 4096\,\xi + 4096D^2(1-2\xi) + 4096D(-2+3\xi)\right)\Big]\,\varepsilon^3 \\ & + \mathcal{O}\,(\varepsilon)^4 \,,\end{aligned} \tag{5.44}$$

The signs $\pm$ correspond to prograde ($\mathtt{s} = +1$) and retrograde ($\mathtt{s} = -1$) motion, respectively. When $\hat{a} = 0$ the two caustic points converge to one point at the origin of the source plane. Note from the third-order term that the caustic points are not symmetric about the vertical axis on the light source plane.

5.4.5 Total Magnification and Centroid

If the two images are too close together to be resolved (as in microlensing), the main observables are the total unsigned magnification and the magnification-weighted centroid position. Using our results above, we compute the total unsigned magnification:

$$\mu_{\rm tot} = |\mu^+| \ + \ |\mu^-| = \frac{\beta^2+2}{|\beta|\,(\beta^2+4)^{1/2}} \ - \ \frac{8\,\mathtt{s}^+\,\hat{a}}{\beta^2(\beta^2+4)^{3/2}}\,\varepsilon \qquad (5.45)$$
$$+\,(\mu_2^+ \ - \ \mu_2^-)\,\varepsilon^2 \ + \ \mathcal{O}\,(\varepsilon)^3\,,$$

where the second-order term is given by eqn. (5.39). The magnification-weighted centroid position (actually, its "horizontal" component, since we are in the regime of quasi-equatorial lensing) is

$$\Theta_{\rm cent} = \frac{\theta^+|\mu^+| - \theta^-|\mu^-|}{|\mu^+| + |\mu^-|} \ = \ \frac{|\beta|\,(\beta^2+3)}{\beta^2+2} \ + \ \frac{(2-\beta^2)\,\mathtt{s}^+\,\hat{a}}{(\beta^2+2)^2}\,\varepsilon$$
$$+ \ \frac{(4+\beta^2)^2\,\mathtt{C}_{2,1}}{384\,|\beta|\,(8+6\beta^2+\beta^4)^3}\,\varepsilon^2 \ + \ \mathcal{O}\,(\varepsilon)^3\,, \qquad (5.46)$$

where

$$\begin{aligned}\mathtt{C}_{2,1} \ = \ & 120\pi\,\mathtt{s}^+\,\hat{a}\,|\beta|\,(2+\beta^2)(3+\beta^2)(4+\beta^2)^{3/2} + 384\,\hat{a}^2\left[(2+\beta^2)(-16-8\beta^2+\beta^4)\right.\\ & \left.+\,4(8+2\beta^2+\beta^4)\right] - \beta^2(2+\beta^2)\left[3(675\pi^2-4096(4+\beta^2))\right.\\ & +\,1024(4+\beta^2)\left(D(6\beta^2-D(-2+9\beta^2+\beta^4))\right.\\ & \left.\left.+3(-1+D)(-\beta^2+2D(6+4\beta^2+\beta^4))\,\xi\right)\right].\end{aligned}$$

In Keeton and Petters (2006a) it was shown that the first-order corrections to the total unsigned magnification and centroid position vanish universally for static, spherical black holes that can be described in the PPN framework. We see that in the presence of spin, the first-order corrections are nonzero (see also Werner and Petters (2007)). Once again, the displacement terms (indicated by ξ) appear only at second order in ε in both eqns. (5.45) and (5.46).

5.4.6 Time Delay

In Appendix 5.8, we show that the lensing time delay can be written as

$$c\tau = T(R_{\rm src}) + T(R_{\rm obs}) - \frac{d_S}{\cos\mathcal{B}} \ ,$$

where

$$R_{\rm obs} = d_L \, , \qquad R_{\rm src} = \left(d_{LS}^2 + d_S^2 \tan^2\mathcal{B}\right)^{1/2} \ , \quad \mathcal{B} = 4\,\beta\,D\,\varepsilon \ ,$$

and $R_{\rm obs}$ and $R_{\rm src}$ are the radial coordinates of the observer and source in the Kerr metric. We derive a Taylor series expansion for the function $T(R)$ in Appendix 5.8 (see eqn. (5.83)). To determine the observable time delay, we evaluate $T(R)$ at $R_{\rm src}$ and $R_{\rm obs}$, and then replace r_0 with b using eqn. (5.63). We change to angular variables using $b = d_L \sin\vartheta$, and then reintroduce the scaled angular variables in eqns. (5.21)–(5.24). Finally, we take a formal Taylor series to second order in our expansion parameter ε. This yields

$$\begin{aligned} \frac{\tau}{\tau_E} \ &= \ \frac{1}{2}\left[1 + \beta^2 - \theta_0^2 - \ln\left(\frac{d_L\,\theta_0^2\,\vartheta_E^2}{4\,d_{LS}}\right)\right] \ + \ \frac{15\pi - 16\,\mathsf{s}\,\hat{a}}{16\,\theta_0}\,\varepsilon \qquad (5.47) \\ &+ \ \frac{\mathtt{T}}{1536\,\theta_0^2\,(\theta_0^2+1)}\,\varepsilon^2 \ + \ \mathcal{O}\,(\varepsilon)^3 \ , \end{aligned}$$

where

$$\begin{aligned} \mathtt{T} \ = \ & -96\pi\,\mathsf{s}\,\hat{a}\,(-7 + \theta_0^2 + \theta_0^4) + 768\,\hat{a}^2\,(2\theta_0^2 + 3\theta_0^4 + \theta_0^6) - (1+\theta_0^2)\left\{675\pi^2\right. \\ & + 3072\,\theta_0^2\,(\theta_0^2+1)\left(2 + \beta^4 + \theta_0 4 - 2\beta^2\,(\theta_0^2+1) - 4\xi\right) \\ & + 3072 D\theta_0^2(1+\theta_0^2)(-8 + \beta^4 + 2\beta^2\theta_0^2 - 3\theta_0^4 + 4\xi + 8\theta_0^2\xi) \\ & \left. + 1024 D^2(1+\theta_0^2)\left(-8 + (24 - 5\beta^4)\theta_0^2 + 5\theta_0^6 - 24\theta_0^4\xi\right)\right\} \ , \qquad (5.48) \end{aligned}$$

and the natural lensing time scale is

$$\tau_E \equiv \frac{d_L d_S}{c\,d_{LS}}\,\vartheta_E^2 = 4\,\frac{\mathsf{m}_\bullet}{c} \ .$$

Notice that retrograde motion ($\mathtt{s} = -1$) leads to a longer time delay than prograde motion ($\mathtt{s} = +1$), which makes sense intuitively. As with our other lensing observables, displacement terms in the time delay (indicated by ξ) begin to appear only at second order in ε.

The differential time delay between the two images, $\Delta\tau = \tau^- - \tau^+$ is such that

$$\begin{aligned}\frac{\Delta\tau}{\tau_E} &= \left[\frac{1}{2}\,|\beta|\,\sqrt{\beta^2+4} + \ln\left(\frac{\sqrt{\beta^2+4}+|\beta|}{\sqrt{\beta^2+4}-|\beta|}\right)\right] + \left[\frac{15\pi}{16}\,|\beta| + \mathtt{s}^+\,\hat{a}\sqrt{\beta^2+4}\right]\varepsilon \\ &\quad + \frac{\mathtt{D}}{1536(\beta^2+4)}\,\varepsilon^2 + \mathcal{O}\left(\varepsilon\right)^3\ , \end{aligned} \tag{5.49}$$

where

$$\begin{aligned}\mathtt{D} &= 96\pi\,\mathtt{s}^+\,\hat{a}\,(4+\beta^2)(7\beta^2-1) - 768\,\hat{a}^2\,|\beta|\sqrt{4+\beta^2} - |\beta|\sqrt{4+\beta^2}\,\left\{-675\pi^2(3+\beta^2)\right. \\ &\quad + 3072(-8+2\beta^2+\beta^4) + 1024D^2(4+\beta^2)(18+5\beta^2-24\xi) \\ &\quad \left. - 3072D(4+\beta^2)(6+\beta^2-8\xi)\right\}.\end{aligned}$$

5.5 Remarks on Lensing Observables

We make a few remarks regarding our results:

1. The procedure for solving the lens equations in the quasi-equatorial regime is as follows: given a source whose (scaled) location on the source plane is $(\beta, \chi_0 + \delta\chi)$, we first solve the "horizontal" lens equation (5.25) term by term to find θ_0, θ_1, and θ_2 (all expressed in terms of β), and then insert these into the "vertical" lens equation (5.29) and solve for $\delta\varphi$. The (scaled) locations of the two images in the lens plane are then

$$\left(\theta_0 + \theta_1^{\pm}\,\varepsilon + \theta_2^{\pm}\,\varepsilon^2\ ,\ \varphi_0 + \delta\varphi^{\pm}\right)\ ,$$

where " $\pm$ " corresponds to $\mathtt{s} = \pm 1$ and where $\varphi_0 = 0$ for retrograde motion ($\mathtt{s} = -1$) and π for prograde motion ($\mathtt{s} = +1$).

2. Note that for all lensing observables—image position, image magnification, total unsigned magnification, centroid, and time delay—the displacement parameter ξ begins to appear only at second order in ε. *Therefore displacement can safely be ignored for studies of first-order corrections to weak-deflection quasi-equatorial Kerr lensing.* Note that the displacement affects the caustic positions only at third order in ε.

3. When there is no spin, we obtain new results on the lensing observables due to Schwarzschild lensing with displacement. Indeed, all of our results in Section 5.4 immediately apply to this regime once we set $\hat{a} = 0$ and the displacement parameter $\xi = 1$. This is equivalent to beginning with the spherically symmetric lens equation with displacement (given in Bozza and Sereno (2006) and eqn. (4.19) in Chapter 4) and then computing lensing observables perturbatively in ε.

4. If one sets $\hat{a} = 0 = \xi$ (i.e., if one turns off spin and ignores displacement), then all of our results in Section 5.4 are consistent with the previous studies of Keeton and Petters (2006b,a).

5. The total magnification and centroid (eqns. (5.45) and (5.46), respectively) are consistent with the corresponding results obtained in Werner and Petters (2007) to first order in ε. (The analysis in Werner and Petters (2007) was carried to first order in ε and did not consider displacement.) In fact we point out that the "horizontal" and "vertical" components of our lens equation (eqns. (5.25) and (5.28)) and our magnification terms (eqns. (5.36) and (5.37)) are all consistent to first order in ε with those in Werner and Petters (2007), after an appropriate change of variables. Furthermore, the "horizontal" and "vertical" components of our bending angle (see eqns. (5.75) and (5.82)

in Section 5.7 below) are also consistent to second order in ε with those in Werner and Petters (2007) (their bending angles were written to second order in ε).

6. Finally, our image correction and magnification terms are also consistent with those in Sereno and De Luca (2006) to first order in ε, while the "horizontal" and "vertical" components of our bending angle are consistent to second order in ε.

5.6 Transformation from Sky Coordinates to Boyer-Lindquist Coordinates

In this section we determine the relation between angular coordinates (ϑ, φ) on the sky as measured by the observer, and the slightly modified Boyer-Lindquist coordinates (t, r, ζ, ϕ) shown in Fig. 4.4.

Recall from Chapter 4 that the latter coincide with the usual Boyer-Lindquist coordinates $(t, r, \wp, \phi)$, except that the polar angle $\wp$ is shifted to $\zeta = \pi/2 - \wp$. To analyze light bending, it is actually convenient to work with another set of coordinates, namely, the lens-centered coordinates (r, Υ, Φ) shown in Fig. 5.2. Our goal is to connect the modified Boyer-Lindquist coordinate angles (ζ, ϕ) to observer-centered angles (ϑ, φ). This will be done in two stages: first, by relating (ζ, ϕ) to (Υ, Φ), and then by relating (Υ, Φ) to (ϑ, φ).

Comparing Fig. 4.4 with Fig. 5.2 below yields the following relation between (ζ, ϕ) and (Υ, Φ):

$$\sin\zeta = \sin\Upsilon \sin\Phi\,, \qquad \tan\phi = \tan\Upsilon \cos\Phi\,. \tag{5.50}$$

In order to relate the observer-centered angles (ϑ, φ) to the lens-centered angles (Υ, Φ), we make the following construction. Consider extending the actual light ray to infinity both "behind" the source and "beyond" the observer. Note that

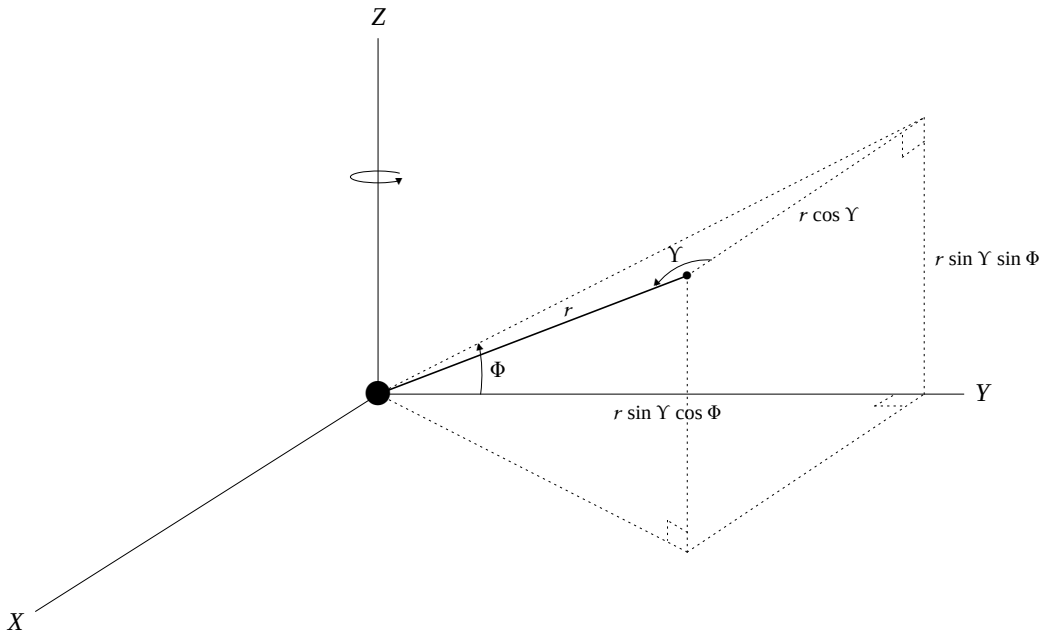

FIGURE 5.2: Lens-centered coordinates (r, Υ, Φ).

evaluating at such points is well-defined because the light ray is a linear path in the asymptotically flat regions where both the source and observer reside. With that said, the asymptotic "final" angular position the light ray reaches is (cf. Section 5.3)

$$\begin{aligned} \Upsilon_f &= \vartheta\,, \qquad \Phi_f = \varphi + \pi \qquad \text{(prograde motion)}, \\ \Upsilon_f &= -\vartheta\,, \qquad \Phi_f = \varphi \qquad \text{(retrograde motion)}. \end{aligned}$$

The asymptotic "initial" angular position from which the light ray originates is

$$\begin{aligned} \Upsilon_i &= \pi - \vartheta_S\,, \qquad \Phi_f = \varphi_S \qquad \text{(prograde motion)}, \\ \Upsilon_i &= \pi + \vartheta_S\,, \qquad \Phi_f = \varphi_S \qquad \text{(retrograde motion)}. \end{aligned}$$

Using eqn. (5.50), we can find the initial and final positions in terms of the angles (ϕ, ζ). For prograde motion, these are:

$$\begin{aligned} \sin\zeta_i &= \sin\vartheta_S \sin\varphi_S\,, & \sin\zeta_f &= -\sin\vartheta\sin\varphi\,, \\ \tan\phi_i &= -\tan\vartheta_S\cos\varphi_S\,, & \tan\phi_f &= -\tan\vartheta\cos\varphi\,. \end{aligned} \tag{5.51}$$

For retrograde motion, they are:

$$\sin\zeta_i = -\sin\vartheta_S \sin\varphi_S\,, \qquad \sin\zeta_f = \sin\vartheta\sin\varphi\,, \tag{5.52}$$
$$\tan\phi_i = \tan\vartheta_S\cos\varphi_S\,, \qquad \tan\phi_f = \tan\vartheta\cos\varphi\,.$$

We will use eqns. (5.51) and (5.52) in our derivation of the "vertical" component of the bending angle vector in Section 5.7.3 below.

5.7 Quasi-Equatorial Kerr Bending Angle

5.7.1 Equations of Motion for Quasi-Equatorial Null Geodesics

Recall from Section A 1 of Chapter 4 that the equations of motion for null geodesics are

$$\hat{\dot{t}} = 1 + \frac{2\mathsf{m}_\bullet\, r(\mathsf{a}^2 - \mathsf{a}\hat{\mathcal{L}} + r^2)}{[\mathsf{a}^2 + r(r-2\mathsf{m}_\bullet)](r^2+\mathsf{a}^2\sin^2\zeta)}\,, \tag{5.53}$$

$$\hat{\dot{r}} = \pm\frac{[r^4 - (\hat{\mathcal{Q}} + \hat{\mathcal{L}}^2 - \mathsf{a}^2)r^2 + 2\mathsf{m}_\bullet((\hat{\mathcal{L}}-\mathsf{a})^2 + \hat{\mathcal{Q}})r - \mathsf{a}^2\hat{\mathcal{Q}}]^{1/2}}{r^2+\mathsf{a}^2\sin^2\zeta}\,, \tag{5.54}$$

$$\hat{\dot{\phi}} = \frac{2\mathsf{a}\mathsf{m}_\bullet r + \hat{\mathcal{L}} r(r-2\mathsf{m}_\bullet)\sec^2\zeta + \mathsf{a}^2\hat{\mathcal{L}}\tan^2\zeta}{[\mathsf{a}^2 + r(r-2\mathsf{m}_\bullet)](r^2+\mathsf{a}^2\sin^2\zeta)}\,. \tag{5.55}$$

$$\hat{\dot{\zeta}} = \pm\frac{(\hat{\mathcal{Q}} + \mathsf{a}^2\sin^2\zeta - \hat{\mathcal{L}}^2\tan^2\zeta)^{1/2}}{r^2+\mathsf{a}^2\sin^2\zeta}\,, \tag{5.56}$$

where $\hat{\mathcal{Q}} = \mathcal{Q}/\mathcal{E}^2$ and $\hat{\mathcal{L}} = \mathcal{L}/\mathcal{E}$, with $\mathcal{E}$ the energy, $\mathcal{L}$ the orbital angular momentum, and $\mathcal{Q}$ the Carter constant $\big(\mathsf{a}$ and $\mathsf{m}_\bullet$ are given by eqn. (5.17)$\big)$. Now consider an equatorial observer and source in the asymptotically flat region. To compute the light bending angle, we focus on null geodesics that remain close to the equatorial plane (which is a plane of reflection symmetry). There are light rays in the equatorial plane that have $\zeta = 0$ everywhere. There are other light rays that remain close to the plane and have $|\zeta| \ll 1$ everywhere. Such quasi-equatorial light rays must have $\varphi = \varphi_0 + \delta\varphi$ with φ_0 equal to either 0 or π, and $|\delta\varphi| \ll 1$. Given the spin configuration, light rays

with $\varphi_0 = 0$ follow retrograde motion and have $\mathcal{L} < 0$, while light rays with $\varphi_0 = \pi$ follow prograde motion and have $\mathcal{L} > 0$. Thus, if we define a sign $\mathtt{s}$ by

$$\mathtt{s} = \mathrm{sign}(\mathcal{L}) = \begin{cases} +1 & \text{prograde motion} \\ -1 & \text{retrograde motion} \end{cases} \tag{5.57}$$

then we can identify

$$\mathtt{s} = -\cos\varphi_0 \,. \tag{5.58}$$

We showed in Chapter 4 that the constants of the motion $\hat{\mathcal{L}}$ and $\hat{\mathcal{Q}}$ can be written as

$$\hat{\mathcal{L}} = -d_L \sin\vartheta \, \cos\varphi \,, \qquad \hat{\mathcal{Q}} = d_L^2 \sin^2\vartheta \, \sin^2\varphi \,.$$

In the quasi-equatorial regime, these become

$$\hat{\mathcal{L}} = \mathtt{s}\, b \, \cos\delta\varphi \,, \qquad \hat{\mathcal{Q}} = b^2 \, \sin^2\delta\varphi \,.$$

We expect $\delta\varphi$ to be of the same order as ζ, so we can Taylor expand eqns. (5.53)–(5.56) in both ζ and $\delta\varphi$. This yields

$$\begin{aligned}
\hat{\dot{t}} &= \frac{r^2}{\mathsf{a}^2 + r(r - 2\mathsf{m}_\bullet)} \left(1 + \frac{\mathsf{a}^2}{r^2} - \frac{2\,\mathsf{m}_\bullet\,\mathsf{a}\,b\,\mathtt{s}}{r^3}\,\mathtt{F} \right) \; + \; \mathcal{O}\left(2\right), \\
\hat{\dot{r}} &= \pm \left(1 - \frac{b^2}{r^2}\,\mathtt{G} + \frac{2\,\mathsf{m}_\bullet\, b^2}{r^3}\,\mathtt{F}^2 \right)^{1/2} \; + \; \mathcal{O}\left(2\right), \qquad (5.59) \\
\hat{\dot{\phi}} &= \frac{b\,\mathtt{s}}{\mathsf{a}^2 + r(r - 2\mathsf{m}_\bullet)} \left(1 - \frac{2\mathsf{m}_\bullet}{r}\,\mathtt{F} \right) \; + \; \mathcal{O}\left(2\right), \qquad (5.60) \\
\hat{\dot{\zeta}} &= \pm \frac{b}{r^2} \left[(\delta\varphi)^2 - \mathtt{G}\,\zeta^2 \right]^{1/2} \; + \; \mathcal{O}\left(2\right), \qquad (5.61)
\end{aligned}$$

where $\mathcal{O}\left(2\right)$ indicate terms that are second order in ζ and/or $\delta\varphi$, and we have defined

$$\mathtt{F} \equiv 1 - \mathtt{s}\,\frac{\mathsf{a}}{b} = 1 - \mathtt{s}\,\hat{a}\,\frac{\mathsf{m}_\bullet}{b} \;, \qquad \mathtt{G} \equiv 1 - \frac{\mathsf{a}^2}{b^2} = 1 - \hat{a}^2\,\frac{\mathsf{m}_\bullet^2}{b^2} \;.$$

Notice that $\dot{t}$, $\dot{r}$, and $\dot{\phi}$ do not depend on ζ or $\delta\varphi$ at zeroth order or first order. In other words, the "in plane" motion is insensitive to small displacements above or below the equatorial plane. By contrast, $\dot{\zeta}$ lacks a zeroth-order term but has a nonzero first-order term. Thus, there is a solution with $\zeta = \delta\varphi = 0$ (i.e., a ray that stays in the equatorial plane), but there are also solutions in which ζ and $\delta\varphi$ are nonzero.

Before evaluating the quasi-equatorial light bending, we need to relate the light ray's coordinate distance of closest approach, r_0, to the invariant impact parameter b. The distance of closest approach is given by the solution of $\dot{r} = 0$. From eqn. (5.59) this is a simple quadratic equation in b, whose positive real solution is

$$\frac{b}{r_0} = \left(\mathtt{G} - \frac{2\mathsf{m}_\bullet}{r_0}\,\mathtt{F}^2\right)^{-1/2}. \tag{5.62}$$

Alternatively, $\dot{r} = 0$ is a cubic equation in r_0, whose one real solution is given by

$$\frac{r_0}{b} = \frac{2}{3^{1/2}}\,\mathtt{G}^{1/2}\cos\left[\frac{1}{3}\cos^{-1}\left(-3^{3/2}\,\frac{\mathtt{F}^2}{\mathtt{G}^{3/2}}\,\frac{\mathsf{m}_\bullet}{b}\right)\right]. \tag{5.63}$$

Taylor expanding in $\mathsf{m}_\bullet/b \ll 1$ yields

$$\begin{aligned}\frac{r_0}{b} \;=\; & \mathtt{G}^{1/2} \;-\; \frac{\mathtt{F}^2}{\mathtt{G}}\left(\frac{\mathsf{m}_\bullet}{b}\right) \;-\; \frac{3\,\mathtt{F}^4}{2\,\mathtt{G}^{5/2}}\left(\frac{\mathsf{m}_\bullet}{b}\right)^2 \;-\; \frac{4\,\mathtt{F}^6}{\mathtt{G}^4}\left(\frac{\mathsf{m}_\bullet}{b}\right)^3 \;-\; \frac{105\,\mathtt{F}^8}{8\,\mathtt{G}^{11/2}}\left(\frac{\mathsf{m}_\bullet}{b}\right)^4 \\ & - \frac{48\,\mathtt{F}^{10}}{\mathtt{G}^7}\left(\frac{\mathsf{m}_\bullet}{b}\right)^5 \;-\; \frac{3003\,\mathtt{F}^{12}}{16\,\mathtt{G}^{17/2}}\left(\frac{\mathsf{m}_\bullet}{b}\right)^6 \;+\; \mathcal{O}\left(\frac{\mathsf{m}_\bullet}{b}\right)^7.\end{aligned} \tag{5.64}$$

(We could further expand $\mathtt{F}$ and $\mathtt{G}$ as Taylor series in $\mathsf{m}_\bullet/b$, but choose not to do that yet.) Note that in the absence of spin ($\mathsf{a} = 0$), $\mathtt{F} = \mathtt{G} = 1$ and so eqns. (5.62)–(5.64) reduce to their respective Schwarzschild values in Keeton and Petters (2006b).

5.7.2 Horizontal Light Bending Angle

We consider the bending of a null geodesic along the ϕ-direction (horizontal). From eqns. (5.59) and (5.60), we can write the equation of motion as

$$\frac{d\phi}{dr} = \frac{\hat{\dot{\phi}}}{\hat{\dot{r}}} = \pm \frac{\mathtt{s}\, b\, r^{1/2}\,(r - 2\,\mathtt{m_\bullet}\,\mathtt{F})}{[\mathtt{a}^2 + r\,(r - 2\mathtt{m_\bullet})][r^3 + b^2\,(2\,\mathtt{m_\bullet}\,\mathtt{F}^2 - \mathtt{G}\,r)]^{1/2}}\ . \tag{5.65}$$

To understand the sign, consider Figs. 4.3 and 4.4. In the case of retrograde motion, $\phi_f = -\hat{\vartheta}$ and $\phi_i = \pi + \hat{\vartheta}_S$, with $\phi_i > \phi_f$ (cf. Section 5.3); recall from Section 5.3 that $\hat{\vartheta}$ and $\hat{\vartheta}_S$ are the respective projections onto the xy-plane of the angles ϑ and ϑ_S. For the "incoming" ray segment (from the source the point of closest approach), we have (see, e.g., (Weinberg, 1972, p. 189)),

$$\phi_i - \phi_0 = \int_{r_0}^{\infty} \left|\frac{d\phi}{dr}\right| dr\,,$$

where ϕ_0 is the value of ϕ at the point of closest approach. For the "outgoing" segment (from the observer the point of closest approach), we have

$$\phi_0 - \phi_f = \int_{r_0}^{\infty} \left|\frac{d\phi}{dr}\right| dr\,.$$

Putting them together yields

$$\pi + \hat{\vartheta}_S + \hat{\vartheta} = \phi_i - \phi_f = 2\int_{r_0}^{\infty} \left|\frac{d\phi}{dr}\right| dr\,.$$

Identifying $\hat{\vartheta} + \hat{\vartheta}_S$ as the "horizontal" bending angle $\hat{\alpha}_{\rm hor}$ (see eqn. (5.7)), we can rewrite this equation in the more familiar form (cf. Keeton and Petters (2006b))

$$\hat{\alpha}_{\rm hor} = 2\int_{r_0}^{\infty} \left|\frac{d\phi}{dr}\right| dr \ - \ \pi\,. \tag{5.66}$$

In the case of prograde motion, we have $\phi_f = \hat{\vartheta}$ and $\phi_i = -(\pi + \hat{\vartheta}_S)$ with $\phi_f > \phi_i$. Similar logic then yields

$$\pi + \hat{\vartheta}_S + \hat{\vartheta} = \phi_f - \phi_i = 2 \int_{r_0}^{\infty} \left| \frac{d\phi}{dr} \right| dr \,. \tag{5.67}$$

Identifying $\hat{\vartheta} + \hat{\vartheta}_S = \hat{\alpha}_{\rm hor}$ again yields eqn. (5.66).

Thus, eqn. (5.66) represents the general expression for the "horizontal" component of the bending angle. The integrand depends on the invariant impact parameter, b, but the integral itself also depends on the coordinate distance of closest approach, r_0. For pedagogical purposes, and to connect with previous studies of lensing by Kerr black holes, it is useful to express the integral purely in terms of r_0, and later to convert back to b.

In the weak-deflection regime, $r - 2\mathsf{m}_\bullet$ and $r - 2\,\mathsf{m}_\bullet\,\mathtt{F}$ are always positive, so all factors in eqn. (5.65) are positive except for $\mathtt{s} = \pm 1$. Hence the absolute value in eqn. (5.66) simply removes the factor of $\mathtt{s}$. Changing integration variables to $x = r_0/r$, we can write the bending angle as

$$\hat{\alpha}_{\rm hor} = 2 \int_0^1 \frac{1 - 2\,\mathtt{F}\,h\,x}{(1 - 2\,h\,x + \hat{a}^2\,h^2\,x^2)\,[\mathtt{G}(1-x^2) - 2\,\mathtt{F}^2\,h(1-x^3)]^{1/2}}\, dx \;-\; \pi \,,$$

where $h = \mathsf{m}_\bullet/r_0$, and we have used eqn. (5.62) to substitute for b in terms of r_0. In the weak-deflection regime $h \ll 1$, so we can expand the integrand as a Taylor series in h and then integrate term by term to obtain

$$\begin{aligned} \hat{\alpha}_{\rm hor}(h) = \;& \mathsf{c}_0\;\pi \;+\; 4\,\mathsf{c}_1\,h \;+\; \left(-4\,\mathsf{c}_2 + \frac{15\pi}{4}\,\mathsf{d}_2\right) h^2 \;+\; \left(\frac{122}{3}\,\mathsf{c}_3 - \frac{15\pi}{2}\,\mathsf{d}_3\right) h^3 \\ & + \;\left(-130\,\mathsf{c}_4 + \frac{3465\pi}{64}\,\mathsf{d}_4\right) h^4 + \mathcal{O}\,(h)^5 \,, \end{aligned} \tag{5.68}$$

where

$$
\begin{aligned}
\mathsf{c}_0 &= \frac{1}{\mathtt{G}^{1/2}} - 1\,, \\
\mathsf{c}_1 &= \frac{\mathtt{F}^2 + \mathtt{G} - \mathtt{F}\,\mathtt{G}}{\mathtt{G}^{3/2}}\,, \\
\mathsf{c}_2 &= \frac{\mathtt{F}^2(\mathtt{F}^2 + \mathtt{G} - \mathtt{F}\,\mathtt{G})}{\mathtt{G}^{5/2}}\,, \\
\mathsf{d}_2 &= \frac{1}{15\,\mathtt{G}^{5/2}}\left[15\,\mathtt{F}^4 - 4\,\mathtt{G}\,(\mathtt{F}-1)\,(3\,\mathtt{F}^2 + 2\,\mathtt{G}) - 2\,\hat{a}^2\,\mathtt{G}^2\right], \\
\mathsf{c}_3 &= \frac{1}{61\,\mathtt{G}^{7/2}}\left[61\,\mathtt{F}^6 - \mathtt{G}\,(\mathtt{F}-1)\,(45\,\mathtt{F}^4 + 32\,\mathtt{F}^2\,\mathtt{G} + 16\,\mathtt{G}^2) - 4\,\mathtt{G}^2\,\hat{a}^2(2\,\mathtt{F}^2 + 2\,\mathtt{G} - \mathtt{F}\,\mathtt{G})\right], \\
\mathsf{d}_3 &= \frac{\mathtt{F}^2}{\mathtt{G}}\,\mathsf{d}_2\,, \\
\mathsf{c}_4 &= \frac{\mathtt{F}^2}{65\,\mathtt{G}^{9/2}}\left[65\,\mathtt{F}^6 - 49(\mathtt{F}-1)\,\mathtt{F}^4\,\mathtt{G} - 8\mathtt{F}^2\,(-4 + \hat{a}^2 + 4\,\mathtt{F})\,\mathtt{G}^2\right. \\
&\qquad \left. + 4\left(4 + \hat{a}^2(\mathtt{F}-2) - 4\,\mathtt{F}\right)\,\mathtt{G}^3\right]\,, \\
\mathsf{d}_4 &= \frac{1}{1155\,\mathtt{G}^{9/2}}\left[1155\,\mathtt{F}^8 - 840(\mathtt{F}-1)\,\mathtt{F}^6\,\mathtt{G} - 140\,\mathtt{F}^4(-4 + \hat{a}^2 + 4\,\mathtt{F})\,\mathtt{G}^2\right. \\
&\qquad \left. + 80(4 + \hat{a}^2(\mathtt{F}-2) - 4\,\mathtt{F})\,\mathtt{F}^2\,\mathtt{G}^3 + 8(16 - 12\hat{a}^2 + \hat{a}^4 + 8(\hat{a}^2 - 2)\,\mathtt{F})\,\mathtt{G}^4\right]\,.
\end{aligned}
$$

(Terms beyond order four in the bending angle series can be derived but are not used in our study.) In the absence of spin, we have $\hat{a} = 0$ and $\mathtt{F} = \mathtt{G} = 1$, so the coefficients become

$$\mathsf{c}_0 = 0, \qquad \mathsf{c}_1 = \mathsf{c}_2 = \mathsf{c}_3 = \mathsf{d}_2 = \mathsf{d}_3 = \mathsf{c}_4 = \mathsf{d}_4 = 1.$$

In this limit, eqn. (5.68) reduces to the Schwarzschild result in Keeton and Petters (2006b).

Let us briefly consider the bending angle to lowest order in $\mathsf{m}_\bullet/r_0$ and a/r_0. At first order, $b \approx r_0$ so from eqn. (5.62) we have $\mathtt{F} \approx 1 - \mathsf{s}\,\mathsf{a}/r_0$ and $\mathtt{G} \approx 1$. This yields

$\mathsf{c}_0 \approx 0$ and $\mathsf{c}_1 \approx 1 - \mathtt{s}\,\mathsf{a}/r_0$. So to lowest order eqn. (5.68) gives

$$\hat{\alpha}_{\rm hor} \approx 4\,\frac{\mathsf{m}_\bullet}{r_0}\,\left(1 - \mathtt{s}\,\frac{\mathsf{a}}{r_0}\right),$$

which recovers the known result for such a regime (see., e.g., Boyer and Lindquist (1967), p. 281).

The expression (5.68) is coordinate-dependent because it involves the coordinate distance of closest approach, r_0. We must rewrite the formula in terms of the impact parameter b to obtain an invariant result. We use eqn. (5.63) to write $h = \mathsf{m}_\bullet/r_0$ as a Taylor series in $\mathsf{m}_\bullet/b$,

$$\begin{aligned} h \;=\; & \frac{1}{\mathtt{G}^{1/2}}\,\left(\frac{\mathsf{m}_\bullet}{b}\right) \;+\; \frac{\mathtt{F}^2}{\mathtt{G}^2}\,\left(\frac{\mathsf{m}_\bullet}{b}\right)^2 \;+\; \frac{5\,\mathtt{F}^4}{2\,\mathtt{G}^{7/2}}\,\left(\frac{\mathsf{m}_\bullet}{b}\right)^3 \;+\; \frac{8\,\mathtt{F}^6}{\mathtt{G}^5}\,\left(\frac{\mathsf{m}_\bullet}{b}\right)^4 \\ & + \frac{231\,\mathtt{F}^8}{8\,\mathtt{G}^{13/2}}\,\left(\frac{\mathsf{m}_\bullet}{b}\right)^5 \;+\; \frac{112\,\mathtt{F}^{10}}{\mathtt{G}^8}\,\left(\frac{\mathsf{m}_\bullet}{b}\right)^6 \;+\; \mathcal{O}\left(\frac{\mathsf{m}_\bullet}{b}\right)^7, \end{aligned} \tag{5.69}$$

and insert this into eqn. (5.68) to obtain a series expansion for the bending angle in $\mathsf{m}_\bullet/b$:

$$\hat{\alpha}_{\rm hor}(b) \;=\; C_0 \;+\; C_1\left(\frac{\mathsf{m}_\bullet}{b}\right) \;+\; C_2\left(\frac{\mathsf{m}_\bullet}{b}\right)^2 \;+\; C_3\left(\frac{\mathsf{m}_\bullet}{b}\right)^3 \;+\; C_4\left(\frac{\mathsf{m}_\bullet}{b}\right)^4 \;+\; \mathcal{O}\left(\frac{\mathsf{m}_\bullet}{b}\right)^5, \tag{5.70}$$

where

$$
\begin{aligned}
C_0 &= \left(\frac{1}{\mathtt{G}^{1/2}} - 1\right)\pi\,, \\
C_1 &= 4\,\frac{\mathtt{F}^2 + \mathtt{G} - \mathtt{F}\,\mathtt{G}}{\mathtt{G}^2}\,, \\
C_2 &= \frac{\pi}{4\,\mathtt{G}^{7/2}}\left[15\,\mathtt{F}^4 - 4\,\mathtt{G}\,(\mathtt{F}-1)\,(3\,\mathtt{F}^2 + 2\,\mathtt{G}) - 2\,\hat{a}^2\,\mathtt{G}^2\right], \\
C_3 &= \frac{8}{3\,\mathtt{G}^5}\left[16\mathtt{F}^6 - 4\,\mathtt{G}\,(\mathtt{F}-1)\,(3\,\mathtt{F}^4 + 2\,\mathtt{F}^2\,\mathtt{G} + \mathtt{G}^2) - \hat{a}^2\,\mathtt{G}^2(2\,\mathtt{F}^2 + 2\,\mathtt{G} - \mathtt{F}\,\mathtt{G})\right]\,, \\
C_4 &= \frac{3\pi}{64\,\mathtt{G}^{13/2}}\left[1155\,\mathtt{F}^8 - 840(\mathtt{F}-1)\mathtt{F}^6\,\mathtt{G} - 140\,\mathtt{F}^4\,(-4 + \hat{a}^2 + 4\,\mathtt{F})\,\mathtt{G}^2\right. \\
&\qquad \left. + 80\left(4 + \hat{a}^2(\mathtt{F}-2) - 4\,\mathtt{F}\right)\,\mathtt{F}^2\,\mathtt{G}^3 + 8\left(16 - 12\hat{a}^2 + \hat{a}^4 + 8(\hat{a}^2 - 2)\,\mathtt{F}\right)\,\mathtt{G}^4\right].
\end{aligned}
$$

Eqn. (5.70) holds for values of $\mathtt{F}$ and $\mathtt{G}$ where the spin is bounded, $\hat{a}^2 < 1$. In other words, when expanding in $\mathsf{m}_\bullet/b$ we really ought to expand in a/b as well. Formally, we may accomplish this by writing $\mathtt{F}$ and $\mathtt{G}$ in terms of $\hat{a}$ and $\mathsf{m}_\bullet/b$ as in eqn. (5.62), expanding the coefficients C_i as Taylor series in $\mathsf{m}_\bullet/b$, and collecting terms to obtain a new series expansion for the bending angle. The result is:

$$
\hat{\alpha}_{\rm hor}(b) \;=\; A_1\left(\frac{\mathsf{m}_\bullet}{b}\right) \;+\; A_2\left(\frac{\mathsf{m}_\bullet}{b}\right)^2 \;+\; A_3\left(\frac{\mathsf{m}_\bullet}{b}\right)^3 \;+\; A_4\left(\frac{\mathsf{m}_\bullet}{b}\right)^4 \;+\; \mathcal{O}\left(\frac{\mathsf{m}_\bullet}{b}\right)^5,
$$

where

$$
A_1 = 4\,, \tag{5.71}
$$

$$
A_2 = \frac{15\pi}{4} - 4\,\mathsf{s}\,\hat{a}\,, \tag{5.72}
$$

$$
A_3 = \frac{128}{3} - 10\,\pi\,\mathsf{s}\,\hat{a} + 4\,\hat{a}^2\,, \tag{5.73}
$$

$$
A_4 = \frac{3465\pi}{64} - 192\,\mathsf{s}\,\hat{a} + \frac{285\pi\,\hat{a}^2}{16} - 4\,\mathsf{s}\,\hat{a}^3\,. \tag{5.74}
$$

(Recall that $\hat{a}^2 < 1$.) When there is no spin ($\hat{a} = 0$), the coefficients reduce to

$A_1 = 4$, $A_2 = 15\pi/4$, $A_3 = 128/3$, $A_4 = 3465\pi/64$ and recover the Schwarzschild values in Keeton and Petters (2006b).

Note that in our scaled angular variables (5.21)–(5.24), the "horizontal" bending angle to third order in ε is

$$\begin{aligned}\hat{\alpha}_{\rm hor}(\varepsilon) &= \frac{4}{\theta_0}\,\varepsilon + \frac{15\pi + 16\,\mathtt{s}\,\hat{a} - 16\theta_1}{4\theta_0^2}\,\varepsilon^2 \\ &+ \frac{256 + 24\,\hat{a}^2 - 60\pi\,\mathtt{s}\,\hat{a} + 64D^2\theta_0^4 - 45\pi\theta_1 + 48\,\mathtt{s}\,\hat{a}\,\theta_1 + 24\theta_1^2 - 24\theta_0\theta_2}{6\theta_0^3}\,\varepsilon^3 \\ &+ \mathcal{O}\left(\varepsilon\right)^4 \ .\end{aligned} \tag{5.75}$$

5.7.3 Vertical Bending Angle

This section presents new results on the vertical component of the bending angle in quasi-equatorial lensing. From eqns. (5.59) and (5.61), the quasi-equatorial light bending in the ζ-direction is governed by the equation of motion

$$\frac{d\zeta}{dr} = \frac{\hat{\dot{\zeta}}}{\hat{\dot{r}}} = \pm i(r)\,\left[\frac{(\delta\varphi)^2}{\mathtt{G}} - \zeta^2\right]^{1/2},$$

where

$$i(r) = \frac{b\,\mathtt{G}^{1/2}}{(r^4 - b^2\,\mathtt{G}\,r^2 + 2\mathtt{m}_\bullet\,b^2\,\mathtt{F}^2\,r)^{1/2}}\ . \tag{5.76}$$

The equation of motion has solutions of the form

$$\zeta(r) = \frac{\delta\varphi}{\mathtt{G}^{1/2}}\ \sin\left[\pm I(r) + p\right]\ ,$$

where

$$I(r) = \int_{r_0}^{r} i(r')\,dr'\,, \tag{5.77}$$

and p is a constant of integration. We are interested in the two asymptotic values ($r \to \infty$),

$$\zeta_\pm = \frac{\delta\varphi}{\mathtt{G}^{1/2}} \, \sin\left(\pm I_\infty + p\right) \, ,$$

where $I_\infty = \lim_{r\to\infty} I(r)$. We can eliminate p and relate the two solutions to one another:

$$\zeta_- = -\frac{\delta\varphi}{\mathtt{G}^{1/2}} \, \sin\left[-2I_\infty + \sin^{-1}\left(\frac{\mathtt{G}^{1/2}}{\delta\varphi} \, \zeta_+\right)\right] . \tag{5.78}$$

The asymptotic values $\zeta_\pm$ must correspond to the initial and final values, ζ_i and ζ_f, introduced in Section 5.6, but we must determine the correspondence. In order to do that, we first examine ζ_i and ζ_f more carefully, using eqn. (5.51). Recall that in the quasi-equatorial regime we have $\varphi = \varphi_0 + \delta\varphi$ and $\varphi_S = \varphi_0 + \pi + \delta\varphi_S$, with $\varphi_0 = \pi$ for prograde motion and $\varphi_0 = 0$ for retrograde motion. Using these relations, eqns. (5.51) and (5.52) both become

$$\sin\zeta_i = \sin\vartheta_S \, \sin\delta\varphi_S, \quad \sin\zeta_f = \sin\vartheta \, \sin\delta\varphi \, .$$

Since we are working to first order in ζ and $\delta\varphi$, we can write these as

$$\zeta_i = \delta\varphi_S \, \sin\vartheta_S \, , \qquad \zeta_f = \delta\varphi \, \sin\vartheta \, .$$

Upon considering the spherical case (see below), we recognize that we want to put $\zeta_- = \zeta_i$ and $\zeta_+ = \zeta_f$ in eqn. (5.78). This substitution yields

$$\delta\varphi_S = \frac{\delta\varphi}{\mathtt{G}^{1/2}\sin\vartheta_S} \, \sin\left[-2I_\infty + \sin^{-1}\left(\mathtt{G}^{1/2}\sin\vartheta\right)\right] \equiv \frac{W(\vartheta)}{\sin\vartheta_S}\delta\varphi \, . \tag{5.79}$$

Notice that the coefficient of $\delta\varphi$ depends only on ϑ, not on φ. (In addition to the explicit ϑ dependence, there is implicit dependence through ϑ_S and I_∞, which

depends on $b = d_L \sin\vartheta$.) We can therefore define it to be the function $W(\vartheta)$, with a factor of $\sin\vartheta_S$ that will prove to be convenient later.

Before evaluating I_∞, let us check the case of a spherical lens to make sure our result is reasonable. For a spherical lens, $\mathsf{a} = 0$ and $\mathtt{F} = \mathtt{G} = 1$, so we have

$$2I_\infty = 2\int_{r_0}^{\infty} \frac{b\,dr}{r^{1/2}[r^3 - b^2(r - 2\mathsf{m}_\bullet)]^{1/2}} = \pi + \vartheta_S + \vartheta\,,$$

where the last equality is obtained after comparison with the spherical limits of eqns. (5.65) and (5.66). Together with our choices $\zeta_- = \zeta_i$ and $\zeta_+ = \zeta_f$, eqn. (5.79) then becomes

$$\delta\varphi_S = \frac{\delta\varphi}{\sin\vartheta_S}\,\sin\left[-\pi - \vartheta_S - \vartheta + \sin^{-1}(\sin\vartheta)\right] = \delta\varphi\,,$$

which is consistent with the symmetry. This verifies our choice of signs above.

We now evaluate the integral (for the general case, not just the spherical limit), in parallel with the analysis in Section 5.7.2. From eqns. (5.76) and (5.77) we have

$$I_\infty = \int_{r_0}^{\infty} \frac{b\,\mathtt{G}^{1/2}}{(r^4 - b^2\,\mathtt{G}\,r^2 + 2\mathsf{m}_\bullet\,b^2\,\mathtt{F}^2\,r)^{1/2}}\,dr\,.$$

Using eqn. (5.62) for b and changing integration variables to $x = r_0/r$ yields

$$I_\infty = \int_0^1 \frac{\mathtt{G}^{1/2}}{[\mathtt{G}(1-x^2) - 2\,\mathtt{F}^2\,h(1-x^3)]^{1/2}}\,dx\,,$$

where $h = \mathsf{m}_\bullet/r_0$. Taylor expanding in h and integrating term by term gives

$$\begin{aligned} I_\infty \;=\; & \frac{\pi}{2} + \frac{2\,\mathtt{F}^2}{\mathtt{G}}\,h + \frac{\mathtt{F}^4}{8\,\mathtt{G}^2}(15\pi - 16)\,h^2 + \frac{\mathtt{F}^6}{12\,\mathtt{G}^3}(244 - 45\pi)\,h^3 \\ & + \frac{5\mathtt{F}^8}{128\,\mathtt{G}^4}(-1664 + 693\pi)\,h^4 + \mathcal{O}\,(h)^5\,. \end{aligned}$$

We now use eqn. (5.69) to write h in terms of $\mathsf{m}_\bullet/b$, and then collect terms to obtain

$$I_\infty = \frac{\pi}{2} \; + \; \frac{2\,\mathtt{F}^2}{\mathtt{G}^{3/2}}\left(\frac{\mathsf{m}_\bullet}{b}\right) \; + \; \frac{15\pi\,\mathtt{F}^4}{8\,\mathtt{G}^3}\left(\frac{\mathsf{m}_\bullet}{b}\right)^2 \; + \; \frac{64\,\mathtt{F}^6}{3\,\mathtt{G}^{9/2}}\left(\frac{\mathsf{m}_\bullet}{b}\right)^3 \; + \; \frac{3465\pi\,\mathtt{F}^8}{128\,\mathtt{G}^6}\left(\frac{\mathsf{m}_\bullet}{b}\right)^4 + \mathcal{O}\left(\frac{\mathsf{m}_\bullet}{b}\right)^5.$$

As in eqn. (5.71), when we expand in $\mathsf{m}_\bullet/b$ we ought to expand in a/b as well. We use eqn. (5.62) to write $\mathtt{F}$ and $\mathtt{G}$ in terms of $\hat{a}$ and $\mathsf{m}_\bullet/b$, and then collect terms to find

$$\begin{aligned} I_\infty \;\; = \;\; & \frac{\pi}{2} \; + \; 2\left(\frac{\mathsf{m}_\bullet}{b}\right) \; + \; \left(\frac{15\pi}{8} - 4\,\mathtt{s}\,\hat{a}\right)\left(\frac{\mathsf{m}_\bullet}{b}\right)^2 \; + \; \left(\frac{64}{3} - \frac{15\pi\,\mathtt{s}\,\hat{a}}{2} + 5\hat{a}^2\right)\left(\frac{\mathsf{m}_\bullet}{b}\right)^3 \\ & + \left(\frac{3465\pi}{128} - 128\,\mathtt{s}\,\hat{a} + \frac{135\pi\,\hat{a}^2}{8} - 6\,\mathtt{s}\,\hat{a}^3\right)\left(\frac{\mathsf{m}_\bullet}{b}\right)^4 \; + \; \mathcal{O}\left(\frac{\mathsf{m}_\bullet}{b}\right)^5. \end{aligned} \tag{5.80}$$

This is to be used with eqn. (5.79) to describe the "vertical" bending (see eqn. (5.29) in Section 5.4.1 above). Note also that the expression inside the square root in eqn. (5.27) is

$$\begin{aligned} 1 - W(\vartheta)^2 \;\; = \;\; & 1 - \left(\frac{1}{\mathtt{G}^{1/2}}\,\sin\left[-2I_\infty + \sin^{-1}\left(\mathtt{G}^{1/2}\sin\vartheta\right)\right]\right)^2 \\ = \;\; & \left(1 - \sin^2\vartheta\right) + 4\sin 2\vartheta\,\left(\frac{\mathsf{m}_\bullet}{b}\right) \\ & - \left[16\cos 2\vartheta + \left(-\frac{15\pi}{4} + 8\,\mathtt{s}\,\hat{a}\right)\sin 2\vartheta\right]\,\left(\frac{\mathsf{m}_\bullet}{b}\right)^2 \\ & - \left[(30\pi - 64\,\mathtt{s}\,\hat{a})\cos 2\vartheta + \hat{a}\,(15\pi\,\mathtt{s} - 10\,\hat{a})\sin 2\vartheta - 4\,\hat{a}^2\tan\vartheta\right]\,\left(\frac{\mathsf{m}_\bullet}{b}\right)^3 \\ & + \; \mathcal{O}\left(\frac{\mathsf{m}_\bullet}{b}\right)^4. \end{aligned}$$

Since $0 < \vartheta < \pi/2$ and $\mathsf{m}_\bullet/b \ll 1$, this expression is nonnegative.

Finally, analogously to the "horizontal" component of the bending angle derived in Section 5.3, we derive the "vertical" component of the bending angle, as follows. Consider the angles ν_i and ν_f shown in Fig. 4.3. We define ν_f to be strictly

nonnegative and within the interval $[0, \pi/2)$, but allow ν_i to be negative, so that $-\pi/2 < \nu_i < \pi/2$, and enforce the following sign convention for ν_i. As shown in Fig. 4.3, ν_i is the angle whose vertex is the point B' on the lens plane, and is measured from a line parallel to the equatorial plane. If ν_i goes *away* from the equatorial plane, then we take it to be positive; otherwise it is negative (e.g., the ν_i shown in Fig. 4.3 is positive). Now denote by $\hat{\nu}_i$ and $\hat{\nu}_f$ the respective projections onto the xz-plane of the angles ν_i and ν_f, and adopt the same sign conventions for them. With these conventions, the "vertical" component of the bending angle can be unambiguously expressed as

$$\hat{\alpha}_{\rm vert} = \hat{\nu}_f - \hat{\nu}_i \ .$$

By the positivity of $\hat{\nu}_f$ and the fact that the bending is nonnegative, we have

$$\hat{\nu}_i \leqslant \hat{\nu}_f \ .$$

(Indeed, with our signs conventions the condition $\hat{\nu}_i > \hat{\nu}_f$ would be equivalent to repulsion of the light ray.) Writing $\hat{\nu}_i$ and $\hat{\nu}_f$ in terms of the angles $\vartheta, \varphi, \vartheta_S, \varphi_S$, we have

$$\begin{aligned} \hat{\nu}_f &= \tan^{-1}(\tan\vartheta \sin\varphi) \ , \\ \hat{\nu}_i &= \tan^{-1}(\tan\vartheta_S \sin(\pi - \varphi_S)) \ , \end{aligned}$$

which in the quasi-equatorial regime reduce to

$$\begin{aligned} \hat{\nu}_f &\approx \pm\delta\varphi \tan\vartheta \ , \\ \hat{\nu}_i &\approx \mp\delta\varphi_S \tan\vartheta_S \ , \end{aligned}$$

where we have set $\varphi = \varphi_0 + \delta\varphi$, $\delta\varphi_S = \varphi_0 + \pi + \delta\varphi_S$, with $\varphi_0 = 0$ (retrograde motion) or π (prograde motion), and expanded to linear order in the small angles $\delta\varphi$ and $\delta\varphi_S$. Using the identities $W(\vartheta)\,\delta\varphi = \sin\vartheta_S\,\delta\varphi_S$ and $\vartheta_S = \hat{\alpha}_{\rm hor} - \vartheta$ given by

eqns. (5.79) and (5.11), we can thus write $\hat{\alpha}_{\rm vert}$ as

$$\hat{\alpha}_{\rm vert} \approx \pm\,\delta\varphi \left[\tan\vartheta + \frac{W(\vartheta)}{\cos(\hat{\alpha}_{\rm hor} - \vartheta)} \right] \ .$$

The expression inside the square brackets is of the form $16D\,\csc\vartheta\,\sec^2\vartheta\,\varepsilon^2 + \mathcal{O}\,(\varepsilon)^4$, so it is positive (recall that $0 < \vartheta < \pi/2$). Since the bending angle is strictly nonnegative, we will adopt " $+$ " for $\delta\varphi \geqslant 0$ and " $-$ " for $\delta\varphi < 0$, so that we may write

$$\hat{\alpha}_{\rm vert} \approx \delta\varphi \left[\tan\vartheta + \frac{W(\vartheta)}{\cos(\hat{\alpha}_{\rm hor} - \vartheta)} \right] \ . \tag{5.81}$$

We now expand eqn. (5.81) in our scaled angular variables (5.21)–(5.24) to third order in ε to obtain

$$\begin{aligned}
\hat{\alpha}_{\rm vert}(\varepsilon) \ &\approx \ \delta\varphi \left\{ \tan\vartheta + \frac{1}{\mathtt{G}^{1/2}} \sin\left[-2I_\infty + \sin^{-1}\left(\mathtt{G}^{1/2} \sin\vartheta \right) \right] \frac{1}{\cos(\hat{\alpha}_{\rm hor} - \vartheta)} \right\} \\
&= \ \delta\varphi \left\{ \frac{4}{\theta_0}\,\varepsilon + \frac{15\pi - 32\,\mathtt{s}\,\hat{a} - 16\theta_1}{4\theta_0^2}\,\varepsilon^2 \right. \\
&\qquad + \frac{256 + 72\,\hat{a}^2 - 90\pi\,\mathtt{s}\,\hat{a} + 64D^2\theta_0^4 + 96\,\mathtt{s}\,\hat{a}\,\theta_1 - 45\pi\theta_1 + 24\theta_1^2 - 24\theta_0\theta_2}{6\theta_0^3}\,\varepsilon^3 \\
&\qquad \left. + \mathcal{O}\,(\varepsilon)^4 \right\} \ .
\end{aligned} \tag{5.82}$$

The result in eqn. (5.82) is new.

5.8 Quasi-Equatorial Time Delay

We now compute the time delays for quasi-equatorial lensed images. Let $R_{\rm src}$ and $R_{\rm obs}$ be the radial coordinates of the source and observer, respectively. From geometry relative to the flat metric of the distant observer, who is assumed to be at rest

in the Boyer-Lindquist coordinates, we can work out

$$R_{\rm obs} = d_L\,, \qquad R_{\rm src} = \left(d_{LS}^2 + d_S^2 \tan^2 \mathcal{B}\right)^{1/2}\,.$$

The radial distances are very nearly the same as angular diameter distances since the source and observer are in the asymptotically flat region of the spacetime. In the absence of the lens, the spacetime would be flat and the light ray would travel along a linear path of length $d_S/\cos\mathcal{B}$ from the source to the observer.

The time delay is the difference between the light travel time for the actual ray, and the travel time for the ray the light would have taken had the lens been absent. This can be written as

$$c\tau = T(R_{\rm src}) + T(R_{\rm obs}) - \frac{d_S}{\cos\mathcal{B}}\ ,$$

with

$$T(R) = \int_{r_0}^{R} \left|\frac{dt}{dr}\right|\, dr = \int_{r_0}^{R} \left|\frac{\dot t}{\dot r}\right|\, dr\,.$$

We use $\dot t$ and $\dot r$ from eqns. (5.59) and (5.59), substitute for b using eqn. (5.62), and change integration variables to $x = r_0/r$. This yields

$$T(R) = r_0 \int_{r_0/R}^{1} \frac{(\mathtt{G} - 2\,\mathtt{F}^2\,h)^{1/2}(1 + \hat a^2\,h^2\,x^2) - 2\,\mathtt{s}\,\hat a\,\mathtt{F}\,h^2\,x^3}{x^2\,(1 - 2\,h\,x + \hat a^2\,h^2\,x^2)\ [\mathtt{G}(1-x^2) - 2\,\mathtt{F}^2\,h(1-x^3)]^{1/2}}\ dx\,,$$

where $h = \mathsf{m}_\bullet/r_0$. We expand the integrand as a Taylor series in h and integrate term by term. The result is a series in h whose coefficients are rational functions of

$\omega = r_0/R$. The first three terms in the expansion are

$$T(R) = \sqrt{R^2 - r_0^2} + h\, r_0 \left[\frac{\mathtt{F}^2\sqrt{1-\omega^2}}{\mathtt{G}(1+\omega)} + 2\ln\left(\frac{1+\sqrt{1-\omega^2}}{\omega}\right)\right] \tag{5.83}$$

$$+ h^2\, r_0 \left[\frac{3\,\mathtt{F}^4 + 4\,\mathtt{F}^2\,\mathtt{G} + 8\,\mathtt{G}^2}{2\,\mathtt{G}^2}\left(\frac{\pi}{2} - \sin^{-1}\omega\right) - 2\,\mathtt{s}\,\hat{a}\,\mathtt{F}\,\mathtt{G}^{-1/2}\sqrt{1-\omega^2}\right.$$

$$\left. - \frac{\mathtt{F}^2\,(4\,\mathtt{G} + (\mathtt{F}^2 + 4\,\mathtt{G})\omega)\sqrt{1-\omega^2}}{2\,\mathtt{G}^2\,(1+\omega)^2}\right] + \mathcal{O}\,(h)^3 \ .$$

The third-order term is easily obtained, and is needed in the derivation of eqn. (5.48), but is too unweildy to write here. Note that if we substitute for F and G using eqn. (5.62) and take the far-field limit, we recover previous results (e.g., Dymnikova (1984, 1986)).

6

Future Goals

One of my future explorations is a systematic study of magnification relations in the Kerr black hole geometry in the non-quasi-equatorial case.

Bibliography

Aazami, A. and Petters, A. (2009a), "A universal magnification theorem for higher-order caustic singularities," *Journal of Mathematical Physics*, 50, 032501.

Aazami, A. and Petters, A. (2009b), "A universal magnification theorem. II. Generic caustics up to codimension five," *Journal of Mathematical Physics*, 50, 082501.

Aazami, A. and Petters, A. (2010), "A universal magnification theorem. III. Caustics beyond codimension 5," *Journal of Mathematical Physics*, 51, 023503.

Aazami, A., Keeton, C., and Petters, A. (2011a), "Lensing by Kerr black holes. II: Analytical study of quasi-equatorial lensing observables," *Arxiv preprint arXiv:1102.4304*.

Aazami, A., Petters, A., and Rabin, J. (2011b), "Orbifolds, the A, D, E family of caustic singularities, and gravitational lensing," *Journal of Mathematical Physics*, 52, 022501.

Adem, A., Leida, J., and Ruan, Y. (2007), *Orbifolds and Stringy Topology*, Cambridge University Press.

Arnold, V. (1973), "Normal forms for functions near degenerate critical points, the Weyl groups of A_k, D_k, E_k and Lagrangian singularities," *Functional Analysis and Its Applications*, 6, 254–272.

Arnold, V., Gusein-Zade, S., and Varchenko, A. (1985), "Singularities of Differentiable Maps, Volume I," *Birkhäuser, Boston*.

Barbeau, E. (2003), *Polynomials*, Springer.

Blandford, R. and Narayan, R. (1986), "Fermat's principle, caustics, and the classification of gravitational lens images," *The Astrophysical Journal*, 310, 568–582.

Boyer, R. and Lindquist, R. (1967), "Maximal analytic extension of the Kerr metric," *Journal of Mathematical Physics*, 8, 265.

Bozza, V. (2003), "Quasiequatorial gravitational lensing by spinning black holes in the strong field limit," *Physical Review D*, 67, 103006.

Bozza, V. (2008a), "Comparison of approximate gravitational lens equations and a proposal for an improved new one," *Physical Review D*, 78, 103005.

Bozza, V. (2008b), "Optical caustics of Kerr spacetime: The full structure," *Physical Review D*, 78, 63014.

Bozza, V. and Scarpetta, G. (2007), "Strong deflection limit of black hole gravitational lensing with arbitrary source distances," *Physical Review D*, 76, 83008.

Bozza, V. and Sereno, M. (2006), "Weakly perturbed Schwarzschild lens in the strong deflection limit," *Physical Review D*, 73, 103004.

Bozza, V., De Luca, F., Scarpetta, G., and Sereno, M. (2005), "Analytic Kerr black hole lensing for equatorial observers in the strong deflection limit," *Physical Review D*, 72, 83003.

Bozza, V., Luca, F., and Scarpetta, G. (2006), "Kerr black hole lensing for generic observers in the strong deflection limit," *Physical Review D*, 74, 63001.

Carter, B. (1968), "Global structure of the Kerr family of gravitational fields," *Physical Review*, 174, 1559–1571.

Castrigiano, D. and Hayes, S. (2004), *Catastrophe Theory*, Westview Press.

Cattani, E., Dickenstein, A., and Sturmfels, B. (1997a), "Residues and resultants," *Arxiv preprint alg-geom/9702001*.

Cattani, E., Cox, D., and Dickenstein, A. (1997b), "Residues in toric varieties," *Compositio Mathematica*, 108, 35–76.

Chiba, M. (2002), "Probing dark matter substructure in lens galaxies," *The Astrophysical Journal*, 565, 17.

Congdon, A. and Keeton, C. (2005), "Multipole models of four-image gravitational lenses with anomalous flux ratios," *Monthly Notices of the Royal Astronomical Society*, 364, 1459–1466.

Dalal, N. (1998), "The magnification invariant of simple galaxy lens models," *The Astrophysical Journal Letters*, 509, L13.

Dalal, N. and Rabin, J. (2001), "Magnification relations in gravitational lensing via multidimensional residue integrals," *Journal of Mathematical Physics*, 42, 1818.

Dymnikova, I. (1984), "The effect of the relative delay of rays focused by a rotating massive body," *Zhurnal Eksperimental noi i Teoreticheskoi Fiziki*, 86, 385–389.

Dymnikova, I. (1986), "Motion of particles and photons in the gravitational field of a rotating body." *Uspekhi Fizicheskikh Nauk*, 148, 393–432.

Evans, N. and Witt, H. (2003), "Fitting gravitational lenses: truth or delusion," *Monthly Notices of the Royal Astronomical Society*, 345, 1351–1364.

Golubitsky, M. and Guillemin, V. (1973), *Stable Mappings and Their Singularities*, Springer Verlag.

Griffiths, P. and Harris, J. (1978), *Principles of Algebraic Geometry*, vol. 1994, Wiley New York.

Hunter, C. and Evans, N. (2001), "Lensing properties of scale-free galaxies," *The Astrophysical Journal*, 554, 1227.

Iyer, S. and Hansen, E. (2009a), "Light's bending angle in the equatorial plane of a Kerr black hole," *Physical Review D*, 80, 124023.

Iyer, S. and Hansen, E. (2009b), "Strong and Weak Deflection of Light in the Equatorial Plane of a Kerr Black Hole," *Arxiv preprint arXiv:0908.0085*.

Keeton, C. (2001), "Computational methods for gravitational lensing," *Arxiv preprint astro-ph/0102340*.

Keeton, C. and Petters, A. (2005), "Formalism for testing theories of gravity using lensing by compact objects: Static, spherically symmetric case," *Physical Review D*, 72, 104006.

Keeton, C. and Petters, A. (2006a), "Formalism for testing theories of gravity using lensing by compact objects. II. Probing post-post-Newtonian metrics," *Physical Review D*, 73, 44024.

Keeton, C. and Petters, A. (2006b), "Formalism for testing theories of gravity using lensing by compact objects. III. Braneworld gravity," *Physical Review D*, 73, 104032.

Keeton, C., Gaudi, B., and Petters, A. (2003), "Identifying lenses with small-scale structure. I. Cusp lenses," *The Astrophysical Journal*, 598, 138.

Keeton, C., Gaudi, B., and Petters, A. (2005), "Identifying lenses with small-scale structure. II. Fold lenses," *Astrophysical Journal*, 635, 35–59.

Lee, J. (2003), *Introduction to Smooth Manifolds*, Springer Verlag.

Majthay, A. (1985), *Foundations of Catastrophe Theory*, Pitman Advanced Pub. Program.

Mao, S. and Schneider, P. (1997), "Evidence for substructure in lens galaxies?" *Arxiv preprint astro-ph/9707187*.

Metcalf, R. and Madau, P. (2001), "Compound gravitational lensing as a probe of dark matter substructure within galaxy halos," *The Astrophysical Journal*, 563, 9.

Moerdijk, I. and Pronk, D. (1997), "Orbifolds, sheaves and groupoids," *K-theory*, 12, 3–21.

O'Neill, B. (1995), *The Geometry of Kerr Black Holes, AK Peters*, AK Peters.

Petters, A. (2010), "Gravity's Action on Light," *Notices of the AMS*, 57.

Petters, A., Levine, H., and Wambsganss, J. (2001), *Singularity Theory and Gravitational Lensing*, Birkhäuser.

Rauch, K. and Blandford, R. (1994), "Optical caustics in a kerr spacetime and the origin of rapid x-ray variability in active galactic nuclei," *The Astrophysical Journal*, 421, 46–68.

Rhie, S. (1997), "Infimum microlensing amplification of the maximum number of images of n-point lens systems," *The Astrophysical Journal*, 484, 63.

Satake, I. (1956), "On a generalization of the notion of manifold," *Proceedings of the National Academy of Sciences of the United States of America*, 42, 359.

Schneider, P. and Weiss, A. (1992), "The gravitational lens equation near cusps," *Astronomy and Astrophysics*, 260, 1–13.

Schneider, P., Ehlers, J., and Falco, E. (1992), *Gravitational Lenses*, Springer Verlag.

Sereno, M. and De Luca, F. (2006), "Analytical Kerr black hole lensing in the weak deflection limit," *Physical Review D*, 74, 123009.

Sereno, M. and De Luca, F. (2008), "Primary caustics and critical points behind a Kerr black hole," *Physical Review D*, 78, 23008.

Vazquez, S. and Esteban, E. (2003), "Strong field gravitational lensing by a Kerr black hole," *NUOVO CIMENTO-SOCIETA ITALIANA DI FISICA SEZIONE B*, 119, 489.

Virbhadra, K. and Ellis, G. (2000), "Schwarzschild black hole lensing," *Physical Review D*, 62, 84003.

Virbhadra, K. and Ellis, G. (2002), "Gravitational lensing by naked singularities," *Physical Review D*, 65, 103004.

Wald, R. (1984), *General Relativity*, University of Chicago Press.

Weinberg, S. (1972), *Gravitation and Cosmology*, vol. 7, Wiley New York.

Werner, M. (2007), "A Lefschetz fixed point theorem in gravitational lensing," *Journal of Mathematical Physics*, 48, 052501.

Werner, M. (2009), "Geometry of universal magnification invariants," *Journal of Mathematical Physics*, 50, 082504.

Werner, M. and Petters, A. (2007), "Magnification relations for Kerr lensing and testing cosmic censorship," *Physical Review D*, 76, 64024.

Witt, H. and Mao, S. (1995), "On the minimum magnification between caustic crossings for microlensing by binary and multiple stars," *The Astrophysical Journal Letters*, 447, L105.

Witt, H. and Mao, S. (2000), "On the magnification relations in quadruple lenses: a moment approach," *Monthly Notices of the Royal Astronomical Society*, 311, 689–697.

Zakharov, A. (1995), "On the magnification of gravitational lens images near cusps." *Astronomy and Astrophysics*, 293, 1–4.

Biography

Amir Babak Aazami was born December 14, 1978, in Tehran, Iran. Together with his family, he immigrated to the United States in 1985. He attended the University of California, Berkeley, graduating in 2001 with a Bachelor's in Physics and English literature. He has since focused on mathematical physics. He hopes to carry on doing research in academia.